THE SOLUBILITY AND THERMODYNAMIC PROPERTIES OF ETTRINGITE, ITS CHROMIUM ANALOGS, AND CALCIUM ALUMINUM MONOCHROMATE ($3CaO \cdot Al_2O_3 \cdot CaCrO_4 \cdot nH_2O$)

by

ROBERT BENJAMIN PERKINS

A dissertation submitted in partial fulfillment of the
requirements for the degree of

DOCTOR OF PHILOSOPHY
in
ENVIRONMENTAL SCIENCES AND RESOURCES: GEOLOGY

Portland State University
2000

DISSERTATION APPROVAL

The abstract and dissertation of Robert Benjamin Perkins for the Doctor of Philosophy in Environmental Sciences and Resources: Geology were presented May 5, 2000 and accepted by the dissertation committee and the doctoral program.

COMMITTEE APPROVALS:

_____
Michael Cummings, Chair

_____
Carl Palmer

_____
William Fish

_____
Georg Grathoff

_____
Jie Lin
Representative of the Office of Graduate Studies

DOCTORAL PROGRAM APPROVAL:

_____
Roy Koch, Director
Environmental Sciences and Resources
Ph.D. Program

ABSTRACT

An abstract of the dissertation of Robert Benjamin Perkins for the Doctor of Philosophy in Environmental Sciences and Resources: Geology presented May 5, 2000.

Title: The Solubility and Thermodynamic Properties of Ettringite, Its Chromium Analogs, and Calcium Aluminum Monochromate ($3CaO \cdot Al_2O_3 \cdot CaCrO_4 \cdot nH_2O$).

Ettringite ($Ca_6[(Al(OH)_6)]_2(SO_4)_3\ 26H_2O$) is a naturally-occurring mineral and an important product of the hydration of Portland cements and fly ash. Substitution of Cr(III) for Al(III) and CrO_4 for SO_4 in the ettringite structure has been demonstrated and may be important with respect to the fate and transport of chromium in alkaline environments.

Ettringite and its chromium analogs were synthesized and their solubilities measured via dissolution and precipitation experiments over a range of temperatures between 5 and 75ºC and pH values between 10 and 13. The log $K_{SP,298}$ for the reaction

$$Ca_6[Al(OH)_6]_2(SO_4)_3 \cdot 26H_2O = 6Ca^{2+} + 2Al(OH)_4^- + 3SO_4^{2-} + 4OH^- + 26H_2O$$

is –44.9 ±0.3.The enthalpy and entropy of reaction are 205 ±12 kJ mol^{-1} and 170 ±38 J mol^{-1} K^{-1}, respectively. The free energy, enthalpy, and entropy of formation are –15211 ±20, –17550 ±16 kJ mol^{-1}, and 1870±59 J mol^{-1} K^{-1}, respectively,

based on the reaction parameters and partial molar properties for the dissolved ions.

The log K_{SP}, free energy, and enthalpy of reaction for the Cr(III) ettringite analog, bentorite, are $K_{SP,298}$ = -52.9 ±0.8, $\Delta G°_{r,298}$ = 302 ±10 and $\Delta H°_r$ = 320 ±76 kJ mol^{-1} based on an equivalent dissolution reaction. Dissolution of bentorite is incongruent due to precipitation of another phase tentatively identified as $Ca_2Cr_2O_5 \cdot 8H_2O$.

The log K_{SP}, free energy and enthalpy of reaction for the dissolution of $Ca_6[(Al(OH)_6)]_2(CrO_4)_3\ 26H_2O$ are $K_{SP,298}$ = –41.46 ±0.30, $\Delta G°_{r,298}$ = 236.6 ±3.9 and $\Delta H°_r$ = 77.5 ±9.6 kJ mol^{-1}. The log K_{SP} varies with pH unless a $CaCrO_{4(aq)}$ complex is included in the speciation model. A log formation constant of K = 2.77 ±0.16 was obtained for the reaction $Ca^{2+} + CrO_4^{2-} = CaCrO_{4(aq)}$ by minimizing the variance of the IAP for $Ca_6[(Al(OH)_6)]_2(CrO_4)_3\ 26H_2O$.

A secondary precipitate, identified as calcium aluminum monochromate or ($3CaO \cdot Al_2O_3 \cdot CaCrO_4 \cdot nH_2O$) was present in Cr(VI)-analog experimental residues. The log K_{SP} for the reaction

$$3CaO \cdot Al_2O_3 \cdot CaCrO_4 \cdot 15H_2O = 4Ca^{2+} + 2Al(OH)_4^- + CrO_4^{2-} + 4OH^- + 9H_2O$$

is –30.38 ±0.28.

$Ca_6[(Al(OH)_6)]_2(SO_{4(1-x)}, CrO_{4x})_3\ 26H_2O$ solids were synthesized and solid-solution aqueous-solution interactions were investigated through dissolution pathway studies. Although thermodynamic equilibrium was not achieved, dissolution pathways approximated stoichiometric saturation curves when plotted on Lippman diagrams.

Acknowledgments

I would first and foremost like to thank Dr. Carl Palmer for providing me with the opportunity to pursue this study and for showing me that, while the devil is in the details, good questions and further opportunities often reside there too. My completion of this study was greatly helped by Carl's boundless enthusiasm for research and patience with those of us new to the world of geochemistry.

I would also like to express my sincere gratitude to Dr. Michael Cummings for his shrewd and practical advice and for his steady push to keep me going. I would certainly like to thank the other members of my committee; Dr. Bill Fish and Dr. Jie Lin for their constructive advice and interesting insights; and last, but not least, Dr. Georg Grathoff for his thorough review of this work and his constant encouragement.

A project such as this requires a lot of help, which I found readily offered by many people here at Portland State. In particular, I would like to acknowledge Dr. Dennis Barnum for the generous use of his lab; the microbiologists on the 5th floor of SB-I for graciously allowing me use of their facilities (often unannounced and unexpected); Dr. Mary Taylor as well as the folks in the limnology lab for letting me fill my carboy when our water filter went out; Inge Wortman and Brent Schauer in Multimedia Production Services for making me look good (at the last second!) on several occasions; and Stuart Cowburn for making the basement geochemistry lab a more lively place to work. I would also like to say thanks to Dr. Alan Yeakley for his advice and encouragement.

Of course, none of this would have been possible without financial support. I would like to acknowledge the U.S. Environmental Protection Agency for initial funding, the Department of Geology and the Environmental Sciences and Resources Program, and the folks in the Graduate Studies Office and the members of the University Club for providing me sufficient freedom so that I could complete the bulk of this work.

My experience here at Portland State University has been greatly enhanced by the many friends I have made - in and out of the Geology Department. I've not the room to list every individual, but thanks to you all! I must, however, say a word of thanks to Chris Hyatt for his good-humored grieve giving and for putting up with the clutter I kept during our Hawthorne day and a very special thanks to Dr. Ayna Alfadhli for her moral support and encouragement.

Most of all, I thank my family, and especially my parents, Fyrl and Clayton Perkins, for their unending and unconditional love and support.

TABLE OF CONTENTS

LIST OF TABLES

LIST OF FIGURES

Chapter 1. General Introduction

1.1 BACKGROUND

Chromium is a prevalent contaminant of soils and waters in many industrialized areas. Major sources of chromium contamination include metal-plating, alloy production, and mining and ore processing operations. Chromium is also widely used in textile dyes, leather tanning, and as a catalyst in various industrial processes (Nriagu, 1988; Richard and Bourg, 1991). The release of chromium into the environment is of concern as it is toxic, carcinogenic, mutagenic, and teratogenic (Nieboer and Shaw, 1988; Nordberg, 1988; O'Brien and Kortenkamp, 1994; Sugiyama, 1994). Understanding the processes that control chromium behavior in the environment is important given its widespread occurrence and potential risks.

Although chromium has received a great deal of study, most of the related research to date has been conducted in neutral to acidic environments. However, chromium can and often does occur in alkaline environments such as concrete, basic waste solutions, fly-ash, flue-gas desulphurization (FGD) wastes, and alkaline soils. The mobility of chromium in alkaline environments is likely to be controlled by precipitation and dissolution of solid phases. This is especially the case with Cr(VI), which typically occurs in an oxyanionic form (CrO_4^{2-}) which has low sorption tendencies under alkaline conditions (Dzombak and Morel, 1990).

Ionic substitution in the mineral ettringite ($Ca_6[(Al(OH)_6)]_2(SO_4)_3\ 26H_2O$ may be important in limiting the mobility of chromium in many alkaline environments of

interest. Ettringite is a naturally-occurring mineral and an important constituent of hydrated portland-type cements and fly ash. Isomorphous substitution of Cr(III) for Al(III) and CrO_4^{2-} for SO_4^{2-} in the ettringite structure (Figure 1-1) has been recognized (Gross, 1980; Myneni et al., 1994; Poellman et al., 1993), and a naturally-occurring Cr(III) analog, bentorite, has been identified (Bensted and Varma, 1971). However, there are few available data regarding the solubility of ettringite and its chromium-analogs.

The objective of the research presented herein is to determine the solubility of ettringite and its chromium analogs and to use these data to calculate thermodynamic properties for these solid phases. Such information is needed to accurately model the fate and transport of chromium in the environment. The results of such modeling could help in the design of waste-stabilization systems and in the development of more effective strategies for environmental cleanups. Thermodynamic data for ettringite and its chromium analogs, in conjunction with data for related phases, could be used to determine stability fields for these solids which may be important for material scientists working with cementitious and refractory materials.

1.2 OVERVIEW

This dissertation contains seven chapters: this introduction, five experimental chapters, and a concluding chapter that summarizes research results, presents overall conclusions, and describes additional avenues for continued research. The experimental chapters have been prepared as stand-alone contributions for publication

in scientific journals. Chapter 2 describes experiments conducted to determine the solubility of ettringite. This work forms the basis for comparison of properties derived for the chromium-substituted ettringite phases. Previously-published values for the solubility of ettringite vary by more than ten orders of magnitude and few data could be found regarding the enthalpy and entropy of ettringite which are needed to calculate the solubility at temperatures other than 25ºC.

Chapter 3 deals with the solubility of the mineral bentorite ($Ca_6[Cr(OH)_6]_2(SO_4)_3 \cdot 26H_2O$), the Cr(III) analog of ettringite. No data regarding the solubility of this phase could be found. Such data are particularly important given the interest in stabilizing chromium-laden wastes in cementitous materials. The chromium in such wastes would, where possible, be reduced to Cr(III) prior to mixing with the cement matrix. Cr(III) has also been proposed as an additive to increase early hydration strengths of cement (Teramato and Koie, 1976)

Chapter 4 presents an investigation of the solubility of $Ca_6[Al(OH)_6]_2(CrO_4)_3 \cdot 26H_2O$, the chromate analog of ettringite. This phase is not naturally-occurring, but previous workers have synthesized it (Kumarathasan et al., 1990; Myneni, 1995) and Palmer (2000) found CrO_4-bearing ettringite crystals in concrete which had been contaminated with chromium-plating solutions. This clearly indicates that ettringite can and does play a role in attenuation of chromium released in the environment. No solubility data could be located for this phase.

A secondary precipitate was determined to have formed in samples prepared as part of the $Ca_6[Al(OH)_6]_2(CrO_4)_3 \cdot 26H_2O$ solubility experiments. This phase was

identified as $3CaO \cdot Al_2O_3 \cdot CaCrO_4 \cdot nH_2O$, the chromate analog of calcium aluminum monosulfate or “monosulfate”, another important product of hydration in cement systems. Chapter 5 deals with the solubility of this phase based on continued interpretation of data obtained from the $Ca_6[Al(OH)_6]_2(CrO_4)_3 \cdot 26H_2O$ study.

The last experimental chapter deals with an investigation of the $Ca_6[Cr(OH)_6]_2(SO_4, CrO_4) \cdot 26H_2O$ solid-solution and corresponding solid solution / aqueous solution reactions. Knowledge of solid solution properties is important since chromium substitution in ettringites is unlikely to be complete under real-world scenarios where SO_4 is likely present in significant quantities and partial substitutions could potentially limit the concentrations of chromium more effectively than would the pure $Ca_6[Al(OH)_6]_2(CrO_4)_3 \cdot 26H_2O$ phase.

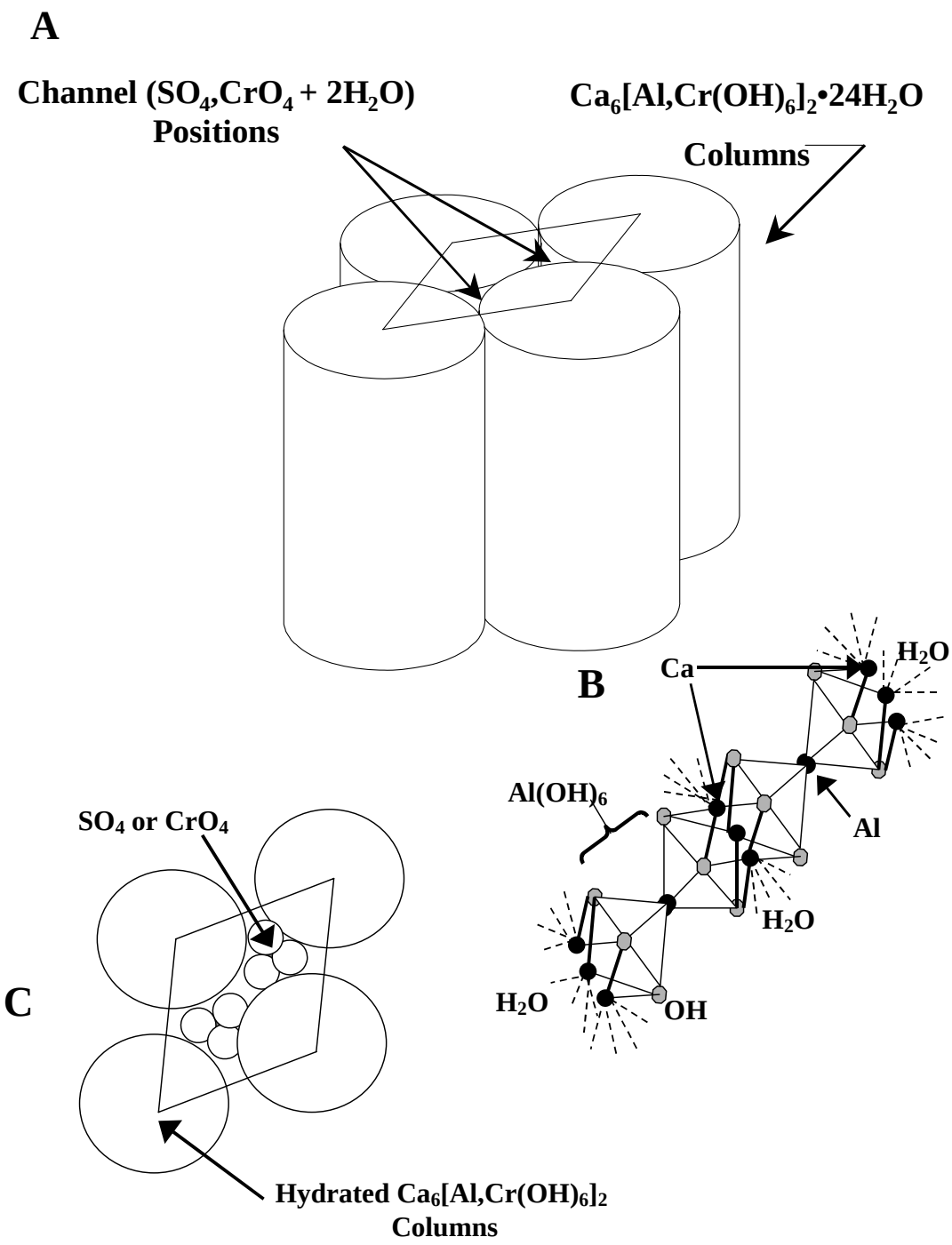

Figure 1-1. Structure of ettringite ($Ca_6[(Al,Cr(OH)_6)]_2(SO_4,CrO_4)_3\ 26H_2O$) A.) schematic showing relationship between calcium aluminum hydroxide columns, channel positions, and hexagonal crystal form; B.) detail of columns; dashed lines represent water molecules; C.) detail showing position of oxyanions in channels. (After Moore and Taylor, 1970; Myneni, 1995)

Chapter 2. Solubility of Ettringite ($Ca_6[Al(OH)_6]_2(SO_4)_3 \cdot 26H_2O$)At 5 - 75° C

2.1 INTRODUCTION

Ettringite is a hydrous calcium alumino-sulfate mineral represented by the formula $Ca_6[Al(OH)_6]_2(SO_4)_3 \cdot 26H_2O$. Ettringite occurs naturally in alkaline environments as a secondary fracture-lining mineral in calcium-rich igneous rocks or in sedimentary units that have undergone contact metamorphism (e.g., Bentor, 1963; Hurlbut and Baum, 1960; Murdoch and Chalmers, 1960). Ettringite is also an important hydration product of Portland and super-sulfated cements and has been used as a coating for paper (Moore and Taylor, 1970).

There is a recognized ettringite group described by the general formula $Ca_6[X_3(OH)_6]_2(Y)_3 \cdot 26H_2O$, where X represents a site occupied by trivalent metals such as Al^{3+}, Fe^{3+}, or Cr^{3+} and Y represents a site occupied by oxyanions such as SO_4^{2-}, CO_3^{2-}, SeO_4^{2-}, or CrO_4^{2-}. Alternative substitutions can involve ions such as $B(OH)_4^-$ and AsO_4^{3-} which require stoichiometric adjustments within the structure (Hassett et al., 1990; Myneni et al., 1994; Poellman et al., 1993; Poellmann et al., 1990). The exchange capacity of ettringite with regard to environmental contaminants such as arsenic, chromium, and selenium, along with its occurrence in common alkaline materials such as concrete and fly ash, make it of particular interest to workers dealing with environmental contamination and waste stabilization in cementitious materials.

There is considerable uncertainty regarding the solubility of ettringite. If the dissolution reaction is written as

(1)

$$Ca_6[Al(OH)_6]_2(SO_4)_3 \cdot 26H_2O = 6Ca^{2+} + 2Al(OH)^-_4 + 3SO^{2-}_4 + 4OH^- + 26H_2O$$

then the solubility product, K_{SP}, is

(2)

$$K_{SP} = \{Ca^{2+}\}^6\{Al(OH)^-_4\}^2\{SO_4^{2-}\}^3\{OH^-\}^4\{H_2O\}^{26}$$

Reported values for log $K_{SP,\ ettringite}$ vary by more than ten orders of magnitude (Table 2-1). In addition, enthalpy and heat capacity data needed to calculate ettringite solubility at temperatures other than 25ºC are sparse and poorly documented.

The purpose of this study was to measure the solubility of ettringite and to determine the log K_{SP} from 5º to 75º C. The thermodynamic properties obtained will be useful to researchers studying rock-water interactions, waste migration in alkaline environments, and waste stabilization in cementitious materials.

2.2 PREVIOUS STUDIES

Jones (1939; 1944a; 1944b; 1944c) made a series of studies involving the systems $CaO\text{-}Al_2O_3\text{-}CaSO_4\text{-}H_2O$, $CaO\text{-}Al_2O_3\text{-}CaSO_4\text{-}K_2O\text{-}H_2O$, and $CaO\text{-}Al_2O_3\text{-}CaSO_4\text{-}Na_2O\text{-}H_2O$. He determined the boundary curves and invariant points for pertinent solid phases, including ettringite. He noted that ettringite dissolves

incongruently, forming an amorphous aluminum oxide. Solution pH values were not specified by Jones. However, log K_{SP} values based on Jones' data were later calculated by both Hampson and Bailey (1982) and Warren and Reardon (1994) who estimated hydroxide ion concentrations from electroneutrality equations. In both cases, the calculated log K_{SP} ranges from greater than –35 to approximately –45.

Atkins et al. (1992; 1991) performed solubility experiments on various cement hydrate phases to model the long term chemistry and stability of cement hydrates proposed for radionucliide immobilization. They observed approximately congruent dissolution of ettringite. Their reported mean log K_{SP} (-111.3 at 25º C) was based on $\{Al^{3+}\}$ rather than $\{Al(OH)_4^-\}$. Some of the charge imbalances in their data exceed 40% (Table 2-1).

Damidot et al. (1992) investigated the stability of ettringite in regards to sulfate attack on concrete. They determined the solubility of ettringite in NaOH and Na_2SO_4 solutions of various strengths. Although pH values are not presented, they reported log K_{SP} values ranging from –43.80 to –44.79 (Table 2-1).

As part of a more comprehensive examination of stability relationships between ettringite and monosulfate, Warren and Reardon (1994) determined the log $K_{SP,298}$ of ettringite over a range of pH values using data from both precipitation and dissolution experiments. They reported an average log $K_{SP,298}$ of -44.91 ±1.06 (2 standard deviations), using an ion interaction approach to calculate activity coefficients. A systematic decrease in the solubility constant values calculated by Warren and Reardon (1994) was noted at pH > 13. They concluded this shift might be

due to: 1) uncertainty in pH measurements, 2) incorrect ion interaction parameters at high pH, or 3) substitution of OH for SO_4 in the ettringite structure at high pH. They did not use the data from high pH samples in calculating their average K_{SP} value.

Table 2-1. Summary of previous studies of ettringite solubility at 25°C.

Ref.	Reported or Mean log Ksp at 25°C	Re-calculated Log Ksp at 25°C[a]	No. of Samples	Mean Charge Balance Error	Comments
1, 4	--	-35 to –45	20	--	Warren and Reardon (1994; Fig. 3) from Jones'(1939).
2	-111.3	-43.88 ±0.65	8	30.4 %	Reported K_{SP} based on Al^{3+}, not $Al(OH)_4^-$.
3	-44.43	--	16	--	No pH values reported.
4	-44.91 ±0.64	-44.61 ±0.56	28	9.6 %	Average of precipitation and dissolution experiments (excluding samples > 13 pH).
4	--	-44.36 ±0.46	16	9.7 %	Dissolution experiments.
4	--	-44.95 ±0.55	12	8.1 %	Precipitation experiments.
5	-111.6 ±0.8	-45.08	12	21.2%	Reported K_{SP} based on $\{Al^{+3}\}$. New K_{SP} & mean charge balance error based on 1 dissolution & 2 precipitation samples w/ reported concentrations.
6	-36.7	--	?	?	Insufficient data to estimate charge balance error(s).
7	-44.90 ±0.32	--	27	5.4%	Average of precipitation and dissolution experiments (excluding samples >13 pH).
7	-44.95 ±0.24	--	14	4.9%	Dissolution experiments.
7	-44.84 ±0.38	--	13	5.9%	Precipitation experiments.

[a] Recalculated using MINTEQA2 (Allison et al., 1990), except for first entry. Sources: 1): Jones, 1939; 2): Atkins et al., 1991; 3): Damidot et al., 1992; 4): Warren and Reardon, 1994; 5): Myneni et al., 1998; 6): Ghorab et al. 1998; 7): Current Study.

Ghorab and Kishar (1985) and Ghorab et al. (1998) investigated the variation in the solubility of ettringite in pure water and in the presence of alite, lime, and monocarboaluminate hydrate. They reported a log Ksp value of –36.7 for ettringite in pure water at 30°C and lower values (~ -40) when in the presence of alite. However, they did not provide detailed methodologies and reported only one set of time-dependent data for each of their experiments.

Myneni et al. (1998) investigated the solubility of ettringite at 25ºC over a range of pH values (10.7 – 12.4). They reported a log $Ksp_{,298}$ value, -111.6 ± 0.8, based on $\{Al^{3+}\}$ rather than $\{Al(OH)_4^-\}$. However, we calculated speciated charge balance errors >20% for two of the three "final" samples for which concentrations were available. Myneni et al. (1998) did report that variations in suspension concentration, while affecting pH and total concentrations, did not affect the log Ksp or significantly alter the dissolution rate.

Wagman et al. (1982) provide the only value for the enthalpy of formation of ettringite which we were able to locate (ΔH^o_f = -17539 kJ mol^{-1}). It is not clear how this value was obtained. Viellard and Rassineux (1992) estimated the Gibbs free energy of formation (ΔG^o_f = -15200.0 kJ mol^{-1}) and entropy value (S^o = 1861.6 J mol^{-1} K^{-1}) from the summation of corresponding oxides and Wagman et al.'s enthalpy value. They also estimated the heat capacity as a function of temperature.

The solubility products calculated from previous ettringite solubility data (Table 1) span more than ten orders of magnitude. Many of these studies suffer from

incomplete data sets, minimal data points, or high charge balance errors. In addition, there is a paucity of data regarding the temperature dependence of ettringite solubility. Our objective is to provide a complete and precise data set from which accurate thermodynamic properties of ettringite can be determined.

2.3 METHODS

2.3.1. Synthesis of Ettringite

Ettringite was synthesized using a modification of methods described by Odler and Abdul-Maula (1984) and Warren and Reardon (1994). Two reactant solutions were initially prepared by adding 6.65 g $Al_2(SO_4)_3 \cdot 18H_2O$ and 4.44 g $Ca(OH)_2$ to 100 ml and 250 ml of ultrapure water (> 14 megaohms-cm), respectively. The reagent water used in preparation of solutions was purged with N_2 gas for 15 to 30 minutes to minimize CO_2 contamination. The reactant solutions were mixed in a N_2-filled glove box in which the atmosphere was continuously bubbled through 1N NaOH. The mixture was diluted to 500 ml with additional reagent water and 0.5 ml of 1N NaOH. The final solution was sealed in a 500-ml high density polyethylene (HDPE) bottle, placed on a 60º C hot plate, and stirred at 400 rpm. After 48 hours, the contents of the bottle were transferred under N_2 to a ceramic filter funnel and rapidly vacuum-filtered through a 7-cm diameter, 1.6-μm filter. The filtered precipitate was dried and stored at room temperature in a desiccator with a saturated $CaCl_2$ solution to maintain a relative humidity of approximately 30%.

2.3.2. Characterization of Synthetic Ettringite

X-ray diffraction (XRD) analyses of the synthesized solid precipitate were performed on a Norelco XRG 3000 unit using CuK_{α} radiation. Fourier Transform Infrared Spectroscopy (FTIR) were conducted on a Perkin-Elmer 2000 unit, utilizing both a KBr pellet and Nujol mull mounted on salt plates. The morphology and size of the synthesized crystallites were determined from images obtained from a Zeiss 960 digital scanning electron microscope (SEM). Qualitative chemistries of the crystallites were obtained with a LINK energy dispersive X-ray spectrometer (EDX) using a 31-mm working distance with an accelerating voltage of 20 kV.

A small portion of solid was digested in HCl and analyzed to verify that the stoichiometry of the synthesized material agreed with ideal ettringite. Total calcium concentrations were measured by atomic absorption spectroscopy (AAS) and total aluminum by graphite-furnace atomic absorption (GFAA) using a Perkin-Elmer Analyst 300 AA spectrophotometer and HGA-800 graphite furnace with auto-sampler. Total sulfate concentrations were determined by high-performance liquid chromatography (HPLC). A Dionex 2010 HPLC unit, equipped with an Ionpac AS11 4 X 250-mm analytical column, a guard column, a Dionex anion self-regenerating suppressor, and conductivity detector was used for sulfate analyses. A 21 millimolar (mM) NaOH solution was used as the eluent.

The amount of water in the synthesized material was determined by thermogravimetric analysis (TGA) using a Perkin-Elmer TGA7 thermogravimetric

analyzer. The analysis was conducted on 5.56 mg of sample material over a temperature range of 40 to 900ºC at a rate of 10ºC/minute.

2.3.3. Dissolution and Precipitation Experiments

A set of dissolution experiments was conducted at 25°C at six different initial pH levels between 10.3 and 13.1. Synthesized ettringite (0.05 to 0.1 g) was placed in 30- or 60-ml HDPE bottles along with a magnetic stir bar. The bottles were subsequently filled under an N_2 with ultrapure water that had been purged with N_2 and adjusted to the desired pH with NaOH. As an additional precaution against CO_2 contamination, the capped HDPE bottles were sealed within N_2-filled glass mason jars. The jarred sample bottles were then placed in circulating water baths to maintain the temperature within 0.2^{o}C of the desired value and mixed with magnetic stirrers. Because of the small volumes of water used in these experiments, an additional experiment using 120 mL of water was conducted in duplicate so that the aqueous solutions could be temporally sampled to determine the time required to achieve steady state.

Samples were also obtained from 25°C solutions initially supersaturated with respect to ettringite. These precipitation experiments were conducted by spiking the suspensions remaining at the end of the dissolution experiments with 20 or 25 ml of 10 or 20 mM $Ca(NO_3)_2$. Other aspects of the precipitation experiments were identical to the dissolution experiments.

Dissolution experiments were conducted at six additional temperatures ranging between 5 and 75°C in order to determine the temperature dependence of the ettringite solubility product. These experiments were otherwise identical to the 25°C dissolution experiment with water bath temperatures maintained within 0.3°C of the temperature of interest.

All sampling was conducted in a N_2-filled glove box. The mason bottles were transferred to the glove box in portable water baths, the HDPE bottles removed, and the samples quickly processed to maintain the desired temperatures. For each sample, approximately 10 ml of suspension were withdrawn. The samples were filtered using 0.45-μm polysulfone membrane filters and separate aliquots allotted for cation and anion analyses. A 5ml/L concentrated HNO_3 solution was used to dilute and preserve the cation subsamples at pH < 2. Samples were stored in HDPE vials for analyses. A representative sample of the solid phase was removed following sampling of the precipitation experiments and analyzed by XRD to verify that no measurable compositional changes had taken place.

Measurements of pH were made at the time of sampling using an Orion Model 290A portable meter and Orion Model 9157BN triode pH electrode. The pH meter was calibrated using three buffers, typically 7.00, 10.00, and 12.45 pH (sodium phosphate, sodium carbonate / bicarbonate, and calcium hydroxide, respectively). Although a slight reduction in the electrode response slope (e.g., ~3 mv/pH) was noted over the higher pH interval, the meter utilizes the slope of the interval corresponding to each measurement in order to reduce “averaging” errors. The buffers were brought

to the temperature of the samples to account for temperature-dependent variations in pH and the meter response adjusted to the appropriate value based on the manufacturer's temperature-dependence data. The low-sodium-error glass used to manufacture the electrode obviated the need to apply alkali interference corrections at the sodium concentration / temperature combinations encountered because the corresponding corrections were < 0.01 pH units. Liquid-junction potential effects were minimized by appropriate conditioning and storage of the electrode and by allowing suspended sediment to settle prior to sampling. Total Ca, Al, and SO_4 concentrations were determined by the same methods used to analyze the solid digest.

2.4 EXPERIMENTAL RESULTS

2.4.1. Solid Characterization

XRD analysis of the synthesized material indicated that the five most intense peaks corresponded to d-spacings of 9.7, 5.61, 3.88, 2.77, and 2.563 Å. These values compare well with the five major peaks of 9.73, 5.61, 3.88, 2.773, and 2.564 Å reported on the JCPDS Card 9-414 for ettringite (JCPDS, 1991; Figure 2-1). Comparisons of other d-spacings with the JCPDS card and McMurdie et al. (1986) show excellent agreement (Table 2-2). All of the sample peaks with relative intensities > 8% were matched with the ettringite JCPDS 9-414 card and all of the listed ettringite peaks with intensities >8% were found in the synthesized material. Two peaks found in the initial synthesized solid at 2.487 and 2.286 Å, with relative intensities of 6 and 2% (of the maximum peak) could not be matched with the JCPDS

9-414 card for ettringite. However, a 2.487 Å peak with a relative intensity of 6% and corresponding to the {224} plane is listed by McMurdie et al. (1986).

Ettringite is in the hexagonal crystal system. Using the Miller indices reported on JCPDS Card 9-414, the d-spacings from the XRD analyses of the initial synthesized material, and the equation for hexagonal system minerals,

(3)

$$d = \frac{\sqrt{3}ac}{\sqrt{4c^2(h^2 + hk + k^2) + 3a^2l^2}}$$

we calculated unit cell dimensions of a_0 = 11.23 ±0.01 and c_o = 21.49 ±0.05 Å. These values correspond extremely well with those listed by the JCPDS 9-414 card (11.23 and 21.44 Å) and by McMurdie et al. (1986) (11.225 and 21.467 Å). Our calculated primitive unit cell volume (2347.1 ±5.4 $Å^3$) is less than one standard error from the volume (2342.5 $Å^3$) reported by McMurdie et al. (1986).

The peak at 2.286 Å can be fit to the calculated cell dimensions using Equation (3) and an hkl of either {315} or {135} with a resulting residual error of 0.0013 Å, which is within the expected analytical error. Alternatively, this peak may be the {113} calcite peak. However, although the principal calcite peak, {104}, occurs at 3.035 Å, which is very near the {116} peak for ettringite, other peaks, including a major peak at 2.095 Å, are not evident in the synthesized ettringite diffraction pattern.

Given the lack of other major calcite peaks and the use of N_2-purged solutions and the N_2-filled glovebox during synthesis, we believe the 2.286 Å peak represents a legitimate ettringite plane.

The XRD analysis of solid residues from the precipitation experiment show additional peaks at 7.60, 4.28, 3.80 and 3.06 Å (Table 2) which correspond to the major peaks (7.56, 4.27, 3.79, and 3.06 Å) reported on the JCPDS Card 6-0046 for gypsum. The residue samples were prepared as wet mounts of suspensions on glass slides and it is possible that the gypsum may have formed during sample drying.

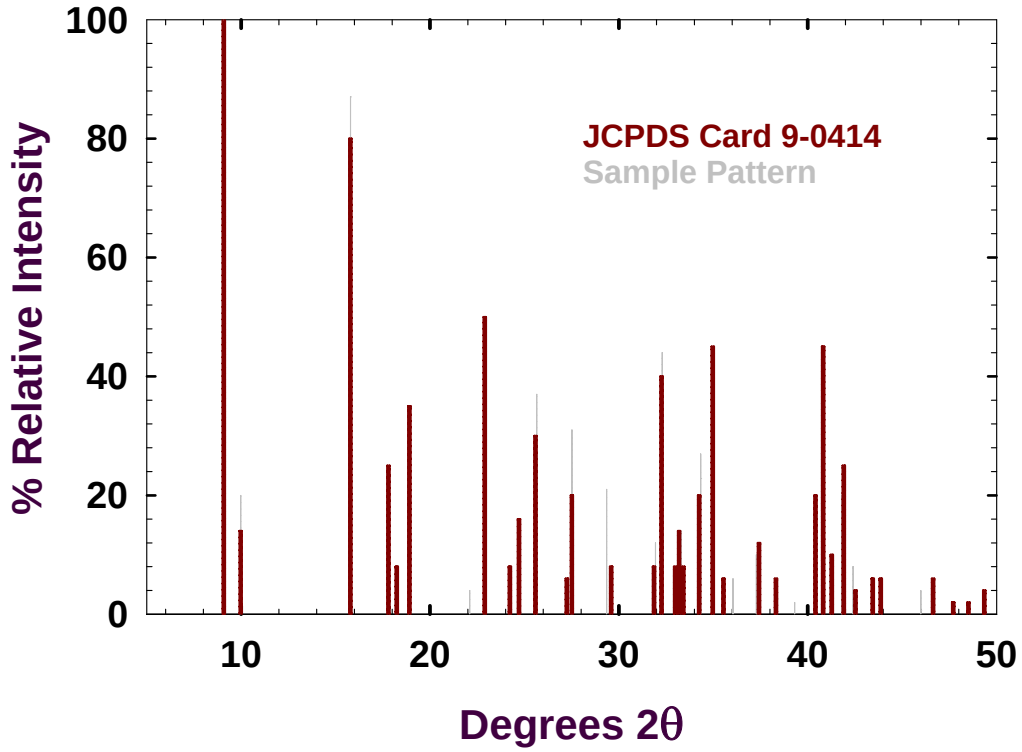

Figure 2-1. Measured X-ray diffraction peaks for synthesized ettringite compared with published powder diffraction peaks for ettringite from JCPDS Card 9-0414

Table 2-2. Comparison of X-ray diffraction peaks from synthetic ettringite used in solubility experiments with peaks from McMurdie et al. (1986) and JCPDS 9-0414.

	Ettringite McMurdie et al. (1986)		Ettringite JCPDS 9-414		Initial Synthesized Ettringite		Solid Filtrate from Precipitation Experiments	
h,k,l[a]	d(Å)	I/Imax	d(Å)	I/Imax	d(Å)	I/Imax	d(Å)	I/Imax
002	10.70	12	--	--	--	--	--	--
100	9.72	92	9.73	100	9.7	100	9.7	100
101	8.88	5	8.86	14	8.9	20	8.9	4
--			--	--	--	--	7.60	10
103	5.758	22	--	--	--	--	--	--
110	5.614	85	5.61	80	5.61	87	5.61	88
112	4.981	30	4.98	25	4.97	19	4.97	14
200	4.867	13	4.86	8	4.86	5	4.86	8
104	4.703	62	4.69	35	4.70	24	4.70	6
314	--	--	4.41	4	--	--	--	--
--	--	--	--	--	--	--	4.28	9
203	4.025	12	4.02	2	4.02	4	4.02	2
114	3.881	100	3.88	50	3.88	45	3.88	15
--	--	--	--	--	--	--	3.80	2
210	3.677	12	3.67	8	3.67	8	3.68	5
211	3.617	17						
204	3.604	24	3.60	16	3.60	13	3.60	3
212	3.477	47	3.48	30	3.47	37	3.48	29
213	3.268	17	3.27	6	--	--	--	--
300	3.241	27	3.240	20	3.24	31	3.24	28
--	--	--	--	--	--	--	3.06	12
116	3.018	15	3.016	8	3.04	21	3.04	29
220	2.807	21	2.806	8	2.805	12	2.809	7
304	2.774	65	2.773	40	2.771	44	2.775	23
222	--	--	2.714	8	--	--	--	--
310	2.697	16	2.697	14	2.690	14	2.698	10
008	2.683	19	2.68	8	--	--	--	--
312	2.615	86	2.616	20	2.614	27	2.614	24
216	2.563	86	2.564	45	2.563	43	2.567	14
313	2.523	6	2.524	6	--	--	2.528	3
224	2.487	6	--	--	2.487	6	2.494	7
400	--	--	2.434	4	--	--	--	--
118	2.420	8	2.422	4	--	--	--	--
314, 306	2.409	15	2.401	12	2.410	10	2.410	6
208	2.350	8	2.347	6	2.346	2	--	--
--			--	--	2.286	2	2.286	6
320	2.230	26	2.23	20	2.232	12	2.232	12
226	2.208	69	2.209	45	2.211	39	2.211	7
322	2.183	13	2.185	10	2.190	10	2.185	7
316	2.152	38	2.154	25	2.155	20	2.155	10
00(10), 323	2.147	14	2.13	4	2.126	8	2.126	4
410	2.122	10	2.124	6	--	--	--	--
412	2.081	7	2.081	6	2.084	5	2.093	5
324	2.059	10	2.062	6	2.062	6	2.062	4
414 , 325	1.9732	6	1.979	4	1.972	4	1.976	7

[a] If two values listed, the first is from McMurdie et al., 1986, the second from JCPDS 9-414.

The FTIR spectra (Figure 2-2, Table 2-3) agree well with that of the ettringite spectrum reported by Bensted and Varma (1971). A comparison of the peaks along with Bensted and Varma's interpretations is presented in Table 2-3. The peaks at 632 (Nujol mull) and 618 cm^{-1} (KBr pellet) correspond to SO_4 ν_4 vibrations (Hassett et al., 1990). However, the peak at 1417 cm^{-1} obtained from analysis of the synthesized material prepared with KBr cannot be due to Nujol mull and may indicate CO_3 contamination. Myneni (Myneni, 1995) assigned peaks near 1450 cm^{-1} to CO_3 and noted that such contamination is difficult to avoid because of the high reactivity of ettringite with respect to CO_2. Such contamination is consistent with the presence of calcite as noted in the XRD results and may have occurred during sample preparation outside the N_2-filled glovebox.

The SEM imaging showed the majority of the synthesized material to be very small (< 1 to ~10 x <0.5 μm) acicular crystals or fibrous crystallites which formed aggregate masses. These observations are consistent with the general prismatic or fibrous morphology of ettringite described by Gougar et al. (1996) and Hampson and Bailey (1982). EDX analyses of the material indicated that most of the crystals had the same general composition (Ca-Al-S), which would be expected for ettringite. One of the eleven random EDX analyses made on a relatively large (tens of μm wide), tabular crystal indicated a lower Ca:S ratio and a relatively smaller proportion of Al than the others. These characteristics are consistent with the presence of a minor amount of gypsum which has been noted as a common minor impurity in synthesized ettringites (Atkins et al., 1992; Atkins et al., 1991; Myneni et al., 1998).

Analysis of the solid phase digest yielded a Ca:Al:SO_4 ratio of 6.23:2.00:3.31 based on the average molarity from replicate analyses normalized to the Al concentration. This compares favorably to the ideal ratio of 6:2:3 for pure ettringite, with the maximum relative percent difference based on the value of 3.31 for sulfate approximating the expected maximum analytical error of 10%. The discrepancies may also be due to the presence of minor impurities. For example, a 0.23 molar excess of Ca could be due to the presence of 1.8% calcite by weight. If the excess Ca and SO_4 concentrations are from gypsum, then the molar excesses correspond to 3.2 to 4.1% gypsum by weight.

The thermogravimetric analysis indicates that mass loss occurs over four distinct temperature intervals (Figure 2-3). Most of the loss occurred between 40 - 180^o C, the range at which loosely bound water would be expected to be lost. The 33% mass loss over this interval corresponds to 23 water molecules. The additional mass loss of 4.3% that occurs between 200 and 280^{o}C (an inflection point) may be explained as the mass loss of the three remaining water molecules. The next interval of mass loss (4.2%) occurs between 280 and 500^{o}C and corresponds closely to the loss of three more water molecules from the unit structure.

The last interval of mass loss (3.8% total) from 600 to approximately 900^{o}C corresponds closely to approximately 2.5 water molecules, resulting in a total mass loss equivalent to 31.5 water molecules. The overall expected mass loss, assuming pure ettringite and conversion to 3 moles of calcium sulfate, 3 moles of calcium oxide and one mole of aluminum oxide, is 45.9% which agrees well with the measured loss

of 45.3%. The 0.6% discrepancy may be due to: 1) incomplete heating/reaction; 2) loss of loosely bound water prior to start of analyses; or 3) the presence of impurities.

Based on the sum of these analyses, we are confident that the synthesized solid is ettringite with near ideal unit cell dimensions and stoichiometry. The variance from the ideal stoichiometry may be explained by minor impurities (e.g., ≤ 4.1% of gypsum or calcite). Although these impurities affect ionic concentrations, they should not alter the calculated values of the resulting IAPs.

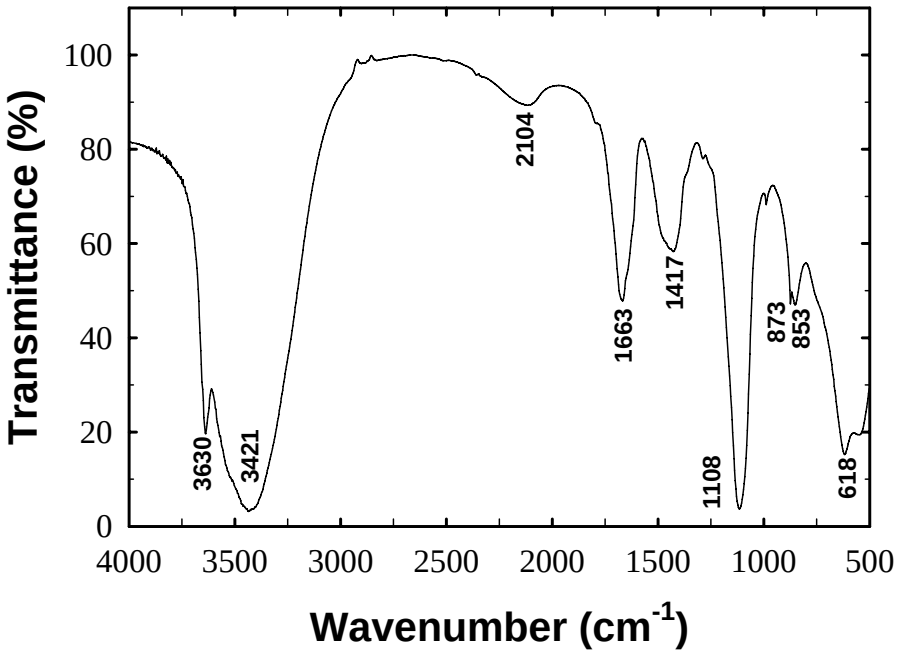

Figure 2-2. FTIR spectrum for synthesized ettringite (in KBr pellet). Major vibrational bands correspond to: free OH-stretching (3641 cm^{-1}); ν_3 H_2O (3429 cm^{-1}); ν_2 H_2O (1684 cm^{-1}); ν_3 SO_4 (1116 cm^{-1}); Al-O-H bending vibration (853 cm^{-1} through 600 cm^{-1}) (Bensted and Varma, 1971). The 1417 cm^{-1} may be due to CO_2

Table 2-3. Comparison of Fourier transform infra-red spectroscopy spectra from synthesized ettringite and previous study.

Synthesized Samples Peak Wavenumbers		**Bensted & Varma's Reported Ettringite Peak Wavenumber**		
in Nujol (cm^{-1})	**In KBr (cm^{-1})**	**(cm^{-1})**		**Comments**
632	608			Bensted et al. did not analyze below 650 cm^{-1}. SO_4 ν_4 suggested by Hassett et al. (1990).
722	--	~720	x	Nujol medium
853	844, 860	855	w	Al-O-H bending vibration
1116	1105	1120	vs	ν_3, SO_4
1377	--	~1375	x	Nujol media
1462	1417	~1470	x	Nujol media. Peak in KBr sample may be due to CO_3^{2-} contamination.
1640	1660	1640	b,	ν_2, H_2O
1684		1675	b,	ν_2, H_2O
2735	2110			No Data Reported from 1750 to 3000 cm^{-1}
2907				Nujol media
3429	3412	3420	vs	ν_3, H_2O
3641	3634	3635	m	Free OH stretching

w = weak; m = medium; s = strong; vs = very strong; b = broad
o = obscured by adjacent stronger peak; x = due to Nujol media

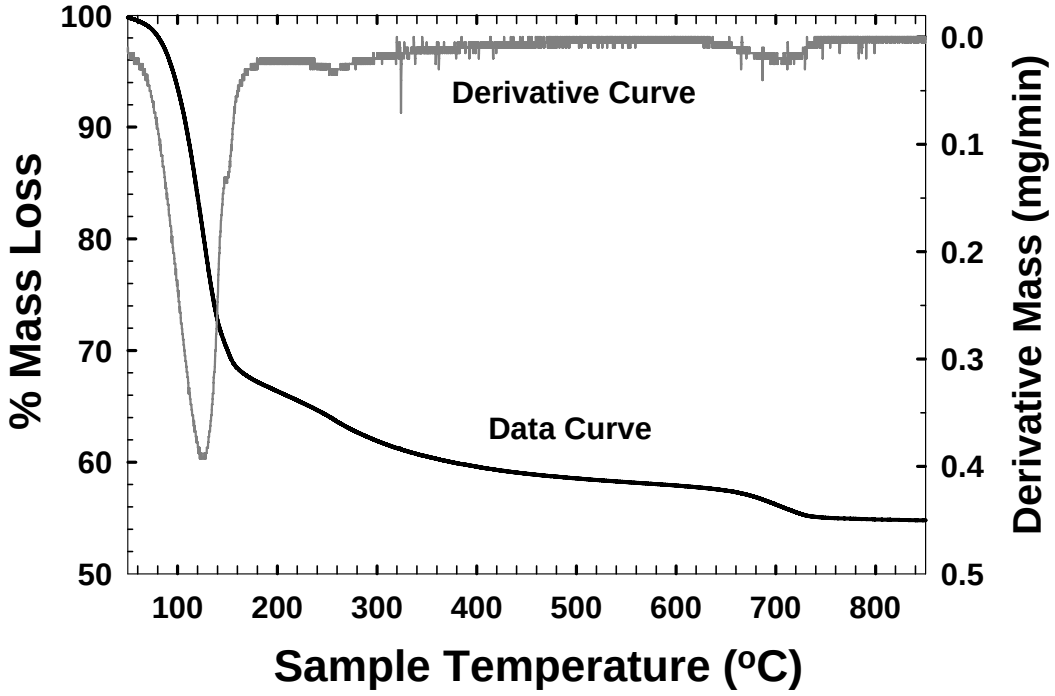

Figure 2-3. Thermogravimetric analysis of synthetic ettringite.

2.4.2. Dissolution and Precipitation Experiments

The greatest variations in ion concentrations occur within the first 50 hours in the dissolution experiment at 25°C and initial pH of 11.5 with steady-state conditions achieved within 100 to 150 hours (Figure 2-4). The highest calcium concentration occurs in the first sample collected at four hours and is likely to be due to rapid dissolution of minor gypsum or calcite impurities. The subsequent decline in calcium concentrations and the concomitant rise in aluminum concentrations and relatively early steady-state conditions for sulfate are consistent with this interpretation.

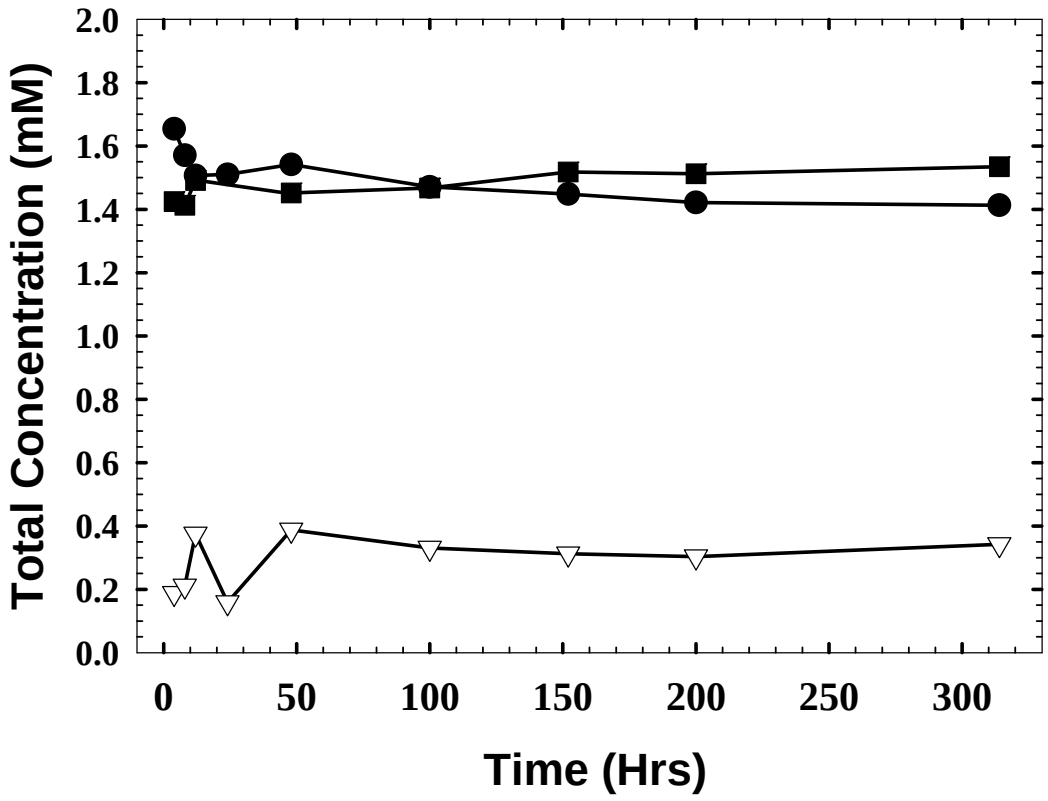

Figure 2-4. Total concentrations of Ca (ℓ), Al (∇), and SO_4 (□) in the 25°C ettringite dissolution experiment with initial pH 11.5.

The averaged analytical results from the 25°C dissolution and precipitation experiment triplicates (Table 2-4) show a clear decrease in the total Ca, Al, and SO_4 concentrations with increasing pH. The ion activities were calculated with the geochemical speciation model MINTEQA2 (Allison, 1990) using modified thermodynamic databases (Table 2-5). Activity corrections were made using the Davies Equation:

(4)

$$\log \gamma_i = -AZ_i^2 \left(\frac{\sqrt{I}}{1+\sqrt{I}} - 0.24I \right)$$

where γ_i is the activity coefficient for ion "i", A is a constant dependent on the dielectric constant of water and temperature, Z is the charge of ion, and I is the ionic strength of the solution.

Ion activity products (IAP) for ettringite (Table 2-6) were calculated from the activities using Equation (2). The charge balance errors calculated for the dissolution samples ranged from 0.2 to 31.8%, with the largest charge balance errors associated with the highest (13.06) pH sample. This sample was not included in subsequent calculations of thermodynamic parameters. The charge balance errors of the remaining samples ranged from 2.1 to 8.0% with an average value of 4.9%. Likewise, excluding the highest pH (12.99) sample, the average charge balance error for the precipitation samples is 5.9%.

There is a general increase in the concentrations of Ca, Al, and SO_4 with increasing temperature (Table 2-7). The calculated activities and IAPs for the temperature-dependent samples are provided in Table 2-8. Again, samples with the highest pH values (12.5 to 13.0) consistently had the highest associated charge balance errors (typically exceeding 20%) and therefore were not included in subsequent calculations of thermodynamic parameters. The mean charge balance error associated with the remaining temperature-dependent samples was 7.2%. The calculated log IAPs

clearly increase with increasing temperature, with average values ranging from –47.11 ±0.64 (total standard deviation) at 5°C to –39.76 ±0.24 at 75°C.

Table 2-4. Final concentrations in 25°C dissolution and precipitation experiments.

Sample Batch[a]	No. Reps.	Meas. pH	(Ca) mmol L^{-1}	(Al) mmol L^{-1}	(SO_4) mmol L^{-1}	(Na) mmol L^{-1}	Duration
D25-10.5	3	11.06 ± 0.02	2.198 ± 0.048	0.511 ± 0.045	1.302 ± 0.083	0.62 ± 0.20	15 days
D25-11.0	3	11.09 ± 0.01	2.165 ± 0.071	0.336 ± 0.020	1.745 ± 0.021	1.336 ± 0.078	15 days
D25-11.5	2	11.43 ± 0.07	1.41 ± 0.13	0.342 ± 0.031	1.53 ± 0.48	4.057 ± 0.058	15 days
D25-12.0	3	11.94 ± 0.07	0.825 ± 0.043	0.309 ± 0.029	0.966 ± 0.084	10[b]	10 days
D25-12.5	3	12.41 ± 0.01	0.637 ± 0.047	0.337 ± 0.020	0.932 ± 0.026	27[b]	10 days
D25-13.0	3	13.06 ± 0.01	0.662 ± 0.083	0.300 ± 0.042	0.9289 ± 0.0009	100[b]	10 days
P25-10.5[c]	3	10.52 ± 0.16	10.22 ± 0.66	0.544 ± 0.073	1.44 ± 0.34	0.58 ± 0.22	25 days
P25-11.0	2	10.57 ± 0.23	10.3 ± 1.3	0.31 ± 0.10	0.64 ± 0.28	0.91 ± 0.25	26 days
P25-11.5	3	11.19 ± 0.10	8.21 ± 0.32	0.144 ± 0.038	0.392 ± 0.078	3.0 ± 1.10	25 days
P25-12.0	2	11.83 ± 0.18	2.63 ± 1.22	0.17 ± 0.18	0.49 ± 0.28	6.2 ± 3.4	25 days
P25-12.5	3	12.44 ± 0.01	3.43 ± 0.38	0.028 ± 0.0032	0.317 ± 0.029	26.3 ± 1.3	26 days
P25-13.0	3	12.99 ± 0.05	1.94 ± 0.87	0.054 ± 0.074	0.57 ± 0.17	69.7 ± 1.1	26 days

[a] Dissolution experiment samples denoted with "D"-prefix; precipitation samples with "P"-prefix.
[b] Sodium concentrations for 25-12.0, -12.5, & -13.0 samples estimated from initial volumes of 1N NaOH added to solutions.
[c] Estimated NO_3 concentrations for precipitation ("P-") samples are as follows:
Samples P25-10.5, -11.5, & 11.5: 16.7 mM NO_3
Samples P25-12.0, -12.5, & 13.0: 6.7 mM NO_3.

Table 2-5. Thermodynamic data used to update MINTEQA2[a] databases.

REACTIONS	kJ/mol $\Delta G°_r$	kJ/mol $\Delta H°_r$	J/mol·K $\Delta S°_r$	J/mol·K ΔC_P	log K	Ref.[b]
$H_2O - H^+ = OH^-$	79.58	55.81	-80.66	-212.5	-13.99	1, 2
Aqueous Species						
$Ca^{2+} + H_2O - H^+ = CaOH^+$	73.22	77.47	14.6	-38.0	-12.82	1, 2
$Ca^{2+} + SO_4^{2-} = CaSO_4^0$	-12.05	5.44	58.6	196	2.11	2, 3
$Al^{3+} + H_2O = AlOH^{2+} + H^+$	28.35	55.65	91.0	0.65	-4.97	2, 4
$Al^{3+} + 2H_2O = Al(OH)^{2+} + 2H^+$	57.70	122.6	218	-225	-10.11	2, 4
$Al^{3+} + 3H_2O = Al(OH)_3^0 + 3H^+$	95.15	176.4	--	--	-16.67	2, 4
$Al^{3+} + 4H_2O = Al(OH)_4^- + 4H^+$	131.3	181.4	167.7	-91.8	-23.00	2, 4
Solid Phases						
$CaSO_4 \cdot 2H_2O = Ca^{2+} + SO_4^{2-} + 2H_2O$	26.15	-0.46	-89.2	-333	-4.58	5
$Ca(OH)_2 = Ca^{2+} + 2H_2O - 2H^+$	-130.1	-129.5	-278.6	--	22.8	5
$Al_2O_{3,\ corundum} = 2Al^{3+} + 3H_2O - 6H^+$	-108.8	-263.6	-533	-93.0	19.06	2, 4, 6
$Al_2O_{3,\ \gamma\text{-Alumina}} = 2Al^{3+} + 3H_2O - 6H^+$	-128.4	-285.8	-542	-93.0	22.49	2, 4, 6
$Al(OH)_{3,\ amph} = Al^{3+} + 3H_2O - 3H^+$	-61.65	-463.9	-1350	--	10.8	2, 4, 6
$Al(OH)_{3,\ crystalline\ gibbsite} = Al^{3+} + 3H_2O - 3H^+$	-46.29	-399.1	-1180	--	8.11	2, 4, 6
$Al(OH)_{3,\ microcrystalline\ gibbsite} = Al^{3+} + 3H_2O - 3H^+$	-53.37	-428.9	-1260	--	9.35	2, 4, 6
$AlOOH,\ _{boehemite} = Al^{3+} + 2H_2O - 3H^+$	-45.70	-116.2	-243	-23.5	8.00	2, 4, 6
$AlOOH,\ _{diaspore} = Al^{3+} + 2H_2O - 3H^+$	-42.10	-112.0	-241	-22.4	7.38	2, 4, 6
$Al(OH)_{3,\ gibbsite} = Al^{3+} + 3H_2O - 3H^+$	-46.36	-105.3	-205	15.0	8.12	2, 3, 4

[a] Allison et al., 1990

[b] Multiple sources indicate sources for individual ion or solid phase data that were used in calculating presented data. 1): Cox et al., 1989; 2): Shock et al., 1997; 3): Sverjensky et al., 1997; 4): Nordstrom and May, 1996; 5): Nordstrom et al., 1990; 6): Hemingway and Sposito, 1996.

2.5 DISCUSSION

The log IAPs calculated using equilibrium activities from the 25°C dissolution experiments range from -44.81 to -45.26 (Table 2-6). The lowest IAP calculated is for the highest pH (13.06) sample (Figure 2-5). This sample is excluded in subsequent calculations because of its large charge balance error (>20%). A Student's t-test indicates that the slope of the remaining log IAP values versus pH is not significantly different from zero at the 90% confidence level (t = -2.58, 3 degrees of freedom), although it does slightly exceed the critical t-value at the 95% level. An F-test indicates that the variance in the log IAP values between samples is not significantly

different than the variance in the replicate values at the 95% confidence level ($F = 1.82$; $n_1 = 5$; $n_2 = 14$; $df_1 = 4$; $df_2 = 9$). The mean log IAP value for the 25°C dissolution experiment is –44.95 ±0.24. The reported error is the total standard deviation (t.s.d.), representing the error in both samples and replicates.

The observed molar ratios of ions in solution do not agree with the ideal or measured solid stoichiometry. The departure from ideal stoichiometry is partially the result of impurities in the synthesized materials. For example, mass balance calculations indicate that the presence of minor amounts of gypsum (0.8 to 6.4%) and trace amounts (< 1%) of $Al_2(SO_4)_3 \cdot 18H_2O$ in the initial solid could explain these discrepancies. The excess aluminum in the solutions with pH > 11.5 could be due to dissolution of minor amounts of aluminum hydroxides or oxyhydroxides which may not be detectable via XRD analysis of the initially synthesized material. The solutions with pH < 11.5 are supersaturated or near saturation with respect to boehmite, diaspore, and gibbsite while solutions with pH > 11.5 are undersaturated with respect to these phases.

Table 2-6. Calculated equilibrium activities and ion activity products; 25ºC ettringite dissolution and precipitation experiments.

Sample Batch	Meas pH	Log $\{Ca^{2+}\}$	Log $\{Al(OH)_4^-\}$	Log $\{SO_4^{2-}\}$	Log $\{OH^-\}$	Log $\{Na^+\}$	Ionic Strgth (m)	C.B. Err. (%)	- Log IAP
25°C Dissolution Samples									
25-10.5	11.06	-2.85	-3.33	-3.10	-2.94	-3.26	0.0075	6.8	44.82 ±0.04
25-11.0	11.09	-2.88	-3.52	-2.98	-2.91	-2.92	0.0085	4.4	44.85 ±0.10
25-11.5	11.43	-3.07	-3.51	-3.03	-2.57	-2.44	0.0090	3.3	44.81 ±0.15
25-12.0	11.94	-3.34	-3.56	-3.25	-2.06	-2.05	0.0134	-2.1	45.18 ±0.39
25-12.5	12.41	-3.59	-3.55	-3.36	-1.59	-1.65	0.0314	-8.0	45.06 ±0.18
25-13.0[b]	13.14	-3.95	-3.65	-3.59	-0.86	-1.12	0.1454	-29.9	45.19 ±0.23
25°C Precipitation Samples									
25-10.5	10.33	-2.30	-3.34	-3.25	-3.66	-3.33	0.0310	1.4	44.91 ±0.16
25-11.0	10.56	-2.28	-3.59	-3.63	-3.43	-3.12	0.0304	6.9	45.50 ±0.21
25-11.5	11.19	-3.92	-3.80	-2.81	-2.62	-1.85	0.0275	-0.67	44.73 ±0.18
25-12.0	11.83	-2.87	-3.95	-3.59	-2.17	-2.18	0.0172	-10.0	44.58 ±0.01
25-12.5	12.44	-2.88	-4.65	-3.88	-1.56	-1.66	0.0394	-10.7	44.47 ±0.23
25-13.0[b]	12.99	-3.44	-4.76	-3.80	-0.99	-1.27	0.1086	-31.9	45.49 ±0.56

[a] Charge balance error

[b] Calculated IAP not used in determining mean log K_{SP} value.

Table 2-7. Final concentrations in temperature-dependent dissolution experiments.

Sample Batch	No Reps	Temp (ºC)	Meas pH	(Ca) mmol L^{-1}	(Al) mmol L^{-1}	(SO_4) mmol L^{-1}	(Na) mmol L^{-1}	Lngth (days)
5-10.5	6	5	11.30 ± 0.05	1.71 ± 0.12	0.288 ± 0.080	1.435 ± 0.074	0.390 ± 0.073	18-35
5-11.5	6	5	12.23 ± 0.033	0.69 ± 0.15	0.260 ± 0.045	0.85 ± 0.25	3.60 ± 0.15	18-35
5-12.5	6	5	13.41 ± 0.04	0.148 ±0.039	0.293 ± 0.036	0.759 ± 0.23	36.30 ± 0.47	18-35
15-10.5	3	15	11.04 ± 0.03	2.164 ±0.095	0.642 ± 0.057	1.81 ± 0.14	0.441 ± 0.028	20
15-11.5	3	15	11.70 ± 0.08	0.97 ±0.21	0.331 ± 0.079	1.41 ± 0.31	3.829 ± 0.062	20
35-10.5	2	35	10.52 ± 0.07	3.609 ±0.037	1.09 ± 0.39	2.89 ± 0.45	0.41 ± 0.10	13
35-11.5	3	35	11.16 ± 0.09	1.142 ±0.007	0.810 ± 0.097	1.386 ± 0.254	3.528 ± 0.023	13
35-12.5	2	35	12.33 ± 0.33	0.528 ±0.057	1.05 ± 0.38	1.17 ± 0.38	38.2 ± 1.4	13
45-10.5	3	45	10.49 ± 0.07	3.93 ±0.42	0.876 ± 0.084	2.78 ± 0.40	0.445 ± 0.004	18
45-11.5	6	45	10.91 ± 0.07	2.65 ±0.12	0.89 ± 0.11	2.51 ± 0.35	4.020 ± 0.094	18-32
45-12.5	3	45	12.13 ± 0.03	0.385 ±0.012	1.045 ± 0.056	1.52 ± 0.16	37.3 ± 1.7	13
60-10.5	3	60	10.38 ± 0.02	4.49 ±0.10	1.64 ± 0.13	3.027 ± 0.090	0.449 ± 0.006	10
60-11.5	3	60	11.83 ± 0.04	3.023 ±0.099	1.44 ± 0.034	2.30 ± 0.11	3.925 ± 0.043	10
60-12.0	2	60	11.80 ± 0.05	0.759 ±0.094	1.402 ± 0.042	1.5818 ± 0.076	25.9 ± 1.2	10
75-11.5	3	75	10.09 ± 0.03	5.30 ±0.18	2.624 ± 0.052	4.21 ± 0.33	4.031 ± 0.069	27
75-12.0	3	75	10.72 ± 0.04	2.615 ±0.079	2.204 ± 0.069	3.12 ± 0.10	12.94 ± 0.15	27

Table 2-8. Calculated equilibrium activities and ion activity products; temperature-dependent ettringite dissolution experiments.

Sample Batch	Meas pH	Log $\{Ca^{2+}\}$	Log $\{Al(OH)_4^-\}$	Log $\{SO_4^{2-}\}$	Log $\{OH^-\}$	Log $\{Na^+\}$	Ionic Strgth (m)	C.B. Err. (%)	Log IAP
5°-10.5	11.30	-2.94	-3.41	-3.05	-3.40	-3.62	0.0062	2.3	47.25 ±0.45
5°-11.5	12.23	-3.35	-3.63	-3.25	-2.47	-2.48	0.0067	-6.4	46.97 ±0.83
5°-12.5[a]	13.41	-4.28	-3.62	-3.51	-1.29	-1.53	0.0513	-26.7	48.63 ±0.91
15°-10.5	11.04	-2.87	-3.23	-2.95	-3.30	-3.40	0.0080	-0.68	45.71 ±0.01
15°-11.5	11.70	-3.22	-3.53	-3.04	-2.64	-2.46	0.0078	0.51	46.05 ±0.20
35°-10.5	10.52	-2.70	-3.05	-2.91	-3.17	-3.64	0.0123	-0.76	43.42 ±0.21
35°-11.5	11.16	-3.17	-3.14	-3.06	-2.52	-2.50	0.0085	-9.6	44.53 ±0.07
35°-12.5	12.33	-3.82	-3.08	-3.34	-1.36	-1.51	0.0519	-18.7	44.54 ±0.39
45°-10.5	10.49	-2.68	-3.11	-2.85	-2.89	-3.41	0.0128	2.4	44.42 ±0.33
45°-11.5	10.91	-2.88	-3.11	-2.87	-2.47	-2.48	0.0130	-6.9	42.00 ±0.18
45°-12.5[a]	12.13	-4.05	-3.08	-3.24	-1.25	-1.52	0.0574	-32.1	45.18 ±0.20
60°-10.5	10.38	-2.66	-2.84	-2.84	-2.59	-3.41	0.0149	-8.2	40.56 ±0.19
60°-11.5	11.83	-2.87	-2.90	-2.94	-2.16	-2.47	0.0155	-19.6	40.45 ±0.18
60°-12.5[a]	11.80	-3.88	-2.95	-3.23	-1.17	-1.69	0.0605	-53.8	43.57 ±0.02
75°-11.5	10.09	-2.66	-2.65	-2.75	-2.51	-2.47	0.0200	-1.9	39.56 ±0.16
75°-12.0	10.72	-3.07	-2.73	-2.86	-1.87	-1.96	0.0247	-17.1	39.95 ±0.07

[a] Samples not used in subsequent calculations due to high charge balance errors.

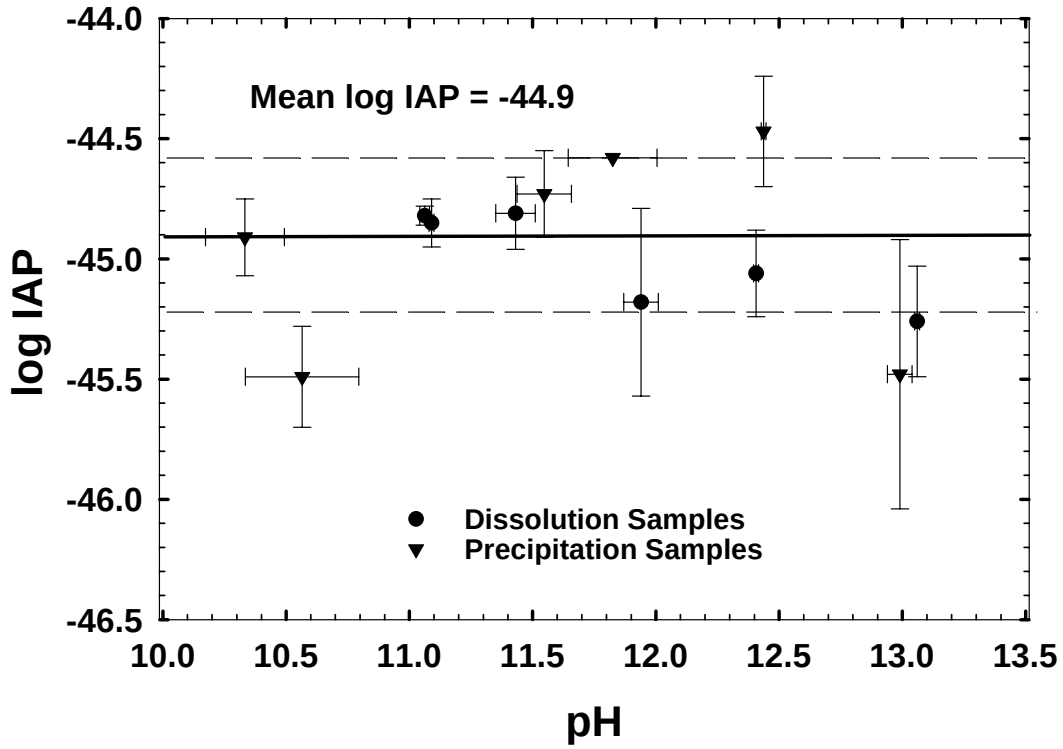

Figure 2-5. Calculated log ion activity products from 25°C ettringite dissolution and precipitation experiments versus pH. Dashed lines represent one standard deviation from mean.

The log IAP values calculated from the precipitation experiment activities range from –44.58 to –45.48. The lowest IAP value is associated with the highest pH sample which has a singularly high associated charge balance error (>30%). A Student's t-test indicates that the slope of the remaining log IAP values versus pH is not significantly different from zero at the 95% confidence level (t = 2.13, 3 degrees of freedom). An F-test indicates that the variance in the log IAP values between samples is significantly different than the variance in the replicate values at the 95% confidence level (F = 11.05; $n_1 = 5$; $n_2 = 13$; $df_1 = 4$; $df_2 = 8$). A contributing factor to

the higher variance in the precipitation samples is the larger range of dilution factors used during analyses of the samples. Estimation of (NO_3^-) based on the volume of the $Ca(NO_3)_2$ spike may have led to additional errors in the calculated ion activities. The mean log IAP value for the 25°C precipitation experiment is –44.84 ±0.38 (t.s.d.).

The relatively low IAP values associated with the highest pH samples were consistently seen in the dissolution experiments conducted at other temperatures as well. Warren and Reardon (1994) also observed such a drop in the log IAPs for ettringite at 25°C. They attributed this apparent drop to uncertainties in the activity coefficient model and possible substitution of OH^- for SO_4^{2-} in the ettringite structure at high pH. Given the charge balance errors calculated for high pH samples in both Warren and Reardon's and our own experiments, it seems likely that the problem is the lack of sound thermodynamic data and uncertainties in measured pH values for high pH conditions.

A Student's t-test for samples with unequal variances shows that the difference between the mean IAPs of the dissolution and precipitation experiments is not significantly different than zero at the 95% confidence level (t = -0.563; 5 degrees of freedom). A Student's t-test of the combined 25°C samples versus pH indicates that the slope is not significantly different than zero at 95% confidence level (t = 1.22; 8 degrees of freedom). Based on the observed steady-state concentrations for individual analytes and the lack of a significant difference in the log IAP values calculated for solutions which were initially under- and over-saturated with respect to ettringite, we are confident that thermodynamic equilibrium was achieved. The average equilibrium

log IAP, obtained from the means of the triplicate dissolution and precipitation experiments, represents the log K_{SP} at 25°C and is calculated as -44.9 ±0.32 (t.s.d.). The calculated log $K_{SP, 298}$ of –44.9 is the same value calculated by Warren and Reardon (1994) using the ion interaction model SIMUL (Reardon, 1990). The similarity of values obtained using the Davies Equation and the ion interaction approach is not entirely surprising given the low ionic strengths of the solutions used in both studies (i.e., <0.15 m for all samples below pH 13). Ion activities calculated by the Davies Equation do not vary extensively from ion interaction models until ionic strengths exceed 0.5 m. Using the MINTEQA2 model and the $\{Al(OH)_4^-\}$, log $K_{SP, 298}$ values of –44.6 and –45.1 were calculated using data from Warren and Reardon (1994) and Myneni et al. (1998), respectively. These values are within one standard deviation of our value and may be considered to be in excellent agreement. These K_{SP}s are considerably lower than many of the previously published values (Table 2-1).

At equilibrium, the Gibbs free energy of the dissolution reaction at 25°C is given by: **(5)**

$$\Delta G^\circ_{reaction} = 6\Delta G^\circ_{f,298}(Ca^{2+}) + 2\Delta G^\circ_{f,298}(Al(OH)_4^-) + 3\Delta G^\circ_{f,298}(SO_4^{2-}) + 4\Delta G^\circ_{f,298}(OH^-) + 26\Delta G^\circ_{f,298}(H_2O) - \Delta G^\circ_{f,298,ettringite.}$$

The free energy of reaction is also related to the K_{SP} by:

(6)

$$\Delta G^\circ_{reaction} = -RT \ln K_{SP}$$

where R is the gas constant (8.3145 J mol^{-1} K^{-1}) and T is the temperature in Kelvin.

Combining Equations (5) and (6), the free energy of formation of ettringite is given by:

(7)

$$\Delta G°_{f,298,ettringite} = 6\Delta G°_{f,298}(Ca^{2+}) + 2\Delta G°_{f,298}(Al(OH)_4^-) + 3\Delta G°_{f,298}(SO_4^{2-}) + 4\Delta G°_{f,298}(OH^-) + 26\Delta G°_{f,298}(H_2O) + RT \ln K_{SP}$$

We calculated $\Delta G°_{r,298,ettringite} = 256 \pm 1.8$ kJ mol^{-1} using Equation (6) and $\Delta G°_{f,298,ettringite} = -15211 \pm 1.8$ kJ mol^{-1} using Equation (7) and the free energies of formation of the individual ions presented in Table 2-9. The error is the uncertainty associated with the K_{SP} value only. An error of 18.5 kJ mol^{-1} is calculated if the maximum possible errors associated with the free energies of the individual ions (Table 2-9) are included.

The calculated log IAPs increase with increasing temperature, ranging from –47.2 at 5°C to –39.7 at 75°C (Table 2-8). Thus, a positive enthalpy of reaction, $\Delta H°_r$, for the dissolution of ettringite is indicated. The dependence of log IAP on the inverse of the temperature (Figure 2-6) appears to be linear ($r^2 = 0.9831$), suggesting that the enthalpy of reaction, $\Delta H°_r$, is constant over the temperature range 5 – 75°C. The log K_{SP} values calculated using the linear regression coefficients (Figure 2-6) were within one standard error of the measured K_{SP} values. The $K_{SP}(T)$ can be written as

(8)

$$\log Ksp = \left(\frac{A}{T}\right) + B$$

where A = $-\Delta H°_r / (\ln(10)R)$ and B = $\Delta S°_r / (\ln(10)R)$. Using Equation (8) and the slope (-10700 ±620 K) of the fitted data (Fig. 2-6), the enthalpy of reaction, $\Delta H°_r$, was calculated to be 205 ±12 kJ mol^{-1}. The entropy of reaction, $\Delta S°_r$, was calculated from the intercept (-8.9 ±1.9) to be -170 ±38 J mol^{-1} K^{-1}. The errors are based on the standard errors of the regressed slope and intercept. A positive enthalpy of dissolution is to be expected given the degree of hydration of ettringite.

The temperature-dependent data were also fitted to a constant heat capacity model (Nordstrom and Munoz, 1994):

(9)

$$\log Ksp = A - \frac{B}{T} + D\log T$$

The resulting coefficients are non-unique and have dependencies which approach unity (>0.999), indicating that the equation is over-parameterized. Corresponding errors, which typically exceed the coefficients by one or more orders of magnitude, particularly for A and D, imply that the coefficients are not significantly different than zero and that the model is therefore inappropriate for our solubility data. Therefore, a constant enthalpy model would appear to best represent the temperature dependence of the log K_{SP} over the temperature range measured.

Using the data in Table 2-9 and equations for $\Delta H°_f$, $\Delta S°$, and $\Delta C°_P$ analogous to Equation (5), and assuming $\Delta C°_{P,r} = 0$, we calculated the enthalpy of formation and entropy and heat capacity for ettringite to be $\Delta H°_{f,ettringite}$ = -17550 ±16 kJ mol^{-1}, $\Delta S°_{ettringite}$ = 1867 ±59 J mol^{-1} K^{-1}, and $\Delta C°_{P,ettringite}$ = 592 ±143 J mol^{-1} K^{-1}. The errors are based on the errors calculated for the dissolution reaction parameters and the maximum calculated errors associated with individual ions. The $\Delta H°_{f,ettringite}$ and $\Delta S°_{ettringite}$ values are within two standard deviations of the values of –17539 kJ mol^{-1} and 1861.6 J mol^{-1} K^{-1} listed by Wagman et al.(1982) and Viellard and Rassineux (1992).

Reported values of $K_{SP,ettringite}$ range over 10 orders of magnitude. Factors contributing to this wide range of values include CO_2 contamination, estimation of ionic concentrations based on the electroneutrality equation, and analytical error. We have made a substantial effort to eliminate CO_2 contamination. In addition, the data set we have presented here is complete, precise, and has relatively small charge balance errors. Therefore, we are confident that our results represent the best available solubility data and that the reported thermodynamic parameters can be used to reliably model ettringite solubility over a wide range of environmentally relevant conditions.

Table 2-9. Relevant thermodynamic data.

	kJ mol^{-1}		J mol^{-1} K^{-1}		
Species	**$\Delta G°_f$**	**$\Delta H°_f$**	**$\Delta S°_f$**	**$\Delta C°_{P,f}$**	**Reference**
H_2O_{liquid}	-237.14 ±0.04	-285.830 ±0.04	69.95±0.03	75.351±0.08	1
OH^-	-157.300 ±2.0	-230.02 ±0.6	-10.7 ±1.9	-137.2 ±16.7	2
Ca^{2+}	-552.790 ±2.0	-543 ±0.6	-56.48 ±1.9	-31.5 ±16.7	2
$CaOH^-$	-716.700 ±2.0	-751.4 ±0.6	28 ±1.9	5.9 ±016.7	2
$CaSO_{4(aq)}$	-1309.300	-1447	20.	-100	3
SO_4^{2-}	-744.460 ±2.0	-909.6 ±0.6	19 ±1.9	-269.4 ±16.7	2
Al^{3+}	-487.7 ±1.5	-540.9 ±4.1	-346 ±10	-120 ±12	4
$AlOH^{2+}$	-696.5 ±2.0	-771 ±5.0	-185 ±15	-44	4
$Al(OH)^{2+}$	-904.3	-990	11.95	-194	4
$Al(OH)_3^0$	-1104	-1222	--	--	4
$Al(OH)_4^-$	-1305 ±2.0	-1502.8 ±1.6	101.5 ±10	89.6 ±12	4
Ettringite	-15211 ±19	-17550 ±12	1460 ±59	590 ±143	5

1): Cox et al., 1989
2): Shock et al., 1997*;
3): Sverjensky et al., 1997;
4): Nordstrom and May, 1996;
5): Current Study
*: Uncertainties are based on maximum values reported by Shock and Helgeson (1988) over the temperature range of 0 to

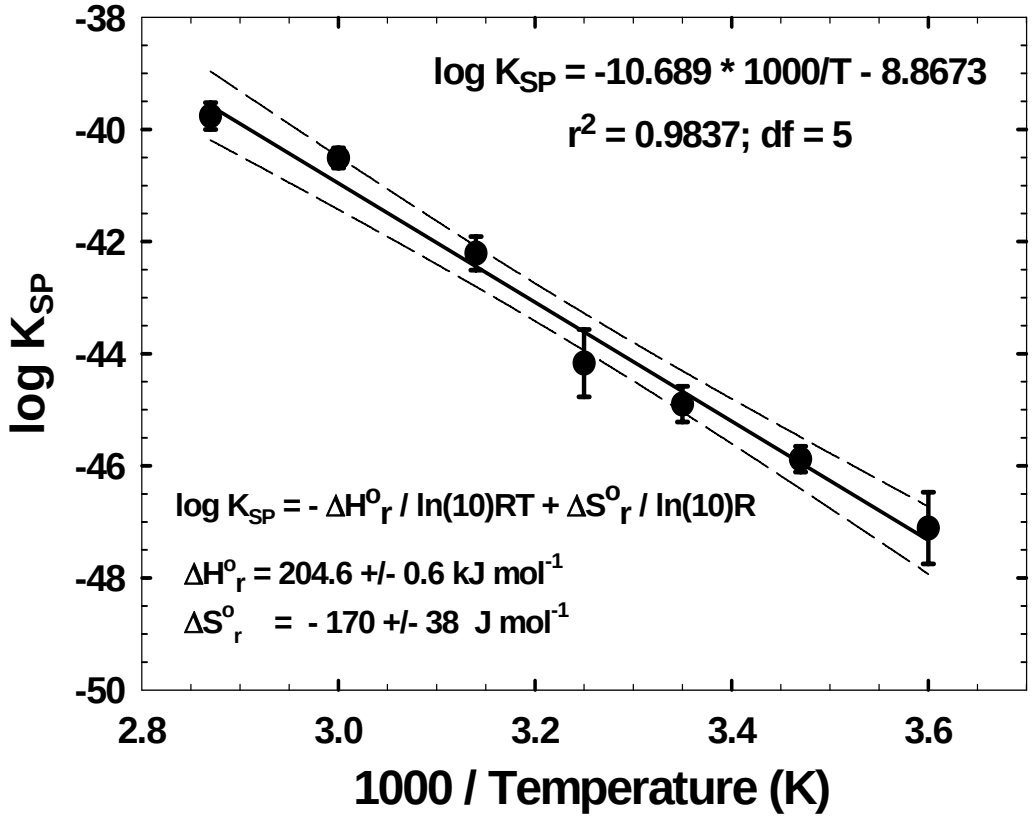

Figure 2-6. Calculated ettringite log K_{SP} values versus inverse temperature. Dashed lines represent 95% confidence intervals.

2.6 SUMMARY

The solubility, free energies of reaction and formation, as well as enthalpies and entropies for a synthetic ettringite were determined from a set of dissolution and precipitation experiments conducted over the temperature range from 5 to 75°C. Our calculated log $K_{SP,298,ettringite}$ of –44.9 ±0.32 is in excellent agreement with values calculated from the data of Warren and Reardon (1994) and Myeni et al. (1998)

although lower than the values reported by or recalculated from other studies (Atkins et al., 1992;1991; Damidot et al., 1992; Ghorab et al., 1998; Jones, 1944a; 1944b, 1944c). Based on the calculated K_{SP} and available thermodynamic data for the constituent ions, the free energy of formation, $\Delta G°_{f,298,ettringite}$, was determined to be -15211 ± 18.5 kJ mol^{-1}.

The K_{SP} values calculated for ettringite via the reaction presented in Equation (1) differ by seven orders of magnitude over the temperature range 5 to 75°C. The log K_{SP} decrease linearly with T^{-1} indicating a constant, positive enthalpy of reaction over this temperature range. A $\Delta H°_r$ of 205 ± 12 kJ mol^{-1} was calculated from the temperature dependent data and a $\Delta H°_f$ of -17550 ± 16 kJ mol^{-1} was obtained from this value and enthalpy data for individual ions gathered from available literature. This value of $\Delta H°_f$ is within one standard deviation of the value of -17539 kJ mol^{-1} listed by Wagman et al. (1982). $\Delta S°_{ettringite}$ and $\Delta C°_{P,ettringite}$ are 1867 ± 59 and 590 ± 143 J mol^{-1} K^{-1}, respectively.

Chapter 3. Solubility of Bentorite ($Ca_6[Cr(OH)_6]_2(SO_4)_3 \cdot 26H_2O$)

3.1 INTRODUCTION

Bentorite is a hydrous calcium chromium-sulfate mineral represented by the formula $Ca_6[Cr(OH)_6]_2(SO_4)_3 \cdot 26H_2O$. This mineral, first identified by Gross (1980), typically occurs as a secondary, low-temperature vein mineral associated with calcite, jennite, and tobermorite, as, for example, in its type location in Israel marble deposits. The name bentorite applies to a mineral having an ettringite structure with $Cr^{3+} > Al^{3+}$. A pure Cr^{3+} solid phase having an ettringite structure was synthesized by Bensted and Varma (1971) as part of an investigation of ettringite and its derivatives.

Bentorite is a member of the ettringite group of minerals described by the general formula $Ca_6[X_3(OH)_6]_2(Y)_3 \cdot 26H_2O$, where X represents a site occupied by trivalent metals such as Al^{3+}, Fe^{3+}, or Cr^{3+} and Y represents a site occupied by oxyanions such as SO_4^{2-}, CO_3^{2-}, SeO_4^{2-}, or CrO_4^{2-} (Dunn et al., 1983; Hassett et al., 1990; Poellman et al., 1993; Poellmann et al., 1990). Substitution of trivalent chromium in ettringite is of interest because chromium is a widespread pollutant that may be acutely toxic, teratogenic, mutagenic, and carcinogenic (Nieboer and Shaw, 1988; Nordberg, 1988; O'Brien and Kortenkamp, 1994; Sugiyama, 1994).

The concentration of chromium in alkaline solutions is typically assumed to be controlled by dissolution / precipitation of $Cr(OH)_3$ (Richard and Bourg, 1991). However, Kindness et al. (1994) suggests that the controlling phase in cement systems is likely a calcium aluminate phase (e.g., hydrogarnet) in which chromium is

substituted for aluminum. Solubility data for calcium aluminate phases are scarce or nonexistent.

Ettringite is an important product resulting from the hydration of Portland-type cements. The natural occurrence of bentorite clearly demonstrates the ability of ettringite to incorporate Cr(III). Therefore, knowledge of the solubility of ettringite and bentorite are required in evaluating potential controls of aqueous Cr(III) concentrations in cement and other alkaline systems.

Addition of Cr(III) to cement blends has also been shown to increase the compressive strength of neat cements (Zamorani et al., 1988). The formation of ettringite is an important factor in cement strength and durability, often associated with weakening of cementitous materials through its role in “sulfate swelling” (Höglund, 1992).

However, other research has shown that ettringite crystals may play a role in increasing early mechanical strength of cements (Teramato and Koie, 1976). Significant changes in the solubility of ettringite due to Cr(III) substitution could therefore alter the strength and long-term durability of cementitous materials.

Understanding and evaluation of the role of the Cr(III) analog of ettringite in these processes could be facilitated by knowledge of its thermodynamic properties. However, we were unable to locate thermodynamic data for this phase.

The objective of this study is to measure the solubility of bentorite and to determine its solubility product (K_{SP}) and thermodynamic properties. The results of this study should be useful to workers dealing with chromium migration and waste

immobilization in alkaline environments as well as to material scientists developing new cements.

3.2 METHODS

3.2.1. Synthesis of Bentorite

Bentorite was synthesized by mixing suspensions of $Ca(OH)_2$ and $Cr_2(SO4)_3$ at appropriate stoichiometries (30.6 and 5.1 mmoles, respectively). Several batches were required to complete all the experiments. The pH of the chromium sulfate solution was initially raised to approximately 12.3 with NaOH to induce dissolution. However, some portion of the solid remained even after stirring for 24 hours at 60°C. All mixing was performed in high-density polyethylene (HDPE) bottles using Teflon-coated magnetic stir bars. Type I reagent water used in preparation of the suspensions was first degassed by purging with nitrogen gas for 30 minutes and the suspensions prepared and mixed in an N_2-filled glove box in which the atmosphere was continuously bubbled through 1M NaOH to minimize CO_2 contamination. The reactants were mixed for one week at 25°C. The resulting suspension was then transferred, still under a N_2 atmosphere, to a polyethylene filter funnel and rapidly vacuum-filtered through a 7-cm diameter, 1.6μm filter to separate the solid precipitate. The precipitate was subsequently dried, crushed to a fine powder, and stored at room temperature under an N_2-atmosphere.

3.2.2. Characterization of Synthetic Bentorite

The synthetic material was characterized using a variety of methods. X-ray diffraction (XRD) analyses, utilizing CuKα radiation were performed on the initial batch using a Norelco XRG 3000 unit while a Phillips X'Pert MPD with a solid state detector was used for the second batch. Qualitative chemistries were also obtained for the first batch with a LINK energy dispersive X-ray spectrometer (EDX) using a 31-mm working distance with an accelerating voltage of 20kV. Replicate portions of both synthesized solids were digested in HNO_3 and analyzed to quantify the stoichiometry of the material. Total calcium concentrations were measured by atomic absorption spectroscopy (AAS) and total chromium by graphite-furnace atomic absorption (GFAA) using a Perkin-Elmer Analyst 300 AA spectrophotometer and HGA-800 graphite furnace with auto-sampler. A lanthanum matrix modifier was used during calcium analyses. A hydrogen peroxide solution was used to oxidize all chromium to Cr(VI) and a $Mg(NO_3)_2$-matrix modifier was used during chromium GFAA analyses. Total sulfate concentrations were determined by high-performance liquid chromatography (HPLC). A Dionex 2010 HPLC unit, equipped with an Ionpac AS11 4 X 250-mm analytical column, a guard column, a Dionex anion self-regenerating suppressor, and conductivity detector was used for sulfate analyses. NaOH solutions of various strengths between 10 and 21 mM were used as eluent.

The amount of water in the synthesized material was determined by thermogravimetric analyses (TGA) using a Perkin-Elmer TGA7 thermogravimetric

analyzer. The TGA analyses were conducted on 3 to 6 mg of sample over a temperature range of 40 to 900ºC at a rate of 10ºC/minute.

3.2.3. Dissolution and Precipitation Experiments

An initial set of dissolution experiments was conducted at 25°C at different initial pH levels between 10.9 and 12.0. The experiments were conducted by placing 0.10 g of the synthesized solid in 30ml HDPE bottles along with a magnetic stir bar. The bottles were subsequently filled under N_2 with ultrapure water that had been purged with N_2 and adjusted to the desired pH with NaOH. As an additional precaution against CO_2 contamination, the capped HDPE bottles were sealed within N_2-filled glass mason jars. The jarred sample bottles were then placed in circulating water-baths to maintain the temperature within 0.4^{o}C of the desired value and mixed with magnetic stirrers. Because of the small volumes of water used in these experiments, an additional experiment using 120 ml of water was conducted in duplicate so that the aqueous solutions could be temporally sampled to determine the time required to achieve steady-state conditions.

All sampling was conducted in an N_2-filled glove box. The jarred bottles were transferred to the glove box in portable water baths and quickly processed to maintain the desired temperatures. Approximately 10 ml of suspension was withdrawn for each sample. The samples were filtered using 0.45-μm polysulfone membrane filters. Separate cation and anion subsamples were prepared using a 5ml/liter solution of concentrated HNO_3 to dilute and preserve the cation samples at pH < 2. Anion samples were diluted with ultrapure water and stored in HDPE vials.

Measurements of pH were made at the time of sampling using an Orion Model 290A portable pH meter and Orion Model 9157BN-triode pH electrode. The pH meter was calibrated using at least three buffers (pHydrion® 7.00, 10.00, 11.00 and / or 12.00 pH). Although a slight reduction in the electrode response slope (e.g., ~ 3 mV/pH) was noted over the higher pH interval, the meter utilizes the slope of the interval corresponding to each measurement in order to reduce "averaging" errors. The buffers were brought to the temperature of the samples to account for temperature-dependent variations in pH and the meter adjusted to the appropriate value based on the manufacturer's temperature-dependence data. The 9157BN triode incorporates low-sodium-error glass obviating the need for alkali interference corrections at the sodium concentrations / temperature combinations encountered (e.g., corrections < 0.01 pH units). Liquid-junction potential effects were minimized by appropriate conditioning and storage of the electrode and by allowing suspended sediment to settle prior to measurements. Total Ca, Cr, and sulfate concentrations were determined using the methods described for the solid digest. A second set of dissolution experiments was carried out to verify the incongruent solution stoichiometry noted in the initial set of experiments.

Precipitation experiments were conducted by two separate methods to verify the solubilities measured by the dissolution experiments. In the first set of precipitation experiments, the suspensions remaining after sampling of the dissolution experiments were supersaturated by spiking the remaining suspension (21 ml) with 0.5 ml of 75 mM $Ca(NO_3)_2$. NO_3 concentrations were obtained by HPLC analyses.

Difficulties with pH measurements at the time of sampling required that the pH values used in subsequent calculations be obtained by minimizing the speciated charge balance error for the solutions. The second round of precipitation experiments were conducted by heating the remaining suspensions from later dissolution experiments to 45ºC for 24 hours to increase the dissolved load and then returning the samples to 25°C to equilibrate for 35 days. Other aspects of these precipitation experiments were identical to the dissolution experiments.

Temperature-dependent dissolution experiments were conducted at six additional temperatures ranging between 5 and 75°C to model the temperature dependence of bentorite solubility. These experiments were conducted in an identical manner as the 25°C dissolution experiment with water bath temperatures maintained within 0.5°C of the temperature of interest. All sampling was conducted in a nitrogen-filled glove box. The jarred bottles were transferred to the glove box in portable water baths and quickly processed to maintain the desired temperatures.

3.3 EXPERIMENTAL RESULTS

3.3.1. Solid Characterization

Examination of the XRD data for the synthesized bentorite (Table 3-1; Figure 3-1) indicate that seventeen of the twenty largest peaks have corresponding peaks listed in the JCPDS Card 33-248 for bentorite (JCPDS, 1991). The twelve peaks listed on the JCPDS card having relative intensities > 5% also match peaks in the sample diffraction patterns. Minor peaks listed in the JCPDS card may represent contaminants

as a natural sample having 0.16 mole fraction of aluminum and possibly other constituents was used for the analyses (Gross, 1980). Ten sample peaks, however, could not be immediately matched with the peaks listed in the JCPDS card.

Ettringite group minerals are in the hexagonal crystal system. Using reported Miller indices, the d-spacings from the XRD analyses of the initial synthesized material which could be matched with JCPDS Card 33-0248, and the equation for hexagonal system minerals,

(1)

$$d = \frac{\sqrt{3}ac}{\sqrt{4c^2(h^2 + hk + k^2) + 3a^2l^2}}$$

we calculated unit cell dimensions of a_0 = 11.19 ±0.01 and c_0 = 21.60 ±0.05 Å and a primitive unit cell volume of 2342.3 ±6.6 $Å^3$. Cell dimensions calculated for the second batch of synthesized bentorite were a_0 = 11.14 ±0.01 and c_0 = 21.73 ±0.07 Å with a resulting cell volume of 2335.4 ±8.5 $Å^3$. Differences in the calculated dimensions and those listed in JCPDS Card 33-0248 (11.21 and 21.48 Å) may be due to the fact that the JCPDS Card is based on analysis of a natural sample containing 0.16 mole fraction aluminum and apparently minor contaminants (e.g., 6.11 Å peak) The calculated cell volumes are, however, within one standard error of the cell volume listed in the JCPDS card (2337.6 $Å^3$).

Table 3-1. Comparison of X-ray diffraction peaks from synthetic bentorite ($Ca_6[Cr(OH)_6]_2(CrO_4)_3 \cdot 26H_2O$) with peaks from bentorite JCPDS card 33-0248.

	Synthesized Bentorite Initial Batch		Synthesized Bentorite Additional Batch		Bentorite JCPDS 33-0248		Solid Residue from B25-11.5 Dissolution Experiment	
h,k,l[a]	d(Å)	I/Imax	d(Å)	I/Imax	d(Å)	I/Imax	d(Å)	I/Imax
002	--	--			10.60	1	--	--
100	9.66	100	9.60	100	9.656	100	9.713	100
101*	8.88	13	8.89	31	--	--	--	--
#	--	--			6.110	4	--	--
103*	--	--	5.770	5	--	--	--	--
110	5.59	69	5.561	79	5.592	40	5.595	55
112	4.94	17	4.948	21	4.980	4	4.975	13
104	4.70	15	4.723	19	4.640	3	4.738	10
005*	--	--	--	--	4.290	3	--	--
203	4.02	5	4.012	10	4.030	3	--	--
114	3.88	73	3.884	77	3.890	8	3.896	39
210	--	--	--	--	3.650	6	--	--
204	3.59	27	3.603	21	3.600	10	3.615	10
212	3.45	20	3.457	27	3.470	6	3.469	15
300	3.22	21	3.218	20	3.230	10	3.228	12
116	3.02	57	3.028	14	3.020	5	3.036	35
206*	2.90	6	2.889	6	--	--	2.897	4
304	2.77	58	2.769	53	2.772	10	2.775	27
008	2.71	10	2.706	9	2.680	3	2.708	5
312	2.61	17	2.601	17	2.610	3	2.608	10
216	2.57	57	2.570	45	2.560	6	2.574	22
224	2.49	15	2.482	11	2.486	3	2.491	9
400*	2.44	8	--	--	--	--	--	--
401	--	--	2.403	17	2.410	3	2.408	9
306	--	--			2.400	3	--	--
217 / 208*	2.39	21	2.359	23	2.359	23	--	--
315*	2.28	8	--	--	--	--	2.282	7
226	2.21	50	2.210	38	2.206	8	2.213	17
322*	2.18	8	--	--	--	--	--	--
316	2.16	28	2.154	21	2.156	4	2.157	9
405*	2.11	10	2.111	9	--	--	--	--
412*	2.09	10	--	--	--	--	2.093	6
324*	2.06	9	2.053	9	--	--	2.059	4
500	1.94	20	1.934	10	1.942	20	1.937	5
502	1.91	15	1.909	5	1.908	5	1.911	4
330*	1.87	20	1.872	6	--	--	1.874	7
241*	1.83	6	--	--	--	--	--	--
422*	1.81	11	--	--	--	--	--	--
334	1.77	6	--	--	1.7660	3	-	--

[a] (hkl)s based on either JCPDS card 33-0248 or regression (*) based on listed cell dimensions. "#" indicates that peak listed in JCPDS card without corresponding (hkl); peak could not be fit to calculated cell dimensions within 0.1 angstrom and is assumed to represent a contaminant. In the case of the 2.359 angstrom peak, the first (hkl) is value listed in JCPDS card; second (hkl) value represents best fit to calculated cell volume.

Table 3-2. X-ray diffraction peaks from analyses of select experimental residues.

	Solid Residue from BP25-10.5c Dissolution Exprmt		Solid Residue from BP25-12.5 Precipitation Exprmt		Solid Residue from BP25-10.5 Precipitation Exprmt		Solid Residue from BP25-10.5b Precipitation Exprmt	
h,k,l[a]	d(Å)	I/Imax	d(Å)	I/Imax	d(Å)	I/Imax	d(Å)	I/Imax
002	--	--	10.69	18	10.71	19	--	--
100	9.71	39	9.66	100	9.68	100	9.712	21
101*	8.636	14	8.80	17	8.84	8	--	--
?	--	--	--	--	--	--	8.04	4
?	--	--	--	--	--	--	7.659	8
?	--	--	6.184	15	6.19	10	--	--
?	--	--	--	--	6.10	14	--	--
103*	--	--	--	--	--	--	--	--
110	5.598	27	5.585	84	5.587	82	5.600	17
?	--	--	--	--	5.246	3	--	--
112	4.949	12	4.964	22	4.967	20	--	--
104	--	--	4.732	10	4.738	11	--	--
005*	--	--	4.311	12	4.314	10	--	--
203	--	--	4.013	14	4.019	7	--	--
114	3.880	21	3.893	49	3.895	46	3.89	8
?	--	--	--	--	3.836	6	3.856	9
210	--	--	--	--	--	--	--	--
204	3.614	5	3.611	15	3.613	15	3.614	2
212	3.475	8	3.465	24	3.466	21	3.469	4
106*	--	--	3.356	7	3.357	3	--	--
213*	--	--	--	--	3.265	5	--	--
300	3.234	7	3.225	24	3.226	18	3.230	3
007*	--	--	3.070	9	3.072	8	3.070	9
116	3.039	100	3.030	38	3.033	17	3.037	100
206*	2.885	8	2.914	16	2.887	7	2.886	3
026*			2.848	9	2.851	7		
304	2.777	16	2.773	43	2.774	35	2.770	7
008	--	--	2.712	6	2.709	5	2.698	1
311*	--	--	2.666	7	2.666	5	--	--
312	--	--	2.606	18	2.606	12	--	--
216	2.570	9	2.573	28	2.576	25	2.568	5
224	2.493	21	2.490	21	2.517	4	2.494	16
401	--	--	2.407	17	2.406	13	Scan Discontinued	
315*	2.283	21	2.281	13	2.280	5		
226	2.212	9	2.213	26	2.212	23		
322*	--	--	--	--	2.175	5		
316	--	--	2.157	14	2.156	12		
405*	--	--	--	--	2.113	6		
412*	2.096	19	2.092	12	2.090	4		
324*	--	--	2.056	7	2.055	5		
500	--	--	1.937	9	1.935	8		
502	1.915	16	1.909	5	1.910	3		
330*	1.875	19	1.873	10	1.871	5		

[a] (hkl)s based on either JCPDS card 33-0248 or regression (*) based on listed cell dimensions. "?" indicates that peak could not be fit to calculated cell dimensions within 0.1 angstrom and is assumed to represent a secondary phase.

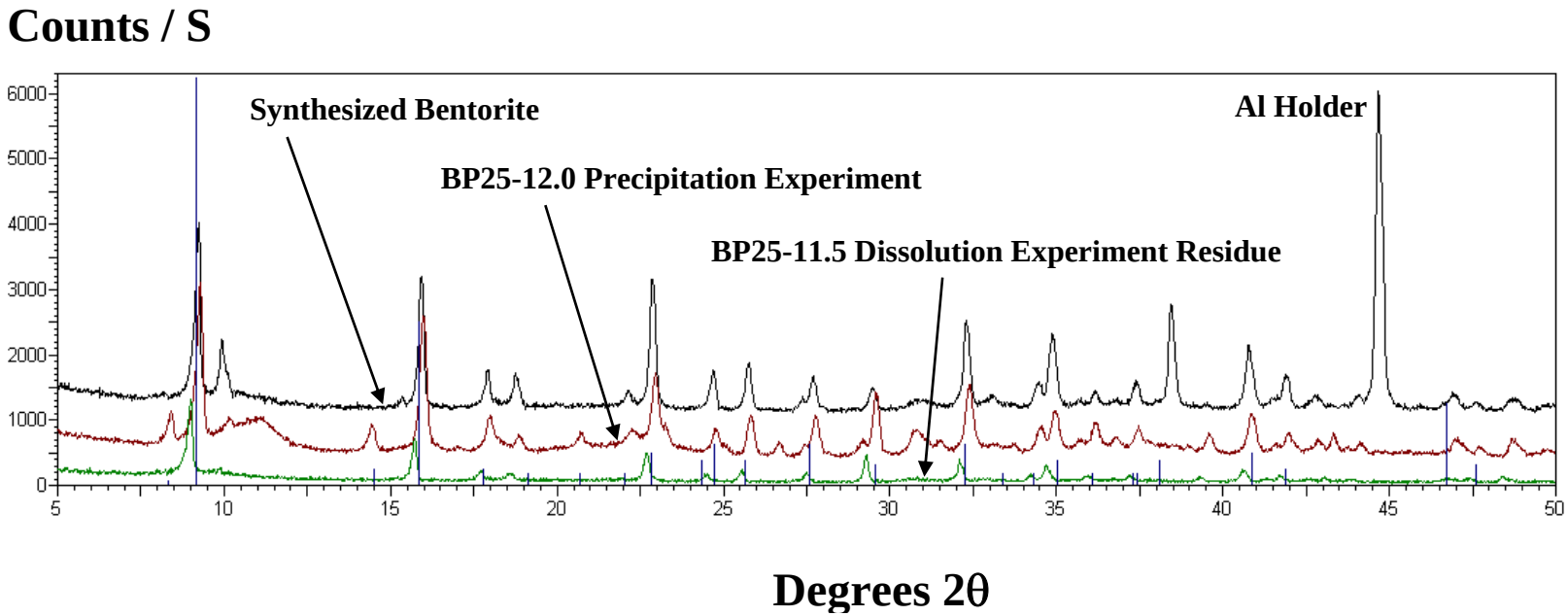

Figure 3-1. X-ray diffraction (raw data) patterns for synthesized bentorite (top), BP25-12.0 precipitation experiment residue (middle), and BP25-11.5 dissolution experiment residue (bottom; not included in Table 3-2). Peaks from bentorite JCPDS powder diffraction file 33-0248 shown as vertical lines (50x vertical exageration)

Based on the calculated cell dimensions, hkls were assigned to the peaks that could not be matched by minimizing the residual error between the measured and calculated d-spacings. The resulting residuals were at or below 0.016 Å for all peaks in both of the samples analyzed except for the 8.88 Å peak, which had a residual < 0.04 Å. Ten random EDX analyses performed on a sample of the initial synthesized solid indicated the same general composition (Ca-Cr-S), which would be expected for bentorite. Very minor peaks corresponding to Al and Si were noted along with the Au and Pd used in the sputter coating. The source of the minor Al and Si is unclear.

Solid digest analyses for the initial solid provided conflicting results. The first replicate had a $Ca:Cr:SO_4$ ratio of 6.00:2.03:3.26 normalized to the Ca molar concentration. This is reasonably close to the expected ratio of 6.00: 2.00: 3.00. However, the second replicate had a ratio of 6.00:2.86:3.28 Clearly the chromium concentration is significantly higher than expected for bentorite. Analyses of an additional batch of synthesized solid resulted in a $Ca:Cr:SO_4$ ratio of 6.00:2.69±0.01:3.01±0.06 normalized to the Ca molar concentrations. Again, although the $Ca:SO_4$ ratios are near ideal, the data indicate higher than expected chromium concentrations. This discrepancy could be explained by the presence of five to six (weight) percent of $Cr(OH)_3$.

Thermogravimetric analyses indicated that mass loss occurs over three distinct temperature intervals (Figure 3-2). Variations of up to 3% within a given range were noted in replicate analyses and in analyses of the different samples. These variations

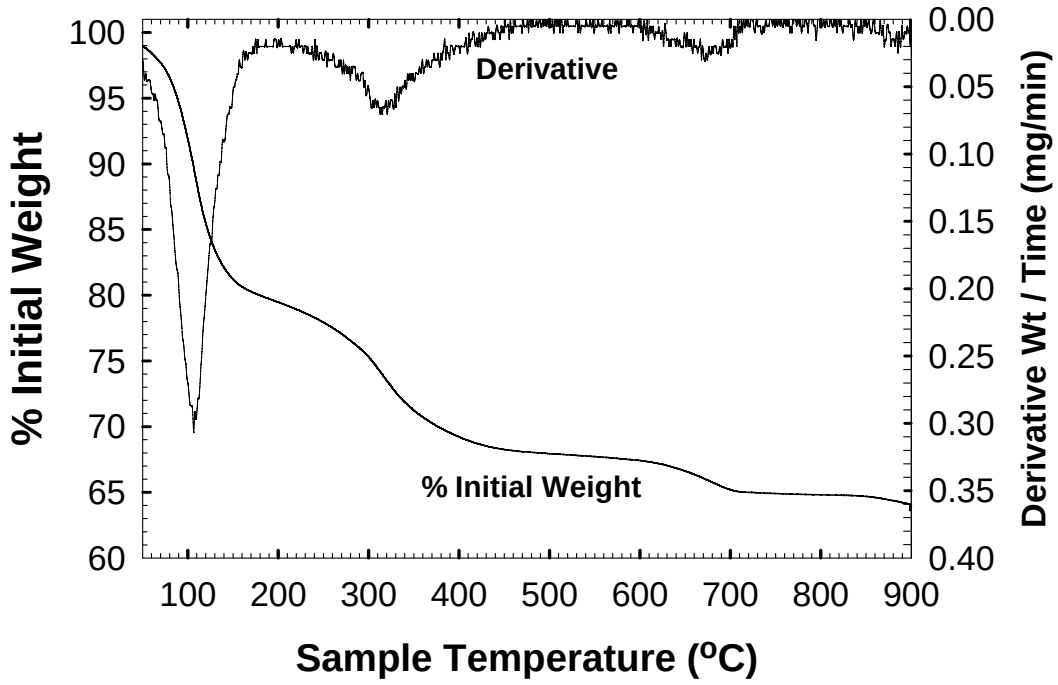

Figure 3-2. Thermogravimetric analyses of bentorite. A 10°C/minute heating rate was used in heating the sample from 40 to 900°C.

may be due to variations in loosely bound water from changes in room humidity or setup time after removal of the samples from the glovebox or they may be due to the presence of impurities. Most of the loss occurred between 40 - 180°C, the range at which loosely bound water would be expected to be lost. The 25 to 28% mass loss over this interval corresponds to approximately 19 or 20 water molecules based on a gram formula weight of 1305 for $Ca_6[Cr(OH)_6]_2(SO_4)_3 \cdot 26H_2O$. An additional mass

loss of 10 to 13% occurs between 180 and 530^{o}C (an inflection point) and may be explained as the mass loss of eight or nine water molecules. Additional mass loss occurred over the temperature interval from 530 to 750^{o}C although a minor loss was noted near 900^{o}C in some samples. Total losses varied between 38 and 40%, correlating approximately with 28 or 29 waters of hydration. The higher limit is nearly identical to the expected mass loss if pure bentorite were converted to 3 moles of calcium sulfate, 3 moles of calcium oxide, and 2 moles of chromium hydroxide. The lower value is very near the mass loss that would result if the initial solid contained 5% by weight of $Cr(OH)_3$, as suggested by the solid digest, and the end product contained 3 moles of calcium hydroxide rather than calcium oxide. The apparent stability of the chromium hydroxide at 900^{o}C is in contrast to the TGA data obtained for ettringite which indicated a breakdown of the corresponding aluminum hydroxide (Perkins and Palmer, 1999).

Based on the sum of these analyses, the synthesized solid appears to be bentorite. However, the characterization data suggests the presence of minor amounts (<6%) of $Cr(OH)_3$ and possibly traces of Al and Si.

3.3.2. Dissolution and Precipitation Experiments

Examination of the measured concentration data (Tables 3-2 and 3-3) clearly indicates that dissolution is not congruent. Chromium concentrations, in particular, are generally two orders of magnitude lower than would be expected with congruent dissolution. This can be explained only by the formation of a secondary solid phase.

$Cr(OH)_3$, suspected of being present in the initial synthesized material, has a

very low solubility and is a reasonable candidate. $Cr(OH)_3$ may precipitate as an amorphous, crystalline, or pseudo-crystalline solid. Saturation indices calculated using MINTEQA2 show the experimental suspensions near saturation or slightly oversaturated (-0.5 to +1) with respect to either or both crystalline or amorphous $Cr(OH)_3$. Several of the major XRD peaks (i.e., ~4.9, 4.6Å) listed for $Cr(OH)_3$ or $Cr(OH)_3 \cdot 3H_2O$ in JCPDS cards 12-0241 and 16-0817 were not observed in XRD patterns obtained for the initial synthesized solid or experimental residues. Amorphous $Cr(OH)_3$ would not be detected in the solid phase by standard X-ray diffraction methods.

The calcium to sulfate ratios are also significantly lower than would be expected from congruent dissolution, suggesting the formation of an additional, calcium-bearing, solid phase. Saturation indices for calcium-bearing phases common to alkaline conditions such as portlandite and gypsum clearly show that the solutions are well below saturation with respect to these minerals and there are no XRD peaks in the diffraction pattern of residues (Table 3-1-b) which are common to these phases. The approximate $Ca:SO_4$ ratios of 1.5:1 to 1:1 observed for many of the dissolution samples does not fit the formation of a Cr(III) analog of monosulfate ($3CaO \cdot Al2O3 \cdot CaSO4 \cdot nH2O$), unless other unidentified solids are also present. The measured diffraction patterns also lack major peaks associated with such a monosulfate phase (e.g., JCPDS 45-0566).

The low chromium concentrations (< 0.1 ppm) are consistent with the data reported by Kindness et al. (1994) in experiments where they placed synthesized

ettringite in chromium nitrate solutions (100 ppm Cr(III)). XRD, SEM, and EDX analyses of the resulting solids showed that Cr(III)-substitution in various calcium aluminate hydrates was an important factor in limiting chromium concentrations. They reported that the most important phases were $Ca_2Al_2O_5 \cdot 6 \cdot 8H_2O$, $Ca_2Al(OH)_7 \cdot 3H_2O$, and $3CaO \cdot Al_2O_3 \cdot 6H_2O$ (hydrogarnet), but that other, less-characterized phases were also present.

Changes in ion concentrations over time in the initial dissolution experiment at 25^{o}C and initial pH of 11.36 are variable (Figure 3-3). This is consistent with the presence of secondary phases. Calcium concentrations appear to reach steady state by 150 hours. However, chromium concentrations continued to increase for the duration of the time-series experiment. This would be consistent with dissolution of minor amounts of $Cr(OH)_3$ following equilibrium with a $3CaO \cdot Cr_2O_3 \cdot 6H_2O$ phase. Sulfate concentrations were not measured but calculated by minimizing the charge balance errors given the pH and calcium, chromium, and sodium concentrations. Unfortunately, the 120-ml sample was exhausted before steady-state conditions with respect to the chromium concentrations were achieved.

The duration of preliminary dissolution experiments were based on the apparent steady state conditions of calcium and prior to completion of the chromium analyses for the initial time series samples. The duration of these initial dissolution experiments (22 days) may have been insufficient for equilibrium to be achieved. Therefore, additional dissolution experiments were conducted with sampling occurring after 48 and 56 days of mixing, to verify the results.

Analyte concentrations varied significantly with pH (Table 3-3). In general, Ca concentrations were lowest at the highest pH, dropping dramatically near pH 12. Saturation indices calculated with MINTEQA2 software indicated that all of the suspension solutions were undersaturated with respect to portlandite. Sulfate and Cr concentrations tended to increase with pH and were less variable overall than Ca.

Analyte concentrations generally increased with temperature within a given pH range (Table 3-4). Maximum Ca concentrations (> 2mM) occurred at 45ºC while maximum SO_4 concentrations (>4.5 mM) occurred at 60ºC. Cr concentrations continued to rise with temperature, with the highest concentrations (~0.05 mM) measured in the 75ºC samples.

3.4 DISCUSSION

The incongruent dissolution and solution stoichiometries imply that bentorite does not directly control Cr(III) concentrations. Therefore, identification of the precipitate(s) responsible for the lower than expected Cr(III) concentrations is an important consideration.

Several peaks observed in XRD patterns for synthesized solids or experimental residues but which were not listed in JCPDS card 33-0248 for bentorite are similar to theoretical peaks calculated for hydrogarnet (JCPDS cards 71-0735 and 84-1353). These include peaks at ~3.35, 2.85, 2.25, 2.05 and 1.85Å. However, some of the reported peaks with the highest relative intensities were not observed in the XRD patterns (e.g., 5.13, 4.44, 3.14 Å). Therefore, it is unlikely that a Cr(III) analog of hydrogarnet is present. The ~10.7 Å peak noted in the XRD patterns for the

precipitation sample residues correspond to the major peak listed for $Ca_2Al_2O_5 \cdot 8H_2O$ in JCPDS card 45-0564. The peak at ~10.7 Å and a minor peak at ~5.25 Å also correspond to major peaks listed for $CaO \cdot Cr_2O_3 \cdot Ca(OH)_2 \cdot 18H_2O$ in JCPDS Card 42-0487.

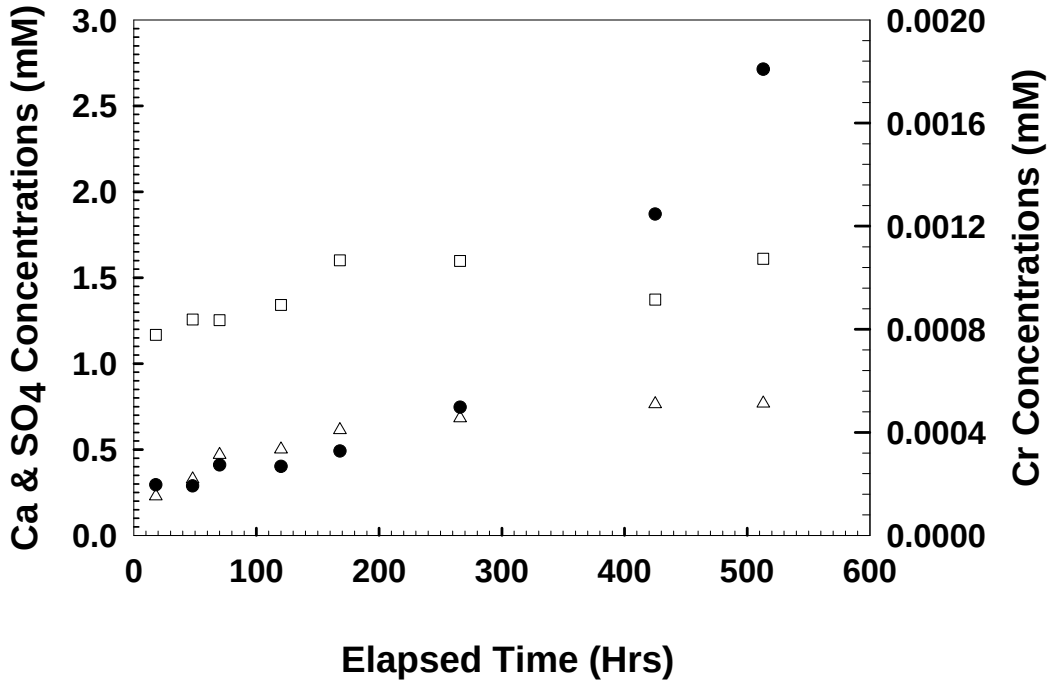

Figure 3-3. Measured calcium (◦), sulfate (Δ), and chromium (ℓ) concentrations over time for bentorite dissolution experiment conducted at 25°C and initial pH of 11.36

Table 3-3. Final concentrations in bentorite dissolution / precipitation experiments conducted at 25ºC.

Sample Batch	No of Reps	Meas. pH	(Ca) mmol L^{-1}	(Cr) mmol L^{-1}	(SO_4) mmol L^{-1}	(Na) mmol L^{-1}	Exprmnt Duration
Initial 25°C Dissolution Experiments							
B25-10.5	3	10.97 ± 0.11	0.87 ± 0.12	0.00106 ± 0.00022	0.992 ± 0.074	0.4506 ± 0.001	22 days
B25-11.0	3	11.132 ± .054	0.68 ± 0.26	0.00071 ± 0.00013	0.9403 ± 0.0010	2.046 ± 0.099	22 days
B25-12.0	3	11.950 ± .013	0.278 ± 0.017	0.00147 ± 0.00015	1.12 ± 0.11	17.428 ± 0.041	22 days
Additional 25°C Dissolution Experiment							
B25-10.5b	3	--	0.93 ± 0.08	0.000387 ±0.000040	0.91 ± 0.06	0.48 ± 0.01	56 days
B25-11.5	3	--	1.06 ± 0.21	0.00053 ± 0.00013	1.00 ± 0.03	3.12 ± 0.07	56 days
B25-12.5	3	--	0.090 ± 0.002	0.000987 ± 0.00008	1.61 ± 0.04	29.80 ± 0.34	56 days
B25-10.0	3	10.312± 0.002	1.81 ± 0.011	0.00168 ± 0.00006	1.676 ± 0.0014	0.081 ± 0.001	48 days
B25-10.5c	3	10.423± 0.086	1.45 ± 0.18	0.00133 ± 0.00010	1.371 ± 0.0022	0.0365 ± 0.001	48 days
25°C Precipitation Experiment							
BP25-10.5	3	--	3.38 ± 0.10	0.00044 ± 0.00007	0.951 ± 0.053	0.475 ± 0.009	56 days
BP25-11.5	3	--	2.840 ± 0.067	0.00065 ± 0.00014	0.826 ± 0.035	3.16 ± 0.10	56 days
BP25-12.5	3	--	0.160 ± 0.007	0.00149 ± 0.00007	2.143 ± 0.053	30.88 ± 0.31	56 days
BP25-10.0	3	10.322± 0.061	2.039 ± 0.0033	0.00069 ± 0.0016	2.04 ± 0.37	0.0657 ± 0.0052	35 days
BP25-10.5b	3	10.638± 0.115	1.33 ± 0.13	0.00107 ± 0.00075	1.26 ± 0.16	0.0309 ± 0.0045	35 days
Synthesis Liquor: Matured							
Bliq1028	2	11.317	1.565 ± 0.0319	0.00070 ± 0.00013	0.851 ± 0.026	0.2079 ± 0.0045	65 days

Table 3-4. Final concentrations in temperature-dependent bentorite dissolution experiments.

Sample Batch	Temp (°C)	No of Reps	Meas pH	(Ca) mmol L^{-1}	(Cr) mmol L^{-1}	(SO_4) mmol L^{-1}	(Na) mmol L^{-1}	Length of Expmt
B5-	5	3	11.438	1.240	0.000270	1.00	0.411	35 days
10.5			±0.021	± 0.138	± .000069	± 0.16	± 0.002	
B5-	5	3	12.912	0.471	0.000348	0.881	12.778	35 days
12.0			±0.028	± 0.033	± .000068	± 0.098	± 0.0028	
B15-	15	3	11.146	1.125	0.00039	0.744	0.412	16 days
10.5			±0.044	± 0.076	± 0.00022	± 0.085	± 0.016	
B15-	15	3	11.86	0662	0.00070	0.824	4.175	16 days
11.5			±0.003	± 0.068	± 0.00014	± 0.028	± 0.024	
B35-	35	3	10.809	1.49	0.00117	1.203	0.4015	13 days
10.5			±0.065	± 0.24	± 0.00011	± 0.166	± 0.036	
B35-	35	3	10.983	1.308	0.000742	1.12	1.136	13 days
11.0			± .032	±0.097	±0.000044	± 0.19	± 0.029	
B35-	35	3	11.349	1.282	0.00111	1.357	3.73	13 days
11.5			±0.004	± 0.024	± 0000086	± 0.081	±0.23	
B45-	45	3	11.043	2.087	0.00744	1.683	4.087	30 days
11.5			±0 .01	± 0.029	± 0.0011	± 0.025	±0.13	
B45-	45	3	10.66	2.41	0.0058	1.60	1.58	30 days
12.0			± 0.16	± 0.23	± 0.0014	± 0.29	±0.15	
B60-	60	2	10.428	1.744	0.0024	0.96	0.428	20 days
10.5			±0.019	± 0.092	± 0.0022	± 0.12	±0.017	
B60-	60	2	10.459	0.735	0.0098	4.50	3.97	20 days
11.0			±0.085	± 0.020	± 0.0017	± 0.11	±0.18	
B75-	75	2	9.796	0.224	0.02.80	1.1945	4.70	20 days
11.0			±0.080	± 0.033	± 0.00093	± 0.0092	±0.89	
B75-	75	3	10.618	0.0579	0.0473	1.370	13.58	20 days
12.0			±0.011	± 0.0033	± 0.0071	± 0.041	± 0.34	

Mass balance calculations were carried out using concentrations of Ca, SO_4, and Cr and stoichiometries of bentorite, $Cr(OH)_3$, and either $Ca_2Cr_2O_5 \cdot 8H_2O$, $Ca_2Cr(OH)_7 \cdot 3H_2O$, $3CaO \cdot Cr_2O_3 \cdot 6H_2O$, or $3CaO \cdot Cr_2O_3 \cdot Ca(OH)_2 \cdot 18H_2O$. These calculations indicate that precipitation of approximately one mole of $3CaO \cdot Cr_2O_3 \cdot 6H_2O$ for each mole of bentorite dissolved is consistent with the observed aqueous compositions of samples at pH < 12. This scenario requires either dissolution or precipitation of minor amounts of $Cr(OH)_3$, suggesting near-saturation

with respect to this phase which is consistent with the calculated saturation indices. The mass balance calculations also suggest that precipitation of 1.5 to 2 moles of $Ca_2Cr_2O_5 \cdot 8H_2O$ per mole of dissolved bentorite is also feasible assuming dissolution of an equal or greater number of moles of $Cr(OH)_3$ than bentorite. The mass of dissolved $Cr(OH)_3$ required is still small (<15% of bulk dissolved material) in comparison to bentorite because of the large difference in molecular weights. The mass balance calculations indicate that precipitation of ~ 1 mole of either $3CaOCr_2O_3 \cdot Ca(OH)_2 \cdot 18H_2O$ or $Ca_2Cr(OH)_7 \cdot 3H_2O$ per mole of dissolved bentorite is likewise feasible with respect to the measured stoichiometries assuming precipitation of $Cr(OH)_3$.

Aqueous activities for Ca^{2+}, $Cr(OH)_4^-$, and SO_4^{2-} as well as Na^+ and NO_3^- were calculated with the geochemical speciation model MINTEQA2 (Allison et al., 1990) using the Davies Equation:

(2)

$$\log \gamma_i = -AZ_i^2 \left(\frac{\sqrt{I}}{1+\sqrt{I}} - 0.24I \right)$$

The databases used by MINTEQA2 were first modified to include pertinent, updated thermodynamic data from available literature (Table 3-5).

Log ion activity products calculated for the reaction:

(3)

$$Ca_2Cr_2O_5 \cdot 8H_2O \rightleftharpoons 2Ca^{2+} + 2Cr(OH)_4^- + 2OH^- + 3H_2O$$

resulted in a mean value of –24.29 ±0.69 based on all of the samples (Table 3-6). The standard error is much lower than that calculated for mean log ion activity products obtained from similarly-written dissolution reactions for $3CaO{\cdot}Cr_2O_3{\cdot}6H_2O$ (-33.28 ±1.81), $3CaOCr_2O_3{\cdot}Ca(OH)_2{\cdot}18H_2O$ (-42.28 ±3.04), $Ca_2Cr(OH)_7{\cdot}3H_2O$ (-20.97 ±1.31). or $Cr(OH)_3$ (3.15 ±1.05). The consistency of the log ion activity product value obtained for $Ca_2Cr_2O_5{\cdot}8H_2O$ strongly suggests that this phase is present and is at equilibrium with the experimental solutions.

We therefore conclude that the low levels of Cr and Ca (relative to SO_4) observed in the experiments are due primarily to precipitation of $Ca_2Cr_2O_5{\cdot}8H_2O$. This phase or other calcium chromium hydrates or hydroxides which may be present may be poorly crystalline and have peaks with d-spacings very similar to bentorite which makes identification difficult using only XRD.

Table 3-5. Thermodynamic data for aqueous species reactions used to update MINTEQA2.

	kJ/mol		J/mol·K			
Reactions	**ΔG°r**	**ΔH°r**	**ΔSr**	**ΔC_p**	**Log KSP**	**Source**
$H_2O - H^+ = OH^-$	79.58	55.81	-80.66	-212.5	-13.99	1, 2
$Ca^{2+} + H_2O - H^+ = CaOH^+$	73.22	77.47	14.6	-38.0	-12.82	1, 2
$Ca^{2+} + SO_4^{2-} = CaSO4^o$	-12.05	5.44	58.6	196	2.11	2, 3
$Cr(OH)^{2+} + H_20 - H^+ = Cr(OH)_3^o$	47.6	67.0	65	-104	-8.34	1,2
$Cr(OH)^{2+} + 2H_2O - 2H^+ = Cr(OH)_4^-$	101.2	104663	12	-33	-17.72	1,2

Multiple sources indicate sources for individual ion data that were used in calculating data presented.
1: Cox et al., 1989; 2: Shock et al., 1997; 3: Sverjensky et al., 1997.

Ion activity products (IAP) for the dissolution of bentorite were calculated from the activities using

(4)

$$Ca_6[Cr(OH)_6]_2(SO_4)_3 \cdot 26H_2O \rightleftharpoons 6Ca^{2+} + 2Cr(OH)_4^- + 3SO_4^{2-} + 4OH^- + 26H_2O$$

The log IAPs for the 25°C dissolution samples (Table 3-6) vary by 2 log units from –53.46 to –51.47. However, if the B25-11.0 sample, which has the highest IAP, is excluded, then the range drops to 0.86 log units. Student's t-tests indicate that there is no significant difference in the mean log IAP values for samples (including B25-11.0) collected at 22, 48, and 56 days at the 95% confidence level (t = <0.9; 3 - 4 degrees of freedom). This implies that equilibrium was achieved by 22 days. Our previous study of the dissolution of ettringite indicated equilibrium occurred within seven days (Perkins and Palmer, 1999).

Regression analyses of the log IAPs vs. pH for all eight dissolution samples indicated that the slope was not significantly different than zero at the 95% confidence level (t = 0.058; 7 degrees of freedom (df)). The mean log IAP value for the 25°C dissolution samples is –52.89 ±0.84 where the error given is the total standard deviation (t.s.d.) calculated from both samples and replicates.

Table 3-6. Calculated equilibrium activities and ion activity products for bentorite dissolution and precipitation experiments conducted at 25ºC.

Sample Batch	pH	Log $\{Ca^{2+}\}$	Log $\{Cr(OH)_4^-\}$	Log $\{SO_4^{2-}\}$	Log $\{OH^-\}$	Log $\{Na^+\}$	Ionic Strgth (mM)	C.B, Error (%)	(-) Log IAP
25°C Dissolution Samples, Mixed 22 days									
B25-	10.97	-3.21	-6.02	-3.19	-3.03	-3.38	4.07	-13.8	53.01
10.5	±0.11	± 0.05	±0.083	±0.029	±0.106	±0.001	±0.23	±7.0	±0.16
B25-	11.13	-3.34	-6.19	-3.18	-2.87	-2.78	4.81	4.56	53.46
11.0	±0.05	±0.12	±0.077	±0.068	±0.054	±0.086	±0.61	±0.35	±1.11
B25-	11.95	-3.85	-6.01	-3.204	-2.048	-1.82	16.40	18.24	52.91
12.0	±0.01	±0.040	±0.17	±0.032	±0.013	±0.007	±0.14	±1.66	±0.64
25°C Dissolution Samples; 1st three mixed 56 days; last two mixed 48 days.									
B25-	11.04	-3.04	-6.46	-3.21	-2.96	-3.40	4.97	--	52.63
10.5b	±0.10	± 0.06	±0.045	±0.020	±0.101	±0.042	±0.56		±0.87
B25-	11.46	-3.18	-6.33	-3.185	-2.54	-2.55	6.88	--	51.47
11.0b	±0.02	± 0.03	±0.11	±0.008	± .017	±0.010	±0.23		±0.47
B25-	12.35	-4.23	-6.08	-3.12	-1.651	-1.600	31.35	--	53.53
12.5	±004	± 0.16	±0.034	±0.013	±0.005	±0.005	± .35		±1.00
B25-	10.340	-2.932	-5.857	-2.969	-3.686	-4.137	6.48	1.82	52.96
10.0	±0.073	±0.003	±0.015	±0.004	±0.025	±0.062	±0.22	±0.69	±0.10
B25-	10.438	-3.014	-5.924	-3.038	-3.533	-4.49	5.361	+/-4.4	53.18
10.5c	±0.103	±0.052	±0.0327	±0.002	±0.069	±0.17	±0.32	±5.3	±0.03
25°C Precipitaiton Samples; Mixed 35 days.									
BP25-	11.173	-2.689	-6.417	-3.319	-2.825	-3.37	10.76	--	50.23
10.5	±0.023	±0.010	±0.065	±0.051	±0.023	±0.008	±0.32		±0.15
BP25-	11.509	-2.770	-6.247	-3.337	-2.489	-2.552	11.65	--	49.09
11.5	±0.010	±0.009	±0.098	±0.017	± .010	±0.022	±0.14		±0.10
BP25-	12.294	-4.186	-5.901	-3.00	-1.704	-2.556	33.07	--	52.75
12.5	±.008	±0.019	±0.021	±0.011	±0.008	±0.037	±0.27		±0.09
BP25-	10.341	-2.908	-6.20	-2.939	-3.665	-4.219	7.14	3.43	53.31
10.0	±0.085	±0.021	±0.14	±0.007	±0.055	±0.031	±0.10	±0.92	±0.35
BP25-	10.523	-3.047	-6.10	-3.072	-3.274	-4.567	5.32	-7.8	52.80
10.5	±0.244	±0.038	±0.33	±0.052	±0.081	±0.072	±0.30	±4.8	±0.84
Synthesis Liquor: Matured at 25°C for 65 days following mixing (56 days after separation of solids used in last round of experiments)									
Bliq-	11.317	-2.979	-6.197	-3.253	-2.681	-3.477	5.79	-7.13	50.75
1028	±0.042	±0.005	±0.081	±0.011	±0.042	±0.005	±0.21	±2.65	±0.07

The log IAPs calculated for the five precipitation samples were highly variable. The two samples in which precipitation was presumably initiated by heating of equilibrated samples yielded nearly identical log IAP values (-53.06 ±0.36) as the dissolution samples. However, the three precipitation experiments conducted by spiking with $Ca(NO_3)_2$ yielded log IAPs of -50.23, -49.09, and -52.75 with a mean value of –50.69 ±1.87. Only the last (higher pH) sample showed a significant decline in Ca concentrations from the spiked level, clearly indicating precipitation of a calcium-bearing phase. The pH values used in calculating ion activities for these samples were calculated by minimizing the charge balance errors. Due to the relatively high Ca and NO_3 concentrations, even relatively minor analytical errors could result in a correspondingly significant contribution to the charge balance error and an erroneous value for the resulting pH and IAP values. The corresponding IAP values were therefore considered suspect.

A log IAP value of -50.75 ±0.07 was obtained from replicate analyses of a portion of the suspension remaining from synthesis of the solid used in the experiments. This suspension was maintained at 25°C for 56 days following collection of the synthesized solid.

The plot of the IAPs calculated for the time series samples vs. time (Figure 3-4) was fit with an exponential curve of the form

(5)

$$\log IAP = a + b \exp(-t/c)$$

(r^2 = 0.994; df = 4) where t is the time in hours. In the limit, as $t \rightarrow \infty$, Equation (5) converges to IAP = a, with a resulting value of -50.45 ±0.74. Examination of the plot of log IAP vs. time (Figure 3-4) shows that a "bench" occurs near the mean log IAP value (~ -53) obtained from the dissolution experiments at ~150 hours. Examination of the plot of analyte concentrations with time (Figure 3-3) indicates that the subsequent rise in IAPs is completely due to a corresponding rise in Cr concentrations. The much lower concentrations of Cr relative to Ca and SO_4 make interpretation difficult as the highest Cr concentrations are within the analytical errors for the other constituents.

A possible explanation for the observed discrepancies between the IAPs calculated for the dissolution samples and the synthesis liquor and time series samples is that coating by secondary precipitates inhibited or prevented diffusion of ions to and from the surface of the bentorite solid. If such coating occurred prior to equilibrium between the solution and bentorite, then the later change in Cr concentrations (> 150 hrs) and IAPs could represent an approach to such equilibrium slowed by diffusion of ions through the coating solids. Alternatively, the late-stage changes in Cr concentrations could represent re-equilibration of the solution with the new coating solid following effective isolation of the bentorite.

We propose that the lower IAP values represent equilibrium with bentorite, based on: 1) the larger range of errors associated with the higher IAP values which were calculated for precipitation samples that had been spiked with $Ca(NO_3)_2$ and for which pH values were estimated by minimizing the charge balance; 2) the achievement of steady-state conditions with respect to Ca and SO_4 concentrations and the fact that

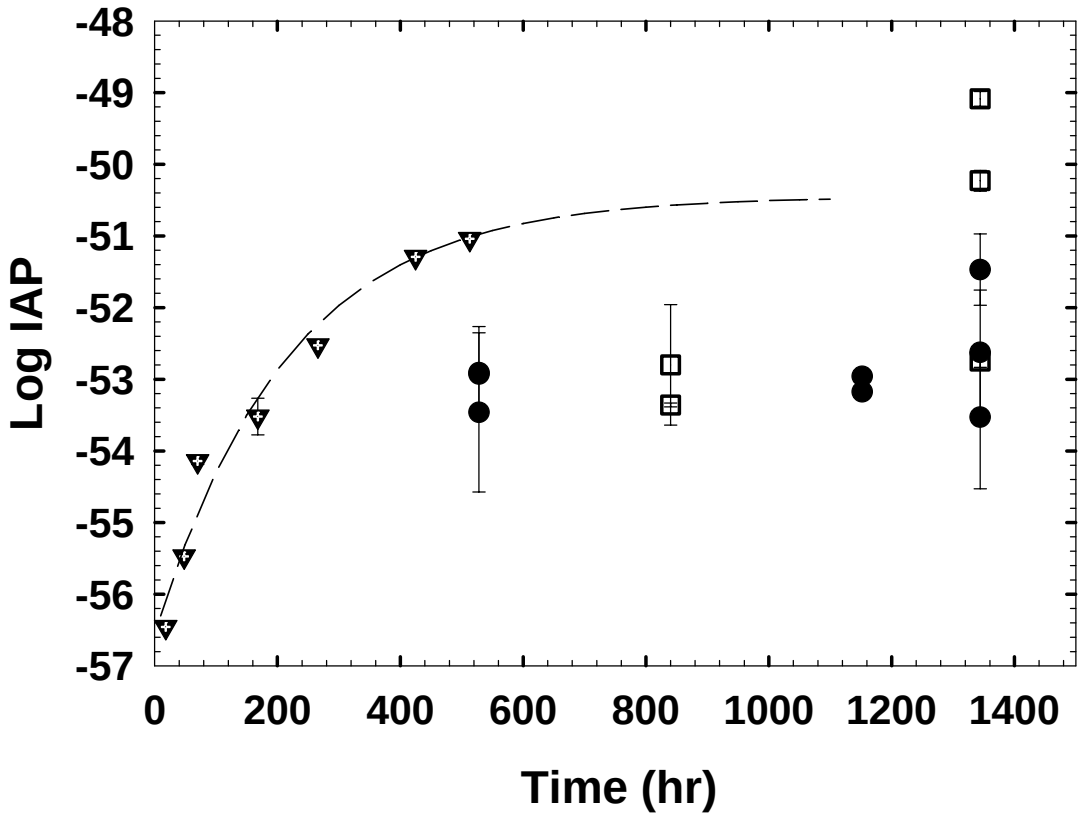

Figure 3-4. Plot of log ion activity product as a function of time in bentorite time series dissolution experiment (↔), dissolution experiments (ℓ), and precipitation experiments (ˬ) conducted at 25°C. Dashed line represents a curve of the form Log IAP = a + b exp(time/c) which was fit to the time series values and which indicates steady-state conditions at ~800 to 1000 hours.

these steady-state concentrations were achieved on a time scale (~150 hrs) analogous to that noted in previous experiments with ettringite (Perkins and Palmer, 1999); 3) the consistency of the IAP values obtained in the dissolution experiments over time periods ranging from 22 to 56 days; and 4) the similarity of the values obtained from the experiments where precipitation was initiated by heating with subsequent cooling and re-equilibration at 25°C. The higher values observed in some of the samples are assumed to represent conditions wherein the initial bentorite was effectively isolated from the solution and Cr concentrations were strictly driven by equilibrium with $Cr(OH)_3$ and possibly Ca-Cr hydroxides.

Assuming that the lower IAP values best represent the solubility of bentorite, the average log value obtained from the means of all of the triplicate dissolution and precipitation samples, excluding BP25-10.5 and BP25-11.5, may then be taken to represent the log K_{SP} at 25°C and is calculated as -52.9 ±0.79 (t.s.d.).

At equilibrium, the Gibbs free energy of the dissolution reaction at 25°C is given by:

(6)

$$\Delta G^\circ_{reaction} = 6\Delta G^\circ_{f,298}(Ca^{2+}) + 2\Delta G^\circ_{f,298}(Cr(OH)_4^-) + 3\Delta G^\circ_{f,298}(SO_4^{2-}) + 4\Delta G^\circ_{f,298}(OH^-) + 26\Delta G^\circ_{f,298}(H_2O) - \Delta G^\circ_{f,298,bentorite.}$$

The Gibbs free energy of reaction is also related to the K_{SP} by:

(7)

$$\Delta G^\circ_{reaction} = -RT \ln K_{SP}$$

where R is the gas constant (8.3145 J mol^{-1} K^{-1}) and T is the temperature in Kelvin.

Combining Equations (6) and (7), the free energy of formation of bentorite is given by: **(8)**

$$\Delta G^\circ_{f,298,bentorite} = 6\Delta G^\circ_{f,298}(Ca^{2+}) + 2\Delta G^\circ_{f,298}(Cr(OH)_4^-) + 3\Delta G^\circ_{f,298}(SO_4^{2-}) + 4\Delta G^\circ_{f,298}(OH^-) + 26\Delta G^\circ_{f,298}(H_2O) + RT \ln K_{SP}$$

We calculated $\Delta G^\circ_{r,298,bentorite} = 302 \pm 10$ kJ mol^{-1} using Equation (7) and $\Delta G^\circ_{f,298,bentorite} = -14625 \pm 24$ kJ mol^{-1} using Equation (8) and the free energies of formation of the individual ions presented in Table 3-7.

Table 3-7. Relevant thermodynamic data

	kJ/mol		J/mol·K		
Species	**ΔG°r**	**ΔH°r**	**ΔS°r**	**ΔC_P**	**Source**
H_2O	-237.14 ±0.04	-285.83 ±0.04	69.95 ±0.03	75.35 ±0.08	1
OH^-	-157.3 ±2.0	-230.0 ±0.6	-10.7 ±1.9	-137.2 ±16.7	2
Ca^{2+}	-552.8 ±2.0	-543.0 ±0.6	-56.5 ±1.9	-31.5 ±16.7	2
SO_4^{2-}	-744.5 ±2.0	-909.6 ±0.6	19 ±1.9	-269.4 ±16.7	2
$Cr(OH)_4^-$	-989 ±2.0	-1192.3 ±0.6	111.9 ±1.9	64.1 ±16.7	3,2
Bentorite	-14625 ±24	-17043 ±79	--	--	4

Multiple sources indicate sources for individual ion data that were used in calculating data presented.
1: Cox et al., 1989; 2: Shock et al., 1997; 3: Ball and Nordstrom, 1998 ; 4: This study.
*: Uncertainties are based on maximum values reported by Shock and Helgeson (1988) over the temperature range of 0 to 100ºC and a pressure of 1 bar.

The log IAP values calculated for the temperature-dependent experiments appear to vary significantly with pH. This discrepancy is particularly evident in the 5 and 15°C experiments, in which samples near or above pH 12 had IAP values approximately two orders of magnitude higher than those at or below pH 11. This could be indicative of non-equilibrium conditions due to slower equilibration times at these lower temperatures. It may also be due to changes in the stability of bentorite or secondary phases at the higher pH. The mass balance calculations using the 25°C dissolution data indicate that the experimental solutions with pH at or above 12 would require a much greater mass (1.5 to 4 times as much) of $3CaO{\cdot}Cr_2O_3{\cdot}6H_2O$ or $Ca_2Cr_2O_5{\cdot}8H_2O$ to be precipitated than in the other experiments in order to achieve the observed stoichiometries, assuming the only other solids present are bentorite and $Cr(OH)_3$. The data from the higher pH solutions were therefore not used in subsequent calculations. The rate of change in IAP values with temperature is approximately the same for both high (> pH 11.5) and low pH (< 11.5 pH) samples (Figure 3-5A). The similarity in slope suggests that the difference in IAPs with pH could be due to incomplete or inaccurate Cr(III) speciation data. IAP values calculated for the 45°, 60°, and 75°C experiments also show a reversal in slope when plotted against temperature, implying a phase change between 35 and 60°C (Figure 3.5A).

Regression of mean log IAP values from the 15, 25, and 35°C experiments (pH < 11.5) versus the inverse of the temperature (Figure 3-5B) resulted in a slope of-16,699 ±3,752 K. The slope appears to be linear ($r^2 = 0.952$), suggesting that the enthalpy of reaction, $\Delta H°_r$, is constant over this range of temperatures. The

log K_{SP} values calculated using the linear regression coefficients were within one standard error of the measured K_{SP} values. The $K_{SP}(T)$ can be written as

(9)

$$\log Ksp = \left(\frac{A}{T}\right) + B$$

where $A = -\Delta H°_r / (\ln(10)R)$ and $B = \Delta S°_r / (\ln(10)R)$. Using Equation (9), and the slope of the fitted data, the enthalpy of reaction, $\Delta H°_{r,}$ was calculated to be 320 ±76 kJ mol^{-1}. The error is based on the standard error of the regressed slope. The entropy of reaction, $\Delta S°_r$, could not be directly calculated from the solubility data as the error of the regressed intercept was greater than the value of the intercept (i.e., the intercept was not significantly different than zero).

Using the data in Table 3-7 and an equation for $\Delta H°_f$, analogous to Equation (6), we calculated the enthalpy of formation for bentorite to be $\Delta H°_{f,ettringite}$ = -17,040 ±79 kJ mol^{-1}. The error is based on the errors calculated for the dissolution reaction parameters and the maximum calculated errors associated with individual ions.

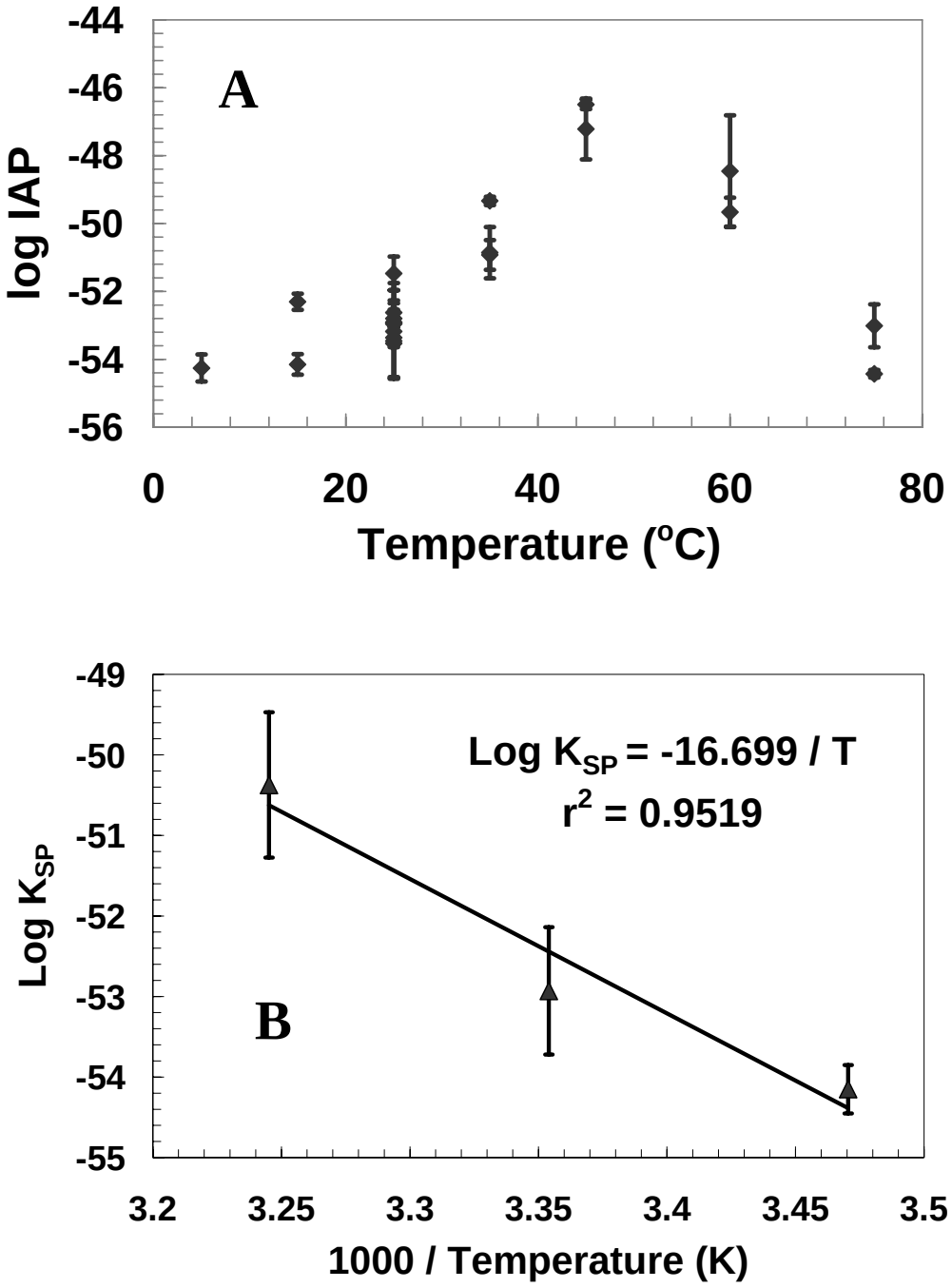

Figure 3-5. A.) Log ion activity products for individual samples as a function of temperature; the 5-12.0 sample is excluded as the corresponding charge balance error exceeded 15%. B.) Mean Log K_{SP} values calculated from 15, 25, and 35ºC samples (pH < 11.5) as a function of inverse temperature.

Table 3-8. Calculated equilibrium activities and ion activity products for temperature-dependent bentorite dissolution experiments.

Sample Batch	Meas pH	Log $\{Ca^{2+}\}$	Log $\{Cr(OH)_4^-\}$	Log $\{SO_4^{2-}\}$	Log $\{OH^-\}$	Log $\{Na^+\}$	Ionic Strngth (mM)	C.B, Error (%)	(-) Log IAP
5-10.5	11.428	-3.06	-6.62	-3.161	-3.273	-3.419	4.67	6.35	54.18
	±0.021	±0.038	±0.11	±0.062	±0.021	±0.001	±0.53	±1.26	±0.50
5-12.0[a]	12.914	-3.62	-6.55	-3.299	-1.80	-1.951	17.99	18.2	51.90
	±0.001	±0.034	±0.067	±0.042	±0.017	±0.001	±0.13	± 1.4	±0.37
15-	11.12	-3.10	-6.37	-3.279	-3.215	-3.422	4.00	10.29	54.04
10.5	±0.018	±0.036	±0.17	±0.052	±0.018	±0.018	±0.01	±7.73	±0.33
15-	11.87	-3.353	-6.206	-3.255	-2.473	-2.92	6.71	1.40	52.08
11.5	±0.003	±0.057	±0.055	±0.018	±0.002	± 0.69	±0.13	±1.40	±0.19
35-	10.809	-3.02	-5.977	-3.108	-2.871	-3.435	5.86	7.60	50.86
10.5	±0.065	±0.061	±0.041	±0.049	± 0065	±0.041	±0.78	±1.67	±0.75
35-	10.983	-3.078	-6.175	-3.105	-2.697	-2.984	6.27	15.05	50.93
11.0	±0.032	±0.021	±0.058	±0058	±0.032	±0.012	±0.57	±3.46	±0.44
35-	11.357	-3.13	-6.003	-3.08	-2.328	-2.475	9.26	12.5	49.33
11.5	±0.009	±0.057	±0.005	±0.025	±0.004	± 0026	±0.14	± 2.5	±0.12
45-	10.66	-2.851	-5.29	-3.041	-2.73	-2.85	9.0	10.7	47.7
11.5	±0.16	±0.023	±0.10	±0.071	± 0.16	±0.040	± 1.2	± 8.1	±1.1
45-	11.042	-2.949	-5.184	-3.022	-2.341	-2.441	11.21	2.43	46.49
12.0	±0.009	±0.007	±0.060	±0.006	±0.009	±0.013	±0.12	±0.99	±0.14
60-	10.43	-2.98	-5.78	-3.237	-2.543	-3.379	6.57	14.5	49.34
10.5	±0.019	± .029	±0.47	±0.058	± .019	± .027	± .12	± 6.0	±0.86
60-	10.46	-3.403	-5.179	-2.933	-2.511	-2.441	8.50	14.0	49.62
11.0	±0.085	±0.001	±0.097	±0.021	±0.085	±0.006	±0.61	± 5.5	±0.59
75-	10.16	-3.884	-4.610	-3.098	-2.798	-2.374	5.91	10.0	53.01
11.0	±0.59	±0.054	±0.014	±0.013	±0.080	±0.081	±0.63	± 5.6	±0.63
75-	10.618	-4.723	-4.391	-3.133	-1.975	-1.943	15.53	4.4	54.43
12.0	±0.011	±0.032	±0.067	±0.012	±0.011	±0.025	±0.15	± 2.3	±0.11

3.5 SUMMARY

Dissolution and precipitation experiments conducted on synthesized bentorite in alkaline solutions (pH 10 to >12) indicate that dissolution of bentorite is non-stoichiometric. Although XRD analyses of experimental residues was inconclusive in determining the secondary phase(s) which would account for this non-stoichiometric dissolution, mass balance calculations and the consistency of calculated ion activity products strongly suggest precipitation of $Ca_2Cr_2O_5 \cdot 8H_2O$. The mean log K_{SP} for $Ca_2Cr_2O_5 \cdot 8H_2O$, assuming it is present at equilibrium with solutions is –24.29 ±0.69. This phase as well as $Ca_2Al_2O_5 \cdot 6 \cdot 8H_2O$, $Ca_2Al(OH)_7 \cdot 3H_2O$, and $3CaO \cdot Al_2O_3 \cdot 6H_2O$ (hydrogarnet) have previously been suggested as potential controls on aqueous Cr(III) concentrations in waters equilibrated with cements (Kindness et al., 1994).

Log IAP values of between -49.05 and -53.53 were calculated for the dissolution of bentorite based on eight dissolution samples and five precipitation samples collected after between 22 and 56 days of mixing at 25ºC. However, the two highest values were calculated for precipitation samples which had been spiked with $Ca(NO_3)_2$ and for which pH values had been calculated by minimizing the charge balance errors. These were discarded as outliers and a log $K_{SP,298,bentorite}$ of –52.9 ±0.79 was calculated based on the mean of the remaining dissolution and precipitation samples. Using the calculated K_{SP} and available thermodynamic data for the constituent ions, the free energy of formation, $\Delta G°_{f,298,bentorite}$, was determined to be –14625 ±24 kJ mol^{-1}. This value is comparable to the value of –15211 ±19 kJ mol^{-1} calculated by Perkins and Palmer (1999) for ettringite.

The log K_{SP} increased with increasing temperatures between 5 and 45°C, indicating a positive enthalpy of reaction over this temperature range. A reversal in the slope of log K_{SP} with T^{-1} between 45 and 75°C was assumed to represent changes in solid phase stabilities and warrants further investigation. A $\Delta H°_r$ of 320 ±76 kJ mol^{-1} was calculated from the linear regression of temperature dependent data between 15 and 35°C and a $\Delta H°_f$ of = -17,043 ±79 kJ mol^{-1} was obtained from this value and enthalpy data for individual ions gathered from available literature. We believe these are the first thermodynamic data published for bentorite.

Chapter 4. Solubility of $Ca_6[Al(OH)_6]_2(CrO_4)_3 \cdot 26H_2O$), the Chromate Analog of Ettringite; 5 - 75° C

4.1 INTRODUCTION

Ettringite ($Ca_6[Al(OH)_6)]_2(SO_4)_3 \cdot 26H_2O$) is a hydrous calcium alumina-sulfate mineral that occurs naturally in alkaline environments as a secondary fracture-lining mineral in calcium-rich igneous rocks, in sedimentary units that have undergone contact metamorphism, and in alkaline soils (e.g.,Bentor, 1963; Hurlbut and Baum, 1960; Murdoch and Chalmers, 1960). Ettringite is also an important constituent in common materials such as cement and fly ash (Kumarathasan et al., 1990; Lea, 1970). Ettringite's widespread occurrence and ability to structurally incorporate potentially toxic ions, such as chromium and selenium, makes it important with regards to the mobility of pollutants in the environment, remediation of contaminated sites, and waste immobilization in cementitious materials.

Ettringite is a member of the ettringite group described by the general formula $Ca_6[X_3(OH)_6]_2(Y)_3 \cdot 26H_2O$, where X represents a site occupied by trivalent metals such as Al^{3+}, Fe^{3+}, or Cr^{3+} and Y represents a site occupied by oxyanions such as SO_4^{2-}, CO_3^{2-}, SeO_4^{2-} or CrO_4^{2-} (Dunn et al., 1983; Hassett et al., 1990; Poellman et al., 1993; Poellmann et al., 1990). Substitution of hexavalent chromium in ettringite is of particular interest as chromium is a widespread pollutant that can be acutely toxic, teratogenic, mutagenic, and carcinogenic (Nieboer and Shaw, 1988; Nordberg, 1988; O'Brien and Kortenkamp, 1994; Sugiyama, 1994). Hexavalent chromium in alkaline

solutions occurs as CrO_4^{2-}. The identical charge, similar structure, and comparable thermochemical radii of CrO_4^{2-} and SO_4^{2-} suggest that CrO_4^{2-} should readily substitute in the crystal structure of many sulfate minerals, including ettringite. Indeed, several researchers have synthesized $Ca_6[Al(OH)_6)_2(CrO_4)_3 \cdot 26H_2O$ (Kumarathasan et al., 1990; Poellman et al., 1993) and we have observed Cr(VI)-rich ettringite crystals in Cr(VI)-contaminated concrete (Palmer, 2000). Thus, the chromate analog of ettringite may provide a solubility control on Cr(VI) concentrations in alkaline environments and may help to immobilize Cr(VI) in cementitious materials.

Understanding and evaluation of the role of the chromate analog of ettringite in these processes could be facilitated by knowledge of its thermodynamic properties. However, we were unable to locate thermodynamic data for this phase. Therefore, the purpose of this study is to measure the solubility of pure $Ca_6[Al(OH)_6)_2(CrO_4)_3 \cdot 26H_2O$ and to determine its solubility product (K_{SP}) from 5 to 75ºC. Thermodynamic properties for this phase are calculated from this information. The results of this study should be useful to workers dealing with chromium migration and waste immobilization in alkaline environments as well as to material scientists developing new cements.

4.2 BACKGROUND

Ionic substitution in ettringite has been well established (Bensted and Varma, 1971; Dunn et al., 1983; Hassett et al., 1990; Hurlbut and Baum, 1960; 1993; Poellmann et al., 1990). However, there is relatively little available literature specifically addressing chromium substitution in ettringites and the studies

that were identified deal chiefly with X-ray and spectroscopic characterization of synthesized solids (Kumarathasan et al., 1990; Myneni, 1995; Poellman et al., 1993). We were unable to find data describing the effect of chromium substitution on ettringite solubility. Such information is needed to accurately model mineral-water interactions important in the solidification and stabilization of chromium-bearing wastes and environmental cleanups involving chromium contamination in alkaline environments.

Teramoto and Koie (1976) investigated the use of chromium, manganese, and fluorine to increase early hydration strengths in cements. As part of their study, they examined the growth of ettringite crystals formed by the reaction of tricalcium aluminate and varying proportions of $CaSO_4$ and $CaCrO_4$. They noted that ettringite containing minor amounts of chromate (9:1 SO_4:CrO_4) grew more quickly and developed thicker crystals than pure sulfate ettringite, but that higher chromate concentrations (1:1 and 1:9 SO_4:CrO_4) produced smaller quantities of relatively very thin acicular ettringite from similar-strength solutions. The latter observation suggests a higher solubility for CrO_4 ettringite.

Kumarathasan et al. (1990) noted a correlation between the precipitation of an ettringite-type phase and reduction of hazardous elements in leaching studies of coal-ash wastes. These investigators synthesized a number of ettringite phases with differing oxyanions, including AsO_4^{3-}, $B(OH)_4^-$, SeO_4^{2-}, VO_4^{3-}, and CrO_4^{2-}, characterizing them by a variety of methods. They noted that the X-ray diffraction (XRD) pattern of the fully substituted chromate phase did not contain many of the

moderate and weak characteristic ettringite peaks and that there were large intensity differences between the chromate and sulfate ettringite peaks. Their chemical analyses indicated a stoichiometry of 6Ca:2.7Al:2CrO_4 as compared to the theoretical stoichiometry of 6Ca:2Al:3CrO_4. Kumarathasan et al. also calculated a heat of hydration for $Ca_6[Al(OH)_6]_2(CrO_4)_3 \cdot 26H_2O$ of 0.47 kJ/g (vs 0.60 kJ/g for ettringite) based on calorimetric analysis of the endotherm at 100-140°C and a total weight loss on ignition (at 850°C for 18h) of 39%.

Poellman et al. (1993) investigated the solid solution of ettringites containing SO_4^{2-}, CrO_4^{2-} and $B(OH)_4^-$. These investigators utilized two different techniques to synthesize their solid solutions: 1) a "paste reaction" combining aqueous mixtures of $CaCrO_4$, $CaSO_4$, $CaAl_2O_4$, and CaO, and 2) a "saccharat-method" involving a lime-sucrose complex. The synthesized solids were characterized by XRD, chemical analyses, and calorimetry. A miscibility gap was noted in the solid solution series synthesized with the saccharat-method, which they attributed to the pH influences and "the low availability of CaO from the lime-sucrose complex." Poellman et al. (1993) also noted a difference in crystal shapes, with a short-prismatic habit noted in ettringites formed by the saccharat-method and a more characteristic elongated prism form resulting from the paste reaction method. Unit cell lattice parameters for the pure $Ca_6[Al(OH)_6]_2(CrO_4)_3 \cdot 26H_2O$ were reported as a_0 = 11.39 Å and c_0 = 21.47 Å (compared with 11.23 Å and 21.52 Å for the sulfate ettringite).

Myneni et al. (1994; 1995) examined sorption and co-precipitation of chromate and arsenate by ettringite. Myneni (1995) noted that chromate uptake was retarded by

aqueous sulfate and that surface complexation was the dominant mechanism for CrO_4^{2-} uptake at sorbate concentrations of <0.02 M while substitution of CrO_4^{2-} for SO_4^{2-} became important at higher (>0.03M) concentrations. Sorbed CrO_4^{2-} was apparently not exchanged by increases in SO_4^{2-} concentrations and was independent of ionic strength.

4.3 METHODS

4.3.1. Synthesis of $Ca_6[Al(OH)_6]_2(CrO_4)_3 \cdot 26H_2O$

The solid material used in the dissolution experiments was synthesized using a modification of a method described by Odler and Abdul-Maula (1984). A suspension of 0.02 moles tricalcium aluminate ($3CaO \cdot Al_2O_3$) and 0.06 moles of $CaCrO_4$ in one liter of ultrapure water (>14 megaohm-cm) was mixed at 400 rpm using a magnetic stirrer at room temperature (~23ºC). To minimize CO_2 contamination, water used in the synthesis was purged with N_2 for 15 to 30 minutes and reactants were mixed in a N_2-filled glove box in which the atmosphere was continuously bubbled through 1 M NaOH (Ewing and Shepard, 1994). After 72 hours, the contents were transferred, under N_2, to a ceramic filter funnel and rapidly vacuum-filtered through a 3.0-μm polysulfone filter to separate the solid precipitate. The precipitate was subsequently dried and stored in the glove box in a desiccator containing a saturated $CaCl_2$ solution to maintain a relative humidity of approximately 30%.

4.3.2. Characterization of Synthetic Ettringite

The synthetic material was characterized using five different methods. X-ray diffraction (XRD) analyses were performed using a Phillips X'Pert MPD unit with CuKα radiation. Qualitative chemistries were obtained with a LINK energy dispersive X-ray spectrometer (EDX) using a 31-mm working distance and an accelerating voltage of 20kV. Fourier Transform Infrared Spectroscopy (FTIR) analysis was conducted on a Perkin-Elmer 2000 unit, utilizing a KBr pellet. Replicate portions (~5mg) of the synthesized solid were digested in HCl and analyzed to quantify the stoichiometry of the material. Total calcium and aluminum concentrations were determined by flame atomic absorption spectroscopy (AAS) using an air-acetylene flame for calcium and a nitrous oxide-acetylene flame for aluminum and a lanthanum matrix modifier for both sets of analyses. Hexavalent chromium concentrations were determined colorimetrically (3500-Cr D; APHA, 1995) by reacting samples with diphenylcarbazide in acid solution and measuring the absorbance at 540 nm with a Beckman DU 640 spectrophotometer. The amount of water in the synthesized material was determined by thermogravimetric analysis (TGA) using a Perkin-Elmer TGA7 thermogravimetric analyzer. The single TGA analysis was conducted on 3.37 mg of sample over a temperature range of 40 to 900ºC at a rate of 10ºC/minute.

4.3.3. Dissolution and Precipitation Experiments

A set of dissolution experiments was conducted at 25°C using initial pH levels between 10.3 and 12.3. The experiments were conducted by placing 0.10 g of the synthesized solid in 30 ml HDPE bottles along with a magnetic stir bar. The

bottles were subsequently filled under N_2 with ultrapure water that had been purged with N_2, then adjusted to the desired pH with NaOH. As an additional precaution against CO_2 contamination, the capped HDPE bottles were sealed within N_2-filled glass mason jars. The jarred sample bottles were then placed in circulating water-baths to maintain the temperature within 0.3°C of the desired value and mixed with magnetic stirrers. Because of the small volumes of suspensions used in these experiments, an additional experiment using 120 ml of water was conducted in duplicate so that the aqueous solutions could be temporally sampled to determine the time required to achieve steady-state conditions and, hence, when to sample the smaller reaction vessels. Several replicate experiments were conducted to verify reproducibility or where the results from the initial experiments were unacceptable because of charge balance errors > 10% or variations in analyte concentrations >20%.

Samples were also obtained from 25°C solutions initially supersaturated with $Ca_6[Al(OH)_6]_2(CrO_4)_3 \cdot 26H_2O$. These precipitation experiments were conducted by spiking the suspensions remaining at the conclusion of dissolution experiments with 7 to 7.5ml of 70 mM $Ca(NO_3)_2$. All other aspects of the precipitation experiments were identical to the dissolution experiments.

Dissolution experiments were conducted at six additional temperatures between 5 and 75°C to determine the temperature dependence of the $Ca_6[Al(OH)_6]_2(CrO_4)_3 \cdot 26H_2O$ solubility. These experiments were conducted in a manner identical to the 25°C dissolution experiment except that water-bath temperatures were maintained within 0.5°C of the temperature of interest.

All sampling was conducted in a N_2-filled glove box. The jarred bottles were transferred to the glove box in portable water baths and quickly processed to maintain the desired temperatures. A hot plate equipped with a digital thermometer was used to maintain temperatures for the 60 and 75ºC samples during pH measurements. A 7.5 ml volume of suspension was withdrawn from each sample and filtered using a 0.45-μm polysulfone membrane filter. Separate cation and anion subsamples were prepared. A 5ml/liter solution of concentrated HNO_3 was used to dilute and preserve the cation samples at pH < 2. Anion samples were diluted with ultrapure water and stored in HDPE vials. A representative sample of the solid phase was removed following some of the experiments and analyzed by XRD to verify that $Ca_6[Al(OH)_6]_2(CrO_4)_3 \cdot 26H_2O$ was still present.

Measurements of pH were made at the time of sampling using an Orion Model 290A portable pH meter and Orion Model 9157BN-triode pH electrode. The pH meter was calibrated using pHydrion® 7.00, 10.00, and 12.00 pH buffers. Although a slight reduction in the electrode response slope (e.g., ~3 mv/pH) was noted over the higher pH interval, the meter utilizes the slope of the interval corresponding to each measurement in order to reduce “averaging” errors. The buffers were brought to the temperature of the samples to account for temperature-dependent variations in pH and the meter was adjusted to the appropriate value based on the manufacturer’s temperature-dependence data. The 9157BN triode incorporates low Na-error glass, obviating the need for alkali interference corrections at the sodium concentrations / temperature combinations encountered (e.g., corrections < 0.01 pH units). Liquid-

junction potential effects were minimized by appropriate conditioning and storage of the electrode and by allowing suspended sediment to settle prior to measurements. Total Ca, Al, and hexavalent chromium concentrations were determined using the methods described for the solid digest.

4.4 EXPERIMENTAL RESULTS

4.4.1. Solid Characterization

The d-spacings from XRD analysis of the synthesized $Ca_6[Al(OH)_6]_2(CrO_4)_3 \cdot 26H_2O$ were compared with the d-spacings listed for the equivalent $Ca_6Al_2Cr_3O_{18} \cdot 32H_2O$ (JCPDS Card 41-0218). Thirty-six of the thirty-seven peaks measured between 5 and 50° 2θ had d-spacings that were within 0.066 Å of corresponding peaks on the JCPDS card (Table 4-1; Figure 4-1), with an average difference of 0.0045 Å. Eight peaks listed on the JCPDS card do not have corresponding measured peaks. However, the relative intensities of five of the eight peaks are 1% and the intensities for the other three are 10% or less. A single measured peak at 7.52 Å could not be matched with a corresponding peak on the JCPDS card. Miller indices {103} for this peak were assigned by minimizing the residual (<0.001 Å) between the measured d-spacing and theoretical d-spacing based on the unit cell dimensions and

(1)

$$d = \frac{\sqrt{3}ac}{\sqrt{4c^2(h^2 + hk + k^2) +}}$$

The cell dimensions were calculated using the equation for hexagonal system minerals (Equation 1), the measured d-spacings of the other 36 peaks, and the corresponding Miller indices from the JCPDS card. The calculated unit cell dimensions are a_0 = 11.41 ±0.019 Å and c_0 = 21.44 ±0.051 Å. These dimensions are within one standard deviation of those reported on the JCPDS 41-0218 card (a_0 = 11.394 Å and c_0 = 21.472 Å). Our calculated primitive unit cell volume (2414.1 ±8.1Å^3) is identical to the value listed on the JCPDS card.

The FTIR spectrum (Figure 4-2) agrees well with previous studies. A strong absorbance peak at 883 cm^{-1} closely matches the 885 cm^{-1} peak Kumarathason et al. (1990) attributed to CrO_4 vibrations. Myneni (1995) also noted peaks at 867 to 902 cm^{-1} in various SO_4 – CrO_4 intermediate phases. He assigned these peaks to CrO_4 based on analogy to aqueous CrO_4^{2-} absorbance. The peak at 1387 cm^{-1} may be due to OH-bending, as suggested by Kumarathason et al. for peaks at ~1427-1435 cm^{-1}.

EDX analyses of crystallites in the synthesized material indicted that all of the crystals had the general composition (Ca, Cr, Al) expected for $Ca_6[Al(OH)_6]_2(CrO_4)_3 \cdot 26H_2O$. No other elements, other than gold and palladium used in sputter coating, were identified. The mean elemental percentages (55.0 ± 3.6% Ca; 31.4 ±6.1% Cr; and 13.7 ±3.8% Al) calculated from twelve EDX scans are in reasonable agreement with the expected relative percentages (54.5: 27.3: 18.2) with a slight excess of chromium and a deficiency of aluminum. However, this technique is considered only semi-quantitative and assumes a flat scanning surface, which was not the case with the sample used.

Table 4-1. Comparison of X-ray diffraction peaks from synthetic $Ca_6[Al(OH)_6]_2(CrO_4)_3 \cdot 26H_2O$ with peaks from JCPDS card 41-0218.

	$Ca_6Al_2Cr_3O_{18} \cdot 32H_2O$ JCPDS 41-0218		**Synthesized $Ca_6[Al(OH)_6]_2(CrO_4)_3 \cdot 26H_2O$**	
h,k,l[a]	**d(Å)**	**I/Imax**	**d(Å)**	**I/Imax**
002	10.7340	5	10.720	10
100	9.872	100	9.938	78
101	8.9719	10	9.000	15
102	7.2663	4	7.250	4
103*	--	--	5.792	21
110	5.6972	80	5.690	100
112	5.0319	23	5.040	51
200	4.9347	5	4.926	8
201	4.8073	1	--	--
104	4.7135	50	4.718	45
202	4.4823	1	4.466	13
203	4.0623	11	4.064	13
105	3.9361	10	--	--
114	3.9053	70	3.908	68
210	3.7292	5	3.733	6
204	3.6317	7	3.631	14
212	3.5227	27	3.527	32
213	3.3079	8	3.360	3
300	3.2899	21	3.284	21
116	3.0303	7	3.035	8
220	2.8482	1	2.874	12
304	2.8038	45	2.806	44
222	2.7534	1	--	--
310	2.737	7	2.737	11
311	2.7144	1	--	--
008	2.6835	10	2.684	11
312	2.6511	15	2.652	19
216	2.5815	45	2.583	40
313	2.5565	4	2.556	6
400	2.4661	1	2.500	12
314	2.4383	5	2.435	7
118	2.4281	5	2.419	9
306	2.4218	1	--	--
208	2.3575	5	2.360	6
320	2.2640	8	2.265	13
226	2.2285	40	2.230	44
322	2.2149	7	--	--
316	2.1735	23	2.176	23
323	2.1581	4	2.155	9
410	2.1532	4	--	--
412	2.1110	2	2.112	4
324	2.0864	1	2.086	4
11(10)	2.0089	1	--	--
325	2.0026	1	2.000	4
500	1.9733	4	1.975	6

[a] (hkl)s from JCPDS Card.; * denotes hkl calculated by minimizing residual between measured and theoretical d-spacings based on cell dimensions.

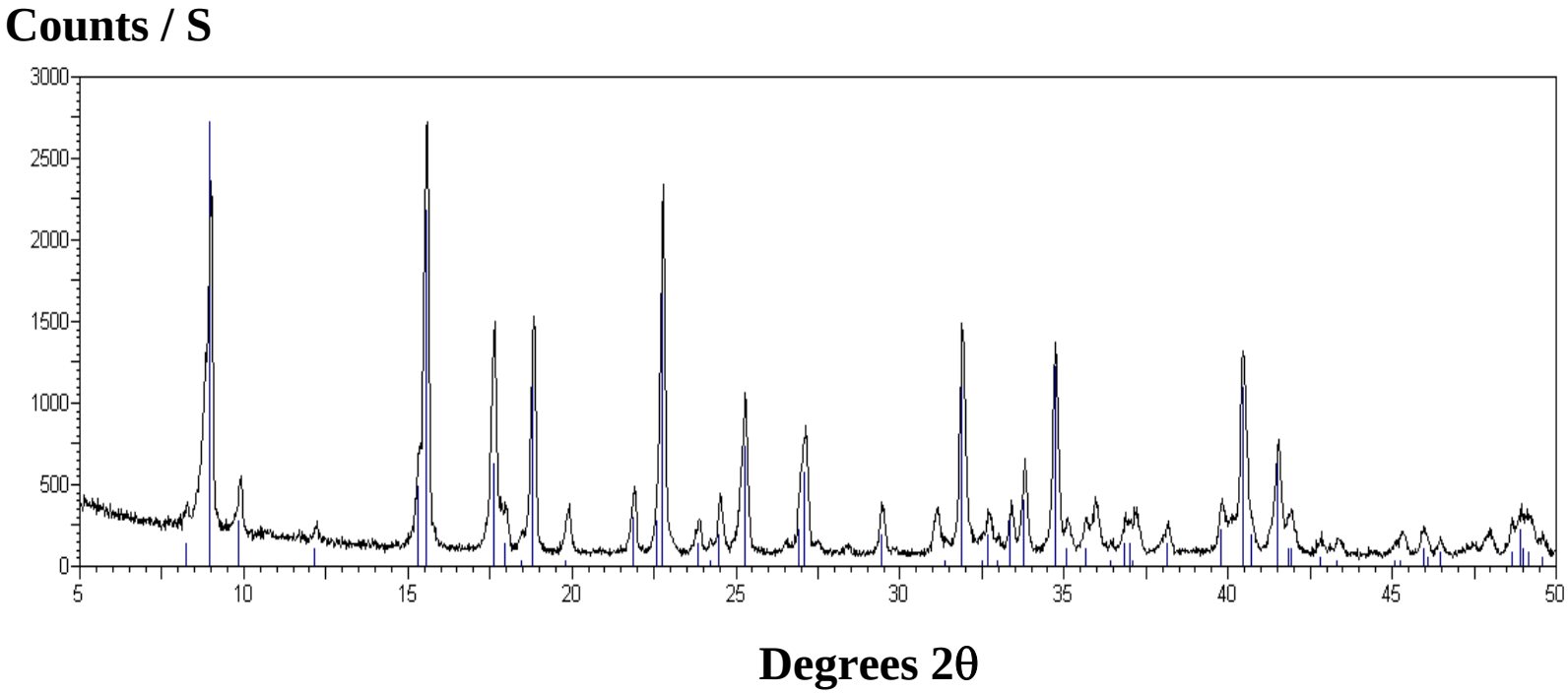

Figure 4-1. X-ray diffraction pattern for synthesized $Ca_6[Al(OH)_6]_2(CrO_4)_3 \cdot 26H_2O$. Peaks from JCPDS powder diffraction file 41-0218 are shown as vertical lines.

Analysis of the solid phase digest yielded a Ca:Al:CrO_4 ratio of 5.92:2.00:2.82 based on the average molarity from replicate analyses normalized to the Al concentration. The standard deviations for the normalized Ca and CrO_4 concentrations are both 0.29. The measured stoichiometry compares closely with the ideal ratio of 6:2:3 for pure $Ca_6[Al(OH)_6]_2(CrO_4)_3 \cdot 26H_2O$. Although this suggests a deficiency of chromate and slight excess of aluminum, the maximum relative percent difference (6%) based on the value of 2.82 for chromate falls within the expected range of analytical error.

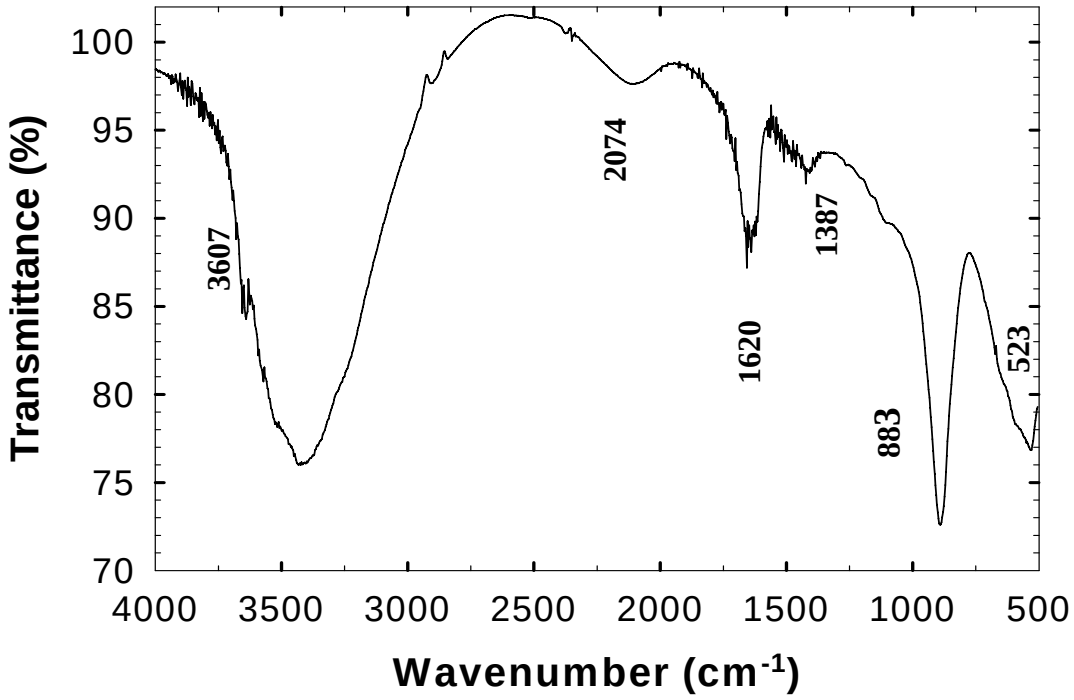

Figure 4-2. FTIR spectra of synthetic $Ca_6[Al(OH)_6]_2(CrO_4)_3 \cdot 26H_2O$ in KBr pellet. Major vibrational bands interpreted to be due to: free OH-stretching (3607 cm^{-1}); H-bonded OH-stretching (3380 cm^{-1}); Cr-O overtone(?) (2074 cm^{-1}); OH-bending (1635 cm^{-1}); ν_3 CrO_4 (883 cm^{-1}); Al-O-H bending (or Cr-O?) vibration (523 cm^{-1}). Interpretations based on discussions from Kumarathasan et al. (1990) and Myneni (1995).

Thermogravimetric analysis indicates that mass is lost over three distinct intervals (Figure 4-3). The greatest loss occurs between 40 - 180^{o} C, the range at which loosely bound water would be expected to be lost. The 30% mass loss over this interval corresponds to 22 water molecules. This loss may be accounted for by the breakdown of ettringite to its constituent hydroxides and calcium chromate, if a variable hydration state of the three calcium chromate molecules is assumed. An additional mass loss of 9.8% that occurs between 180 and 540^{o}C (an inflection point) corresponds to the loss of seven additional water molecules. The total mass loss at 540^{o}C may be explained by the dehydration of the hydrated calcium chromate that resulted from initial heating and by the conversion of aluminum hydroxide to aluminum oxide. The last interval of mass loss (3.9%) from 540 to 900^{o}C corresponds to 2.9 water molecules. Three additional water molecules would be expected from conversion of the calcium hydroxide to calcium oxide. The measured mass loss of 43.7% is consistent with the expected mass loss of 43.8% based on loss of 32 waters.

The sum of these analyses demonstrates that the synthesized solid is $Ca_6[Al(OH)_6]_2(CrO_4)_3 \cdot 26H_2O$ with near-ideal unit cell dimensions. The slight variations from the expected stoichiometry (1.3 to 6.1%) are less than the corresponding analytical errors.

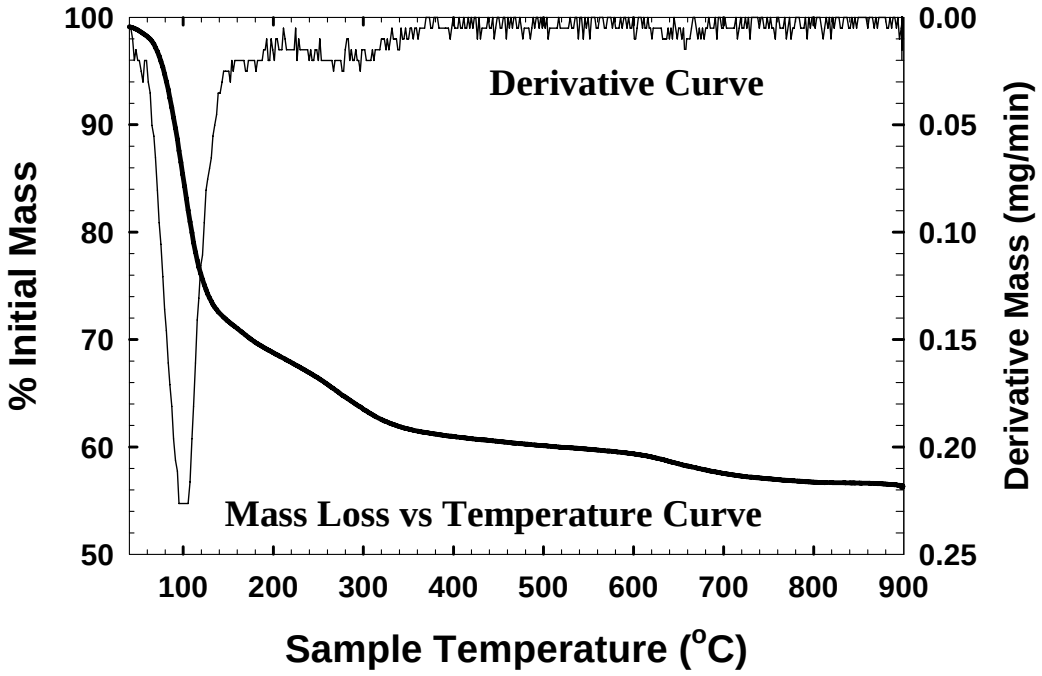

Figure 4-3. Thermogravimetric analysis of $Ca_6[Al(OH)_6]_2(CrO_4)_3 \cdot 26H_2O$.

4.4.2. Dissolution and precipitation experiments

Examination of the ion concentrations in time-series samples collected from the dissolution experiment at 25°C and initial pH of 11.0 indicates that steady-state conditions were achieved in 50 hours or less. No significant changes were noted in subsequent samples collected up to 336 hours (Figure 4-4).

The averaged analytical results from the 25°C dissolution and precipitation experiments (Table 4-2) clearly show the increased Ca and decreased Al and CrO_4 concentrations resulting from the $Ca(NO_3)_2$ spike added to induce precipitation. A decrease in total Ca, Al, and CrO_4 concentrations with increasing pH is also evident as

expected at elevated hydroxide activities. The reported aqueous concentration stoichiometry is not congruent with respect to chromate-ettringite dissolution. In the 25ºC dissolution samples, CrO_4 consistently appears in relative excess based on the expected stoichiometry normalized to Ca or Al. Ca:Al ratios appear to be near their expected stoichiometric values at pH values <11.35 but increase dramatically at higher pH. There is a general increase in the concentrations of Ca, Al, and CrO_4 with increasing temperature from 5 to 45ºC (Table 4-3). Al concentrations continue to increase at 60 and 75ºC but Ca and CrO_4 concentrations decrease.

Table 4-2. Final concentrations in 25°C dissolution and precipitation experiments.

Sample Batch[a]	No. Reps.	Meas. pH	(Ca) mmol L^{-1}	(Al) mmol L^{-1}	(CrO_4) mmol L^{-1}	(Na) mmol L^{-1}	Duration (days)
D25-10.5	3	11.06 ± 0.04	6.06 ± 0.31	2.05 ± 0.28	4.33 ± 0.21	0.977 ± 0.028	14
D25-11.0	2	11.14 ± 0.02	5.465 ± 0.060	1.814 ± 0.081	4.60 ± 0.10	1.619 ± 0.038	14
D25-11.5	3	11.35 ± 0.04	4.21 ± 0.14	1.109 ± 0.087	4.307 ± 0.060	3.902 ± 0.025	14
D25-11.5r	3	11.42 ± 0.02	4.76 ± 0.10	0.661 ± 0.013	4.38 ± 0.13	3.818 ± 0.043	18
D25-12.0r	3	11.85 ± 0.03	3.68 ± 0.17	0.209 ± 0.019	3.25 ± 0.21	10.23 ± 0.38	18
D25-12.0pp[b]	3	10.62 ± 0.04	10.133 ± 0.081	0.118 ± 0.023	2.85 ± 0.21	8.72 ± 0.11	22
D25-12.5pp[b]	3	12.13 ± 0.01	9.761 ± 0.075	0.018 ± 0.001	2.24 ± 0.29	28.15 ± 0.24	22
P25-10.5	3	10.90 ± 0.03	20.259 ± 0.032	1.305 ± 0.085	2.89 ± 0.17	0.673 ± 0.017	8
P25-10.5r[c]	2	10.97 ± 0.06	15.98 ± 0.26	0.920 ± 0.022	2.40 ± 0.23	0.322 ± 0.032	13
P25-11.5[c]	3	11.14 ± 0.01	19.91 ± 0.44	0.635 ± 0.034	2.720 ± 0.031	3.07 ± 0.16	8
P25-11.5r[c]	2	11.298 ± 0.005	15.96 ± 0.44	0.296 ± 0.006	2.350 ± 0.003	3.418 ± 0.092	13
P25-12.0[c]	2	11.54 ± 0.06	17.454 ± 0.065	0.130 ± 0.004	2.47 ± 0.12	7.91 ± 0.49	11
P25-12.5[c]	3	12.164 ± 0.004	17.76 ± 0.44	0.003 ± 0.0006	2.40 ± 0.23	24.79 ± 1.33	11

[a] "D" prefix designates dissolution experiment samples, "P" precipitation experiment samples.
[b] "pp" suffix designates post-precipitation dissolution experiments (i.e., dissolution of solid phase, spiking w/ $Ca(NO_3)_2$ to induce precipitation, then, following equilibrium, dilution with NaOH solution). NO_3^- concentration estimated by minimizing charge balance error (<1%).
[c] NO_3^- concentrations determined from amount and strength of $Ca(NO_3)_2$ spike used. NO_3^- concentration of 0.03 M used for samples P25-12.0 and P25-12.5; 0.035M used for all other samples.

Table 4-3. Final concentrations in temperature-dependent dissolution experiments.

Sample Batch	No. Reps	Temp (°C)	Meas. pH	(Ca) mmol L^{-1}	(Al) mmol L^{-1}	(CrO_4) mmol L^{-1}	(Na) mmol L^{-1}	No of days
5-10.5	3	5	11.79 ± 0.04	4.30 ± 0.57	1.68 ± 0.18	2.61 ± 0.70	0.502 ± 0.0237	8
5-10.5r	3	5	11.98 ± 0.03	3.575 ± 0.009	1.079 ± 0.046	2.156 ± 0.029	0.739 ± 0.021	20
5-11.5r	3	5	12.29 ± 0.06	2.96 ± 0.13	0.529 ± 0.058	2.482 ± 0.045	3.584 ± 0.038	20
15-10.5	3	15	11.64 ± 0.02	4.282 ± 0.091	1.185 ± 0.032	2.982 ± 0.050	0.846 ± 0.095	13
15-11.5	3	15	11.89 ± 0.03	3.75 ± 0.17	0.551 ± 0.009	3.30 ± 0.23	3.687 ± 0.031	13
35-10.5	2	35	10.95 ± 0.02	6.12 ± 0.15	1.503 ± 0.029	4.34 ± 0.16	0.497 ± 0.003	30
35-11.5	3	35	11.11 ± 0.05	5.061 ± 0.058	5.35 ± 0.16	0.801 ± 0.066	4.628 ± 0.073	30
45-10.5	3	45	10.57 ± 0.04	8.14 ± 0.32	2.230 ± 0.048	6.08 ± 0.28	0.558 ± 0.014	8
45-12.0	3	45	11.30 ± 0.06	3.82 ± 0.10	0.59 ± 0.046	4.24 ± 0.24	12.10 ± 0.43	8
60-10.5	3	60	10.15 ± 0.01	7.43 ± 0.25	2.090 ± 0.003	4.85 ± 0.29	0.808 ± 0.027	10
60-11.5	3	60	10.53 ± 0.10	5.55 ± 0.20	1.312 ± 0.071	4.296 ± 0.083	4.909 ± 0.022	10
75-10.5	3	75	9.90 ± 0.03	7.13 ± 0.24	2.642 ± 0.065	5.21 ± 0.23	0.847 ± 0.038	9
75-11.5	2	75	10.03 ± 0.02	5.19 ± 0.14	1.860 ± 0.015	4.80 ± 0.41	5.01 ± 0.16	9

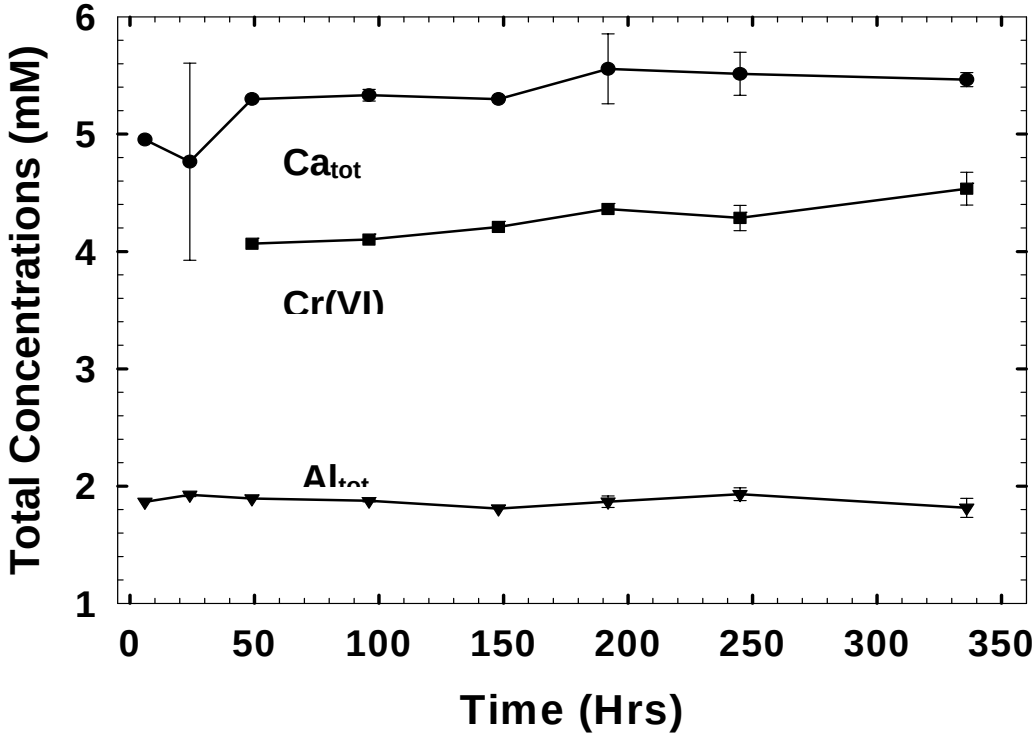

Figure 4-4. Total concentrations of Ca (ℓ), CrO_4 (◆) and Al (↔) in the 25°C $Ca_6[Al(OH)_6]_2(CrO_4)_3 \cdot 26H_2O$ dissolution experiment with initial pH 11.

4.5 DISCUSSION

Aqueous activities for Ca^{2+}, $Al(OH)_4^-$, and CrO_4^{2-} as well as Na^+ and NO_3^- were calculated with the geochemical speciation model MINTEQA2 (Allison et al., 1990) using the Davies Equation:

(2)

$$\log \gamma_i = -AZ_i^2 \left(\frac{\sqrt{I}}{1+\sqrt{I}} - 0.24I \right)$$

The databases used by MINTEQA2 were first modified to include pertinent, updated thermodynamic data from available literature (Table 4-4). Ion activity products (IAP) were calculated from the activities using the dissolution reaction:

(3)

$$Ca_6[Al(OH)_6]_2(CrO_4)_3 \cdot 26H_2O = 6Ca^{2+} + 2Al(OH)_4^- + 3CrO_4^{2-} + 4OH^- + 26H_2O$$

The initial log IAPs for the 25°C samples (Table 4-5) vary by 1.5 log units from –41.08 to –39.44, with the lowest values associated with the highest pH sample (12.15 pH). Regression analyses of the IAPs vs pH indicates that the slope is significantly different than zero and that there is a significant trend at the 95% confidence level (t = 4.96; 11 degrees of freedom (df)). The apparent trend suggests measurement or calculation errors or inaccurate thermodynamic data because the

equilibrium IAP should equal the solubility product and therefore be constant.

Subsequent XRD analyses of solid filtrate from dissolution and precipitation experiments showed $Ca_6[Al(OH)_6]_2(CrO_4)_3 \cdot 26H_2O$ to be present in all the samples except those obtained from the "12.5" pH experiments. This determination is based on the lack of {100} and {110} peaks and significantly different cell dimensions calculated for the "12.5" pH samples. Consequently, these samples were excluded in subsequent calculations of the log K_{SP}. Additional peaks were observed in all samples indicating formation of a secondary precipitate during equilibration with the chromate analog of ettringite. This result is consistent with the observed incongruent dissolution inferred from the solution stoichiometry. The peaks associated with the secondary phase dominate the XRD pattern obtained for the "12.0" pH sample. However, a peak matching the {100} peak of the initial synthesized material is present and cell dimensions calculated from peaks not attributed to the secondary phase are in reasonable agreement with those from the initial solid.

Exclusion of the "12.5" pH samples lessened but did not remove the observed trend in IAPs with pH. A plausible explanation for this trend is the lack of sufficient or accurate thermodynamic data for aqueous complexes, which may impact calculated ion activities. A strong candidate for consideration is the $CaCrO_{4(aq)}$ complex, which is not included in the MINTEQA2 database. Although we could find no data regarding this complex, its existence is implied by analogy with the $CaSO_{4(aq)}$ complex and the similar radii of CrO_4^{2-} and SO_4^{2-} (2.4 and 2.3 Å, Waddington, 1959). In our study of the solubility of ettringite (Perkins and Palmer, 1999), the $CaSO_{4(aq)}$ complex

consistently accounted for >5% of total Ca and >10% of total SO_4 in some samples. Thus, an analogous CrO_4 complex would be expected to have a significant impact on final calculated ion activities.

We performed a series of MINTEQA2 runs varying the log values of the association constant for the $CaCrO_{4(aq)}$ complex,

(4)

$$K_{CaCrO4(aq)} = \{CaCrO_4(aq)\} / \{Ca^{2+}\}\{CrO_4^{2-}\}$$

and found that the variance between all 25ºC samples (excluding the "12.5" pH samples) was minimized using a value of 2.69. This value falls well within the expected range (2.3 to 3.2) of log K_{assoc} values for $M^{2+}L^{2-}$ complexes (Langmuir, 1979). However, the value is greater than would be expected based on a linear interpolation of previously published log K_{assoc} values for calcium complexes as a function of the electrostatic function $[z_+z_-/(r_+ + r_-)]$. Such interpolation suggests that the association constant for $CaCrO_{4(aq)}$ should be very close to that of $CaSO_{4(aq)}$ ($\leq$2.3) due to the close similarity in the charges and thermochemical radii of CrO_4 and SO_4. The higher value of 2.69 suggests some degree of covalent bonding. Certainly other factors, including the presence of other complexes not included in the activity calculations, analytical errors, and the choice of the activity coefficient model, may affect estimates based on minimizing the variance in IAPs. Additional investigation of this complex is warranted but is beyond the scope of this study.

Table 4-4. Thermodynamic data used in modified MINTEQA2 database.

Reactions	kJ mol^{-1} $\Delta G°_r$	kJ mol^{-1} $\Delta H°_r$	J mol^{-1} K^{-1} $\Delta S°_r$	J mol^{-1} K^{-1} ΔC_P	Log K_{SP}	Source[a]
$H_2O - H^+ = OH^-$	79.85	55.81	-80.66	-212.5	-13.99	1,2
Aqueous Species						
$CrO_4^{2-} + 2H^+ = H_2CrO_4^o$	-39.8	-26.0	85	--	6.97[b]	3
$CrO_4^{2-} + H^+ = HCrO_4^-$	-37.10	5.13	141.6	163.2	6.50	9
$2CrO_4^{2-} + 2H^+ - H_2O = Cr_2O_7^{2-}$	-83.45	20.7	210.3	661	14.62	9
$Ca^{2+} + CrO_4^{2--} = CaCrO_4^0$	-15.81	--	--	--	2.77	4
$Ca^{2+} + H_2O - H^+ = CaOH^+$	73.22	77.47	14.6	-38.0	-12.83	1,2
$Al^{3+} + H_2O = AlOH^{2+} + H^+$	28.35	55.73	91.0	0.65	-4.97	1,5
$Al^{3+} + 2H_2O = Al(OH)^{2+} + 2H^+$	57.70	122.6	218	-225	-10.11	1,5
$Al^{3+} + 3H_2O = Al(OH)_3^0 + 3H^+$	95.15	176.4	--	--	-16.67	1,5
$Al^{3+} + 4H_2O = Al(OH)_4^- + 4H^+$	131.3	181.4	167.7	-91.8	-23.00	1,5
Solid Phases						
$Ca(OH)_2 = Ca^{3+} + 2H_2O - 2H^+$	-129.6	-129.6	0.02	31.71	22.70	1,2,6
$Al_2O_{3,\ corundum} = 2Al^{3+} + 3H_2O - 6H^+$	-96.63	-243.6	-491	-125	16.93	1,5
$Al_2O_{3,\ \gamma\text{-Alumina}} = 2Al^{3+} + 3H_2O - 6H^+$	-104.6	-265.9	-533	-93.0	18.33	1,5
$Al(OH)_{3,\ amph} = Al^{3+} + 3H_2O - 3H^+$	-61.65	-110.8	--	--	10.8	7
$AlOOH,\ _{boehemite} = Al^{3+} + 2H_2O - 3H^+$	-43.60	-116.2	-243	-23.5	7.64	1,2,8
$AlOOH,\ _{diaspore} = Al^{3+} + 2H_2O - 3H^+$	-40.00	-112.0	-241	-22.4	7.01	1,2,8
$Al(OH)_3,\ _{gibbsite} = Al^{3+} + 3H_2O - 3H^+$	-44.26	-105.3	-205	14.3	7.75	1,2,8
$Ca_6[Al(OH)_6]_2(CrO_4)_3 \cdot 26H_2O \rightleftharpoons 6Ca^{2+} + 2Al(OH)_4^- + CrO_4^{2-} + 4OH^- + 26H_2O$	236.6 ± 3.9	77.5 ± 9.5	-534 ± 87	-1510 ± 140	-41.46 ± 0.30	4

[a] Multiple sources indicate sources for individual ion or solid phase data that were used in calculating data presented. 1. Cox et al., 1989; 2. Shock et al., 1997; 3. Ball and Nordstrom, 1998; 4.This Study; 5. Nordstrom and May, 1996; 6. Garvin et al., 1987; 7. Nordstrom et al., 1990; 8: Hemingway and Sposito, 1996; 9: Baron and Palmer, 1998.

[b] Calculated from $\Delta G°r$ from Ball and Nordstrom, 1998.

Table 4-5. Equilibrium activities and ion activity products calculated without $CaCrO_{4(aq)}$ for 25ºC $Ca_6[Al(OH)_6]_2(CrO_4)_3 \cdot 26H_2O$ dissolution experiments.

Smple Batch	pH	Log $\{Ca^{2+}\}$	Log $\{Al(OH)_4^-\}$	Log $\{CrO_4^{2-}\}$	Log $\{OH^-\}$	Log $\{Na^+\}$	Ionic Strngth (m)	C.B. Err[a] (%)	-Log IAP
25-10.5	11.04	-2.48	-2.75	-2.62	-2.94	-3.08	0.02283	3.82	40.01 ±0.13
25-11.0	11.14	-2.52	-2.81	-2.59	-2.85	-2.70	0.02487	±0.71	39.98 ±0.14
25-11.5	11.35	-2.63	-3.02	-2.62	-2.65	-2.47	0.02059	±1.27	40.28 ±0.03
25-11.5r	11.42	-2.59	-3.24	-2.62	-2.58	-2.49	0.02175	2.93	40.17 ±0.05
25-12.0	11.85	-2.73	-3.74	-2.76	-2.15	-2.06	0.02297	7.34	40.76 ±0.07
25-12.0r[b]	11.62	-2.34	-4.01	-2.88	-2.38	-2.14	0.04123	<1%	40.20 ±0.12
25-12.5[b,c]	12.13	-2.42	-4.88	-3.04	-1.87	-1.64	0.05757	<1%	40.94 ±0.11

[a] Charge balance error. Charge balance errors represent means of absolute values from replicate errors. Positive values indicate excess cations, negative values indicate excess anions; ± indicates both excess cations and anions within sample replicates.

[b] "Post-precipitation" samples; dissolution induced in precipitation experiment samples by diluting with NaOH solution. (NO_3^-) calculated via charge balance equation.

[c] Samples not included in subsequent calculations based on lack of confirmation of $Ca_6[Al(OH)_6]_2(CrO_4)_3 \cdot 26H_2O$ from XRD analyses of solid residues.

Table 4-6. Equilibrium activities and ion activity products calculated without $CaCrO_{4(aq)}$ for 25ºC $Ca_6[Al(OH)_6]_2(CrO_4)_3 \cdot 26H_2O$ precipitation experiments[d].

Smple Batch	pH	Log $\{Ca^{+2}\}$	Log $\{Al(OH)_4^-\}$	Log $\{CrO_4^{-2}\}$	Log $\{OH^-\}$	Log $\{Na^+\}$	Ionic Strngth (m)	C.B. Err[a] (%)	-Log IAP
P25-10.5	10.90	-2.08	-2.96	-2.91	-3.12	-3.26	0.0634	-4.55	39.68 ±0.07
P25-10.5r	10.97	-2.16	-3.13	-2.98	-3.03	-3.58	0.0684	-6.84	40.24 ±0.35
P25-11.5	11.14	-2.09	-3.29	-2.95	-2.86	-2.61	0.0651	±0.70	39.44 ±0.04
P25-11.5r	11.30	-2.16	-3.61	-2.99	-2.70	-2.56	0.0542	-3.30	39.99 ±0.08
P25-12.0	11.54	-2.15	-3.98	-3.03	-2.46	-2.21	0.06236	-1.92	39.78 ±0.07
P25-12.5[b]	12.15	-2.20	-5.52	-3.14	-1.84	-1.71	0.07489	0.75	41.09 ±0.02

[a] Charge balance error. Charge balance errors represent means of absolute values from replicate errors. Positive values indicate excess cations, negative values indicate excess anions; ± indicates both excess cations and anions within sample replicates.

[b] "Post-precipitation" samples; dissolution induced in precipitation experiment samples by diluting with NaOH solution. (NO_3^-) calculated via charge balance equation.

[c] Samples not included in subsequent calculations based on lack of confirmation of $Ca_6[Al(OH)_6]_2(CrO_4)_3 \cdot 26H_2O$ from XRD analyses of solid residues.

[d] Log $\{NO_3^-\}$ values are: -1.66 for P25105r; -1.61 for P25115r; -1.55 for all other samples.

In an attempt to determine a standard state enthalpy for the formation of $CaCrO_{4(aq)}$ we conducted a series of MINTEQA2 runs on the data collected at the other temperatures (Table 4-6) to determine the values at which sample variance was minimized. Four of the six resulting log $K_{CaCrO4(aq)}$ values were similar to that determined for the 25ºC samples, ranging from 2.60 to 3.02. The remaining two values, 0.29 for the 5ºC samples and 3.80 for the 35ºC samples, were considered outliers. The 35ºC samples had the highest variability, suggesting that experimental errors overshadowed the effects of the $CaCrO_{4(aq)}$ complex. The 5ºC samples exhibited the smallest degree of variation in pH. Attempts to fit the log $K_{CaCrO4(aq)}$ from the five remaining temperatures (2.81 for 15ºC; 2.69 for 25ºC, 3.02 for 45ºC, 2.74 for 60ºC; and 2.60 for 75ºC samples) to both a constant enthalpy and constant heat capacity model resulted in statistically insignificant coefficients. However, the similarity of the five log $K_{CaCrO4(aq)}$ values and the fact that they are well within the range listed by Langmuir (1979) for divalent complexes suggests that the mean value of 2.77 ±0.16 (standard deviation) represents a reasonable estimate and should provide more meaningful results for chemical speciation calculations than would be obtained by ignoring this complex.

Using log $K_{CaCrO4(aq)}$ = 2.77, the log IAPs calculated for the 25ºC samples, excluding the "12.5" pH samples, varied between –41.87 and –40.93 (Figure 4-5). Student t-tests indicate that the slope of the IAPs versus pH for the dissolution samples, precipitation samples, and all 25ºC samples are not significantly different from zero at the 95% confidence level (e.g., t = -1.08, df = 9 for all samples). An F-

test indicates that the variance in log IAP values between samples is significantly different than the variance in the replicate values at the 95% confidence level (F = 19.4; df1 = 10; df2 = 17). Clearly the factors influencing random variability were more closely controlled within a given set of replicates. The charge balance errors calculated for the dissolution samples range from <1% to 9% (Table 4-7). It should be noted that activities for two of the seven dissolution samples (post-precipitation samples) were calculated by estimating (NO_3^-) based on minimizing the charge balance errors. The mean charge balance error, excluding these samples, is 3.4%. The charge balance errors for precipitation samples ranged from <1% to 7.5%, with a mean value of 2.3%.

The mean log IAP values for the 25ºC dissolution and precipitation samples are –41.62 ±0.16 and –41.26 ±0.28, respectively. The reported errors are total standard deviations (t.s.d.), representing the error in both samples and replicates. A Student's t-test for samples with unequal variances shows that the difference between the means of the IAPs of the dissolution and precipitation samples is significantly different than zero at the 95% confidence level (t = 2.54; df = 6) but not at the 97.5% confidence level. The difference in the means of both groups (0.36 log units) is approximately that expected from a nominal 5% analytical error (0.33 log units). The slightly higher IAPs and the greater degree of variability of IAPs calculated for the precipitation samples may be due to: 1) the estimation of (NO_3^-) based on the strength and amount of $Ca(NO_3)_2$ spike used; and 2) the possibility that precipitation kinetics may have been slower than dissolution and that some of the sample replicates may not have fully

achieved equilibrium. The average log IAP obtained from the means of both dissolution and precipitation experiments is –41.46 ±0.30 (t.s.d.).

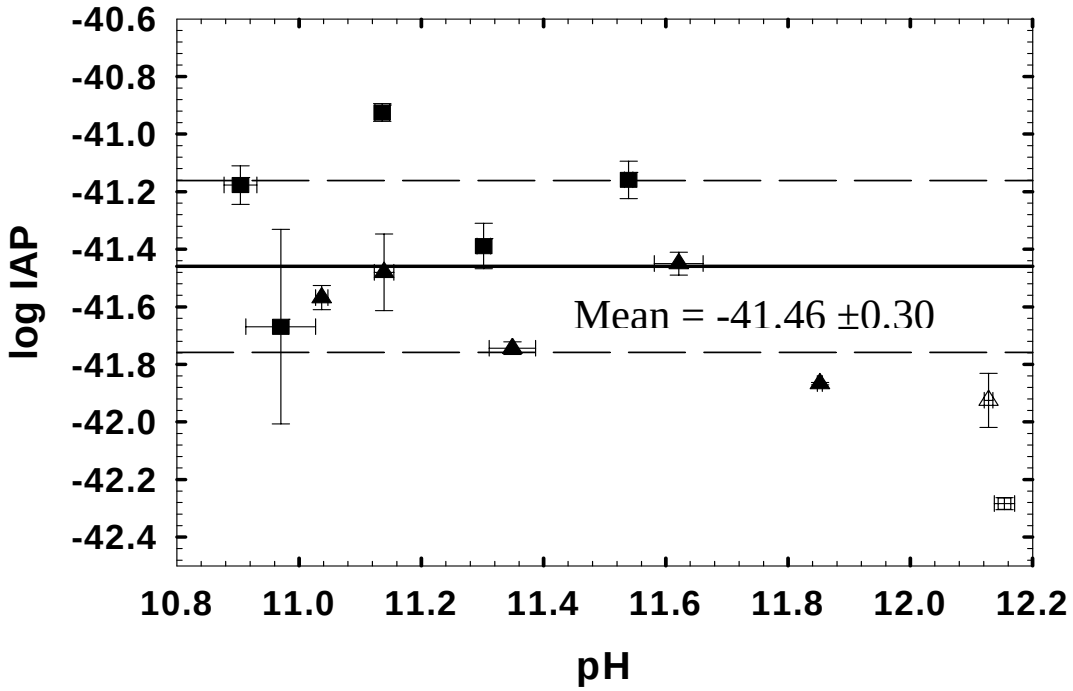

Figure 4-5. Calculated log ion activity products of $Ca_6[Al(OH)_6]_2(CrO_4)_3 \cdot 26H_2O$ dissolution (←) and precipitation (□) experiments versus pH at 25ºC. The open symbols represent samples from 12.5 pH experiments that were discarded based on XRD results.

Table 4-7. Equilibrium activities and ion activity products calculated with $CaCrO_{4(aq)}$ for 25ºC $Ca_6[Al(OH)_6]_2(CrO_4)_3 \cdot 26H_2O$ dissolution and precipitation experiments.

Sample Batch	pH	Log $\{Ca^{2+}\}$	Log $\{Al(OH)_4^-\}$	Log $\{CrO_4^{2-}\}$	Log $\{OH^-\}$	Log $\{Na^+\}$	Ionic Strngth (m)	C.B. Err.[a] (%)	(-) Log IAP
25°C Dissolution Samples									
25-10.5[b]	11.04	-2.63	-2.72	-2.83	-2.96	-3.07	0.01469	3.12	41.57 ±0.04
25-11.0	11.14	-2.68	-2.80	-2.80	-2.86	-2.85	0.01448	±1.03	41.48 ±0.13
25-11.5	11.35	-2.80	-3.01	-2.78	-2.65	-2.47	0.01442	±1.53	41.74 ±0.02
25-11.5r	11.42	-2.74	-3.23	-2.79	-2.58	-2.48	0.01499	4.54	41.63 ±0.05
25-12.0	11.85	-2.85	-3.74	-2.91	-2.15	-2.05	0.01860	8.99	41.86 ±0.07
25-12.0r[c]	11.62	-2.39	-4.01	-3.20	-2.38	-1.82	0.03522	<1%	41.45 ±0.10
25-12.5[c,d]	12.13	-2.46	-4.88	-3.30	-1.87	-1.67	0.05386	<1%	41.93 ±0.09
25°C Precipitation Samples[e]									
P25-10.5	10.90	-2.12	-2.98	-3.37	-3.09	-3.26	0.05583	-4.98	41.18 ±0.07
P25-10.5r	10.97	-2.18	-3.12	-3.40	-3.03	-3.58	0.04804	-7.47	41.67 ±0.34
P25-11.5	11.14	-2.11	-3.29	-3.40	-2.86	-2.61	0.05802	±1.86	40.93 ±0.03
P25-11.5r	11.30	-2.19	-3.61	-3.41	-2.70	-2.55	0.04843	-3.53	41.39 ±0.08
P25-12.0	11.54	-2.17	-3.98	-3.44	-2.46	-2.19	0.05676	-1.98	41.16 ±0.07
P25-12.5[c]	12.15	-2.22	-5.52	-3.50	-1.84	-1.71	0.07069	0.94	42.28 ±0.02

[a] Charge balance error. harge balance errors represent means of absolute values from replicate errors. Positive values indicate excess cations, negative values indicate excess anions; ± indicates both excess cations and anions within sample replicates.

[b] Excluding one replicate which had charge balance error > 10%.

[c] "Post-precipitation" samples; dissolution induced in precipitation experiment samples by diluting with NaOH solution. (NO_3^-) calculated via charge balance equation.

[d] Samples not included in subsequent calculations based on lack of confirmation of $Ca_6[Al(OH)_6]_2(CrO_4)_3 \cdot 26H_2O$ from XRD analyses of solid residues.

[e] Log $\{NO_3^-\}$ values are: -1.66 for P25105r; -1.61 for P25115r; -1.55 for all other samples.

The calculated log IAPs increase with increasing temperature with average values ranging from –42.63 ±0.52 at 5°C to –39.05 ±0.48 (t.s.d.) at 75°C (Table 4-8). Such a trend indicates a positive enthalpy of dissolution that is expected given the high degree of hydration for ettringite. However, there is no significant difference between the IAP values calculated for 60ºC and 75ºC samples based on t-testing of replicates (t = 0.94, 8 degrees of freedom). The apparent decrease in the slope of log IAP vs temperature indicates that the enthalpy of reaction is not constant. Filtrate from one of the 75ºC dissolution samples was analyzed by XRD to ensure that $Ca_6[Al(OH)_6]_2(CrO_4)_3 \cdot 26H_2O$ was still present. Although the largest peaks were attributed to the secondary solid, a prominent peak at 9.87 Å matches the {100} peak determined for the initial synthesized solid. Charge balance errors for the temperature-dependent samples range from <1% to 10.0% with an average value of 3.7%.

The temperature-dependent data (Table 4-8) were fitted to a constant heat capacity of reaction model (e.g. Nordstrom and Munoz, 1994):

(5)

$$\log Ksp = A - \left(\frac{B}{T}\right) + D \log T$$

where T is the temperature (K). The KSP values used to obtain the regression were not weighted. The calculated regression coefficients, A = 498.94 ±48.99, B = 27,499 ±2,257 K, and D = -181.11 ±16.74, are statistically significant (t-values of 10.16, 12.16, and 10.80, respectively) and the highest residual error is 0.06 log units for the 45ºC sample (Figure 4-6).

Table 4-8. Equilibrium activities and ion activity products calculated with $CaCrO_{4(aq)}$; temperature-dependent $Ca_6[Al(OH)_6]_2(CrO_4)_3 \cdot 26H_2O$ dissolution experiments.

Sample Batch	pH	Log $\{Ca^{2+}\}$	Log $\{Al(OH)_4^-\}$	Log $\{CrO_4^{2-}\}$	Log $\{OH^-\}$	Log $\{Na^+\}$	Ionic Strngth (m)	C.B. Err.[a] (%)	-Log IAP
5º-10.5	11.81	-2.68	-2.79	-2.97	-2.89	-3.34	0.01172	3.71	42.11 ±0.05
5º-10.5r	11.97	-2.75	-3.00	-3.07	-2.73	-3.17	0.00983	2.98	42.59 ±0.17
5º-11.5	12.32	-2.88	-3.33	-2.98	-2.39	-2.49	0.01174	±4.07	42.47 ±0.23
15º-10.5	11.64	-2.71	-2.97	-2.96	-2.70	-3.10	0.01158	±0.82	41.92 ±0.12
15º-11.5	11.90	-2.79	-3.31	-2.88	-2.44	-2.49	0.01377	±0.93	41.91 ±0.23
35º-10.5	10.94	-2.61	-2.88	-2.85	-2.73	-3.36	0.01479	2.14	40.91 ±0.10
35º-12.5	11.11	-2.76	-3.16	-2.71	-2.57	-2.40	0.01685	1.38	41.28 ±0.15
45º-10.5	10.45	-2.54	-2.71	-2.76	-2.93	-3.32	0.01841	5.03	40.66 ±0.31
45º-11.0	11.29	-2.90	-3.29	-2.79	-2.10	-2.00	0.02157	±2.52	40.74 ±0.16
60º-10.5	10.27	-2.55	-2.74	-2.85	-2.82	-3.16	0.01723	10.03	40.64 ±0.08
60º-11.5	1053	-2.70	-2.94	-2.84	-2.44	-2.37	0.0175	6.98	40.38 ±0.39
75º-10.5	9.90	-2.61	-2.64	-2.80	-2.69	-3.14	0.0178	±2.97	40.07 ±0.04
75º-11.5	10.03	-2.75	-2.80	-2.76	-2.56	-2.37	0.01751	2.19	40.70 ±0.03

a Charge balance error Charge balance errors represent means of absolute values from replicate errors. Positive values indicate excess cations, negative values indicate excess anions; ± indicates both excess cations and anions within sample replicates.

The temperature-dependent data were also fitted to a variable (linear) heat capacity of reaction model. However, the resulting coefficients were not significant (i.e. t-values < 1), implying that this model is over-parameterized and inappropriate for our solubility data. Therefore, the constant heat capacity of reaction model best represents the temperature dependence of the log K_{SP} over the temperature range of 5 to 75ºC.

The Gibbs free energy, heat capacity, entropy, and enthalpy of dissolution were calculated from

$$G^{o}_{r,T} = -\ln(10)RT \log K \quad \textbf{(6)}$$

$$\Delta C^{o}_{p,r} = DR \quad \textbf{(7)}$$

$$\Delta H^{o}_{r,T} = \ln(10)RB + \Delta C^{o}_{p,r} T \quad \textbf{(8)}$$

$$\Delta S^{o}_{r,T} = \ln(10)RA + \ln(10) \Delta C^{o}_{p,r} \log T + \Delta C^{o}_{p,r} \quad \textbf{(9)}$$

where R is the gas constant (8.31441 J mol^{-1} K^{-1}). The resulting standard state thermodynamic properties, using the regression value for log K, were $\Delta G^{o}_{r,298}$ = 236.6 ±3.9 kJ mol^{-1}, $\Delta C^{o}_{p,r}$ = -1,510 ±140 J mol^{-1} K^{-1}, $\Delta H^{o}_{r,298}$ = 77.5 ±9.5 kJ mol^{-1}, and $\Delta S^{o}_{r,298}$ = -533 ±87 J mol^{-1} K^{-1}. The errors are based on the standard errors of the regression coefficients except for the Gibbs free energy, for which the error is based on the t.s.d. of all 25ºC samples.

The Gibbs free energy of formation for $Ca_6[Al(OH)_6]_2(CrO_4)_3 \cdot 26H_2O$ is given by: **(10)**

$$\Delta G^\circ_{f,298,CrO4\text{-}ettringite} = 6\Delta G^\circ_{f,298}(Ca^{2+}) + 2\Delta G^\circ_{f,298}(Al(OH)_4^-) + 3\Delta G^\circ_{f,298}(CrO_4^{2-}) + 4\Delta G^\circ_{f,298}(OH^-) + 26\Delta G^\circ_{f,298}(H_2O) + \Delta G^\circ_{r,298,CrO4\text{-}ettringite.}$$

We calculated $\Delta G^\circ_{f,298} = -15{,}130 \pm 19$ kJ mol^{-1} using Equation (10) and the free energies of formation of the individual ions (Table 4-9). The error is calculated using the uncertainty associated with the K_{SP} value and the maximum calculated errors associated with the free energies of the individual ions. This value is slightly higher than the value of $-15{,}211 \pm 19$ kJ mol^{-1} previously calculated for ettringite (Perkins and Palmer, 1999).

Using the data in Table 8 and equations for ΔH°_f, ΔS°, and ΔC°_P analogous to Equation (10), we calculated the enthalpy of formation and entropy and heat capacity for $Ca_6[Al(OH)_6]_2(CrO_4)_3 \cdot 26H_2O$ to be $\Delta H^\circ_f = -17{,}330 \pm 15$ kJ mol^{-1}, $\Delta S^\circ = 2.19 \pm 0.11$ kJ mol^{-1} K^{-1}, and $\Delta C^\circ_P = 2.12 \pm 0.53$ kJ mol^{-1} K^{-1}. The errors are based on the errors calculated for the dissolution reaction parameters and the maximum calculated errors associated with individual ions. The calculated enthalpy and entropy values are similar to the values of $-17{,}550 \pm 16$ kJ mol^{-1} and 1.87 ± 0.059 KJ mol^{-1} K^{-1} previously calculated for ettringite (Perkins and Palmer, 1999). The temperature dependence of the ettringite log IAP was sufficiently linear over the same temperature range that

$\Delta C°_{P,r}$ was assumed to be zero, which helps to explain why the $\Delta C°_{P,ettringite}$ value of 590 ±143 J mol^{-1} K^{-1} is much lower than that calculated for the chromate analog.

Table 4-9. Thermodynamic data used in calculation of formation parameters.

	kJ mol^{-1}		J mol^{-1} K^{-1}		
Species	**$\Delta G°_f$**	**$\Delta H°_f$**	**$\Delta S°_f$**	**$\Delta C°_{P,f}$**	**Reference**
H_2O_{liquid}	-237.14	-285.83	69.95	75.351	1
	± 0.040	± 0.40	± 0.03	± 0.08	
OH^-	-157.3	-230.02	-10.7	-137.2	2
	± 2.0	± 0.6	± 1.9	± 16.7	
Ca^{2+}	-552.79	-543	-56.48	-31.5	2
	± 2.0	± 0.6	± 1.9	± 16.7	
CrO_4^{2-}	-724.2	-879	5.4	-261.9	3
	± 1.0	± 1.0	± 0.5	± 16.7	
$Al(OH)_4^-$	-1305	-1502.8	101.5	89.6	4
	± 2.0	± 1.6	± 10	± 12	
$Ca_6[Al(OH)_6]_2(CrO_4)_3 \cdot 26H_2O$	-15131	-17330	2190	2120	5
	± 19	± 15	± 110	± 530	

1). Cox et al., 1989;
2). Shock et al., 1997*;
3). Ball and Nordstrom , 1998; $\Delta C°_{P,f}$ from Shock et al., 1997;
4). Nordstrom and May, 1996;
5). Current Study.
*: Uncertainties are based on maximum values reported by Shock and Helgeson ,1988 over the temperature range of 0 to 100C

4.6 SUMMARY

$Ca_6[Al(OH)_6]_2(CrO_4)_3 \cdot 26H_2O$, the chromate analog of the mineral ettringite, was synthesized and the solubility product, standard-state Gibbs free energies and enthalpies of reaction and formation, as well as entropies and heat capacities were calculated from the data obtained in a series of dissolution and precipitation experiments conducted from 5 to 75°C. Equilibrium conditions were reached within 50 hours. IAPs decreased significantly with increasing pH (10.9 – 11.9) unless a $CaCrO_{4(aq)}$ complex was included in the thermodynamic data-set used to calculate ion

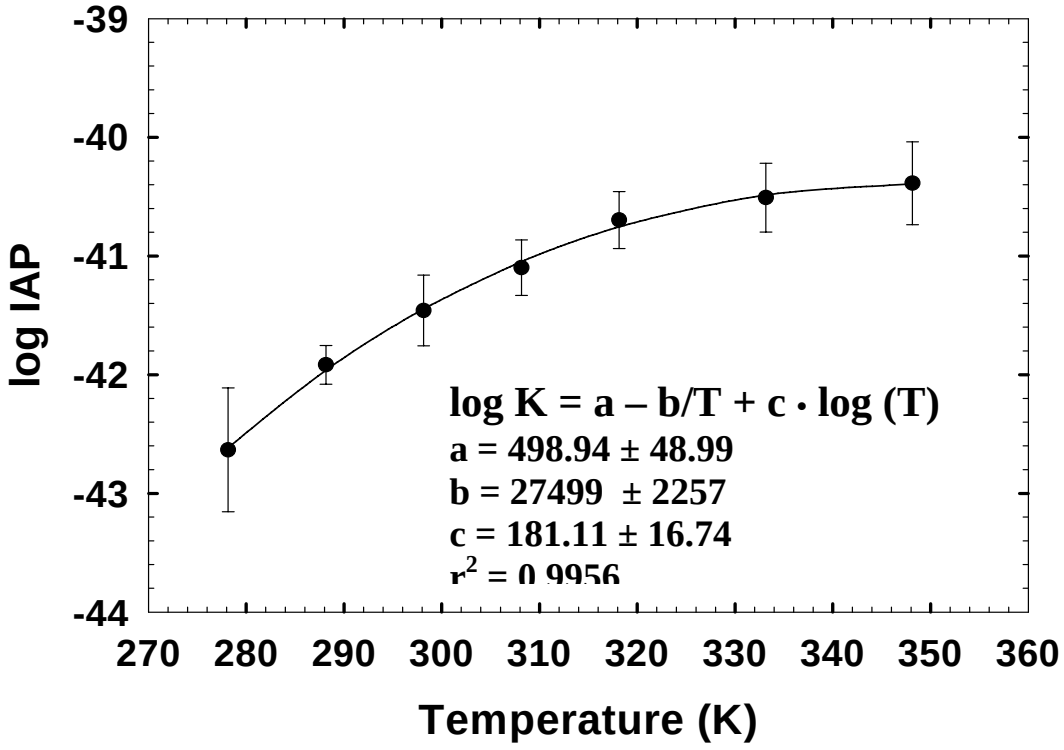

Figure 4-6. Log K_{SP} values for $Ca_6[Al(OH)_6]_2(CrO_4)_3 \cdot 26H_2O$ versus temperature.

activities. A formation constant for $CaCrO_{4(aq)}$ ($\log K_{CaCrO4(aq)} = \log\{CaCrO_{4(aq)}\} - \log\{Ca^{+2}\} - \log\{CrO_4^{-2}\} = 2.68$) was estimated by minimizing the variance in 25ºC samples. Values estimated in like manner for data collected at other temperatures were similar but we were unable to demonstrate significant temperature dependence for the $CaCrO_{4(aq)}$ formation constant and no enthalpy of formation was determined. The mean $\log K_{CaCrO4(aq)}$ value of 2.77 ±0.16 was therefore used in calculating ion activities for all experiments.

The solubility product and free energy of formation for $Ca_6[Al(OH)_6]_2(CrO_4)_3 \cdot 26H_2O$ were calculated to be log $K_{SP,298}$ = –41.46 ±0.30 and $\Delta G°_{f,298}$ = −15130 ±19 kJ mol^{-1}. A $\Delta H°_r$ of 77.5 ±9.5 kJ mol^{-1} was calculated from the temperature dependence of the solubility product and a $\Delta H°_f$ of -17330 ±15 kJ $mol^{-1}$was obtained from this value and enthalpy data for individual ions gathered from available literature. Similarly, $\Delta S°$ and $\Delta C°_P$ values of 2.19 ±0.11 and 2.12 ±0.53 kJ mol^{-1} K^{-1}, respectively, were also calculated. To our knowledge, these are the first solubiliy data published for $Ca_6[Al(OH)_6]_2(CrO_4)_3 \cdot 26H_2O$.

Chapter 5. The Solubility of Monochromate ($3CaO \cdot Al_2O_3 \cdot CaCrO_4 \cdot nH_2O$)

5.1 INTRODUCTION

Monosulfate ($3CaO \cdot Al_2O_3 \cdot CaSO_4 \cdot nH_2O$) is typically the dominant hydrated calcium alumina-sulfate phase present in mature Portland cement pastes. It is formed as the sulfate concentrations in the pore water decrease due to the formation of early hydration products, primarily ettringite ($Ca_6(Al(OH)_6)_2(SO_4)_3 \cdot 26H_2O$). The ettringite then reacts with tricalcium aluminate ($Ca_3Al_2O_6$), one of the primary clinker phases, to form the more sulfate-depleted monosulfate (Lea, 1970; Odler and Abdul-Maula, 1984). Both monosulfate and ettringite are known to allow ionic substitution, including Fe^{3+} for the Al^{3+} and OH^-, CO_3^{2-}, SeO_4^{2-}, and CrO_4^{2-} for SO_4^{2-} (Carlson and Berman, 1960; Lea, 1970; Odler and Abdul-Maula, 1984; Poellman et al., 1993; Poellmann et al., 1990; Reardon, 1990). The widespread use of cement and concrete and the ability of monosulfate to structurally incorporate toxic ions makes it important with regards to the mobility of pollutants in the environment, remediation of contaminated sites, and waste immobilization in cementitious materials.

Substitution of hexavalent chromium in monosulfate is of particular interest as chromium is a widespread pollutant that is acutely toxic, teratogenic, mutagenic, and carcinogenic (Nieboer and Shaw, 1988; Nordberg, 1988; O'Brien and Kortenkamp, 1994; Sugiyama, 1994). Chromium is a frequently cited contaminant at hazardous waste sites and may be found in several types of alkaline environments including naturally alkaline soils, fly ash, cement and concrete, chromite ore processing wastes,

and basic waste mixtures. Hexavalent chromium in alkaline solutions primarily occurs as CrO_4^{2-}. The identical charge, similar structure, and comparable thermochemical radii of CrO_4^{2-} and SO_4^{2-} suggest that chromate should readily substitute in the crystal structure of monosulfate. However, although chromate substitution in ettringite has been documented (Kumarathasan et al., 1990; Poellman et al., 1993), we are unaware of any similar reports for monosulfate. Given that monosulfate is typically present in mature cements, often in the absence of ettringite, it is especially important to understand the potential for its chromate analog (monochromate) to act as a solubility control with respect to long-term immobilization of Cr(VI) in cementitious materials.

The purpose of this study is to measure the solubility of $3CaO{\cdot}Al_2O_3{\cdot}CaCrO_4{\cdot}15H_2O$ and to determine its solubility product (K_{SP}) from 5 to 75ºC. Thermodynamic properties for this phase will be calculated from this information. The results of this study should be useful to workers dealing with chromium migration and waste immobilization in alkaline environments as well as material scientists developing new cements.

5.2 BACKGROUND

The formation of monosulfate from tricalcium aluminate ($Ca_3Al_2O_6$) and gypsum ($CaSO_4{\cdot}2H_2O$) in water has long been thought to occur in two stages. In the first step, hydration of $Ca_3Al_2O_6$ in the presence of gypsum yields ettringite ($Ca_6(Al(OH)_6)_2(SO_4)_3{\cdot}26H_2O$):

$$Ca_3Al_2O_6 + 3CaSO_4 \cdot 2H_2O + 30H_2O = Ca_6(Al(OH)_6)_2(SO_4)_3 \cdot 26H_2O \quad \textbf{(1)}$$

As the aqueous sulfate concentrations decrease and the hydration of $Ca_3Al_2O_6$ continues, the ettringite is converted to monosulfate:

(2)

$$Ca_6(Al(OH)_6)_2(SO_4)_3 \cdot 26H_2O + 2Ca_3Al_2O_6 + 4H_2O = 3CaO \cdot Al_2O_3 \cdot CaSO_4 \cdot 12H_2O$$

The degree of hydration of monosulfate is variable and the subject of some dispute. The hydration state having twelve waters of hydration as shown in Equation (1) is the most commonly cited hydration state. However, Kuzel (1996) determined 14 waters of hydration based on X-ray diffraction (XRD) analyses performed in the presence of water. Differing hydration states alter some d-spacings and Lea (1970) lists the characteristic d-spacings for monosulfates with 7, 10, 12, and 15 waters of hydration. The hydration largely depends on the relative humidity of the atmosphere in contact with the solid and the changes in the hydration are generally reversible (Lea, 1970).

Of greater dispute is the manner in which the intermediate phase, ettringite, reacts to form monosulfate. The initial hydration has been thought to proceed according to Equation (1) until one third of the tricalcium aluminate is utilized in the formation of ettringite. The newly-formed ettringite then forms a protective coating around the remaining tricalcium aluminate, allowing only diffusive transport of H_2O and SO_4^{2-} to the reactive tricalcium aluminate surface. However, once the

gypsum has been entirely consumed and the aqueous SO_4^{2-} concentration drops below a critical threshold, the ettringite becomes unstable and undergoes transformation to monosulfate (Hampson and Bailey, 1982). Studies of mature cement pastes show the presence of monosulfate and, typically, an absence of ettringite. However, XRD studies utilizing "wet cell" samples of hydrated cements indicate that ettringite may persist and that monosulfate appears only in pastes free of CO_2 (Kuzel, 1996). In pastes with greater than 0.5% CO_2, hemicarbonate ($4Ca_3Al_2O_6 \cdot CaCO_3 \cdot Ca(OH)_2 \cdot 22H_2O$) was formed in the presence of ettringite. $Ca_4Al_2O_7 \cdot 13H_2O$ forms as a metastable phase from hydration of the tricalcium aluminate (Warren and Reardon, 1994). The reaction of ettringite with $Ca_4Al_2O_7 \cdot 13H_2O$ yields monosulfate. However, any remaining $Ca_4Al_2O_7 \cdot 13H_2O$ eventually transforms to the more stable $Ca_3Al_2O_6 \cdot 6H_2O$ (hydrogarnet) and ettringite is more stable than monosulfate in the presence of this phase. Ettringite transforms to monosulfate and gypsum at temperatures >90ºC (Ghorab and Kishar, 1985).

5.3 METHODS

The results discussed in the following sections are based on continued interpretation of data obtained from a previous study. The specific methodology for synthesis and characterization of the initial solid, dissolution and precipitation experiments, and analyses of the resulting solutions are detailed in our $Ca_6[Al(OH)_6]_2(CrO_4)_3 \cdot 26H_2O$ solubility study (Perkins and Palmer, 2000).

Equilibrium with monochromate was achieved by equilibrating solutions with $Ca_6[Al(OH)_6]_2(CrO_4)_3 \cdot 26H_2O$ which was synthesized from suspensions of

$3CaO \cdot Al_2O_3$ and $CaCrO_4$ using a modification of a method described by Odler and Abdul-Maula (1984). Both dissolution and precipitation experiments were conducted at 25ºC in HDPE bottles using N_2-purged solutions.

Solutions were prepared in a glove box equipped with a CO_2-scrubber. HDPE bottles were sealed in glass mason jars before removing them from the chamber. The jars were kept in a water bath at a constant temperature (±0.3ºC) for a minimum of 14 days, well after the 2 days required to achieve steady-state concentrations of analytes. In addition to the experiments conducted at 25ºC, a series of experiments were conducted at 5, 15, 35, 45, 60 and 75ºC.

Measurements of pH were made within the glove box at the time of sampling. The pH meter was calibrated using pHydrion® 7.00. 10.00, and 12.00 buffers. The samples were filtered through 0.45-μm polysulfone membrane filters. Samples intended for cation analysis were preserved with HNO_3 (5% solution). Ca and Al were analyzed by atomic absorption spectroscopy using a lanthanum matrix modifier. Cr(VI) was analyzed colorimetrically (3500-Cr D; APHA, 1995) using the diphenylcarbizide method and measuring the absorbance at 540 nm on a Beckman DU 640 spectrophotometer. Powder X-ray diffraction (XRD) analyses of the solids that were present at the end of the experiments were obtained using CuKα radiation on a Norelco XRG 3000 unit.

5.4 RESULTS AND DISCUSSION

5.4.1. Powder X-ray Diffraction

The concentrations of Ca, Al, and Cr(VI) obtained from solutions equilibrated with synthesized $Ca_6[Al(OH)_6]_2(CrO_4)_3 \cdot 26H_2O$ are presented in Perkins and Palmer (2000). The stoichiometry of these solutions was found to differ from that of the initial solid, suggesting the formation of a secondary precipitate. XRD patterns of solid residue from the dissolution experiments show the presence of peaks not observed in the initial solid. These peaks were attributed to a secondary precipitate. Specifically, the XRD patterns (Table 5-1) show a decrease in the relative intensity of the {100} peak (d-spacing of 9.87 Å) and the appearance of a prominent peak at 10.21-10.27 Å. Likewise, the {110} peak (d-spacing of 5.05-5.08 Å) is also diminished and the {112} peak strengthened in relative intensity. A new peak at ~5.15-5.18 Å was observed in some samples. The peaks associated with the secondary phase dominate the XRD pattern of the highest pH samples. The XRD pattern for the "12.5" pH sample residue was missing both the {100} and {110} peaks (Figure 5-1). Unit cell dimensions were calculated for all residues, both with and without the 10.21- 10.27 and 5.15-5.18 Å peaks. Residual errors for the 10.21 and 10.27 Å peaks were higher than the errors calculated for the other peaks, exceeding 0.1 Å. The a_0 dimension calculated for the "12.5" pH sample was significantly different than the initial synthesized material and the standard errors calculated for both dimensions were relatively large (a_0 = 12.03 ±1.18 and c_0 = 21.36 ±3.89 Å). Based on these results, the

"12.5" pH samples were not included in subsequent calculations of the solubility product for $Ca_6[Al(OH)_6]_2(CrO_4)_3 \cdot 26H_2O$.

Myneni (1995) also observed a diminished {100} peak and the appearance of a new peak at 10.33 Å when Cr(VI) concentrations exceeded 1.29 mM in coprecipitation experiments conducted with sulfate ettringite. Although not specifically noted, Myneni's XRD patterns also show the {112} peak diminishing in relative intensity with increasing Cr(VI) concentrations. The XRD pattern for the chromate ettringite phase synthesized by Kumarathasan et al. (1990) has a larger d-spacing (e.g., ~10.1 Å) than did our initial synthesized material, and lacks the {110} peak which should occur near 15.5° 2θ.

Myneni (1995) notes that the slightly larger radius of CrO_4^{2-} over SO_4^{2-} does not adequately explain the increase in d-spacing to 10.33 Å. He also concluded, as did we, that Ca and Al chromate compounds listed in the ICDD database do not exhibit strong reflections at d-spacings of 10.2-10.3 Å. However, monosulfate exists in several forms, presumably dependent on the degree of hydration, each having a different X-ray pattern. Lea (1970) lists 10.3, 5.15, 4.03, and 2.87 Å d-spacings for $C_3A \cdot CaSO_4 \cdot 15H_2O$. Two of these d-spacings correspond well with major peaks (10.27, 5.15 Å) that appeared in the XRD patterns of the experimental residues but not in the initial solid. A third peak (2.87 Å) was noted but was also present in the initial synthesized solid XRD pattern. The JCPDS card 44-0602 for $Ca_4Al_2SO_{10} \cdot 16H_2O$ lists d-spacings of 10.23, 5.11, 3.41, 2.56, and 2.04 Å. The first four of these d-spacings correspond to XRD peaks (10.21-10.27, 5.15-5.18, 3.38-3.44, and 2.53 Å) obtained for

the experimental residues but which were not observed in XRD patterns for the initial synthesized solid. The relative intensity of the fifth peak is only 4% and so the corresponding peak in our XRD pattern may not be distinguishable from the background. Three other peaks which do not correspond to $Ca_6[Al(OH)_6]_2(CrO_4)_3 \cdot 26H_2O$ correspond to calcite (Table 5-1) which may have formed during XRD sample preparation which took place outside the glove-box.

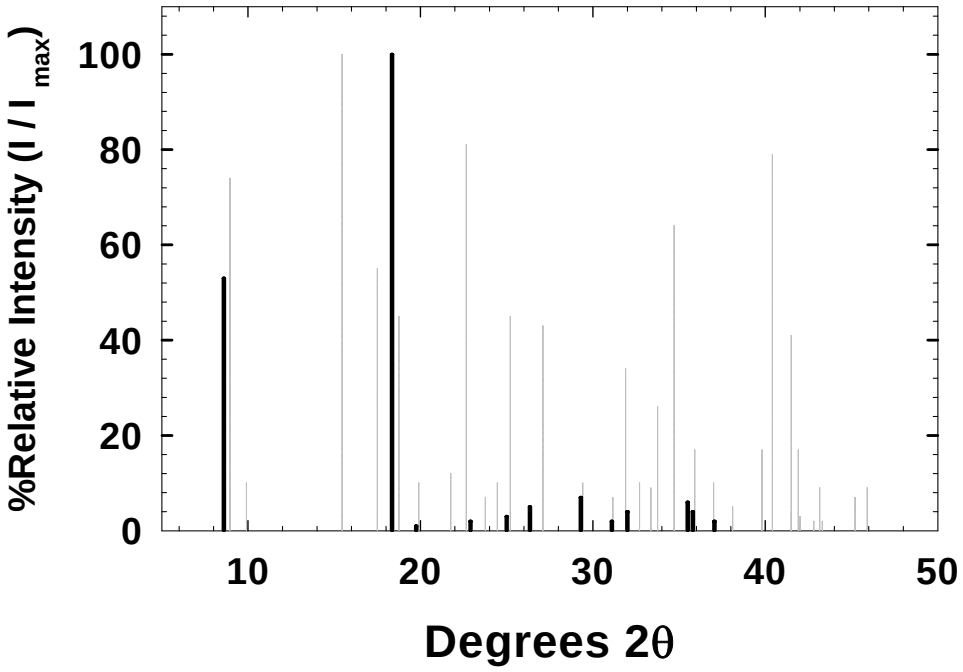

Figure 5-1. X-ray diffraction peaks from analyses of synthesized $Ca_6[Al(OH)_6]_2(CrO_4)_3 \cdot 26H_2O$ (gray) and solid residues from solubility experiments at initial pH ≈ 12.5 (black).

The presence of a corresponding "monochromate" would be consistent with the discrepancies observed in our XRD results and in Kumarathasan et al.'s (1990) solid stoichiometry. The coexistence of monochromate and the Cr(VI) analog of ettringite is not unexpected as mixtures of monosulfate and ettringite are known to form when the $CaSO_4$:Al_2O_3 ratio exceeds unity (Lea, 1970). Palmer (2000) also found a Cr(VI)-bearing ettringite phase together with an almost pure monochromate in samples of concrete which had been contaminated with chrome-plating solutions. Based on the analogy with the Ca-Al-SO_4-H_2O system, the observations of monochromate and a Cr(VI) analog of ettringite in Cr(VI)-contaminated concrete, and the correspondence of secondary XRD peaks with available monosulfate XRD patterns, we have identified the secondary phase as a heavily hydrated "monochromate."

The stability of ion concentrations over time suggests that equilibrium was achieved in our experiments. The presence of the peaks for both the Cr(VI) analog of ettringite and monochromate in all samples with pH < 12.5 suggests that equilibrium is attained with both phases. For the "12.5" pH samples, the ion activity products (IAPs) calculated for the dissolution of the chromate analog of ettringite were significantly lower than those calculated for the other samples. The low IAPs and decidedly uncharacteristic ettringite XRD patterns obtained for these samples indicate they were equilibrated only with the monochromate phase.

The relative intensities of the monochromate XRD peaks also increase with the temperature of the dissolution experiment. Filtrate from one of the 75ºC dissolution

samples was analyzed by XRD to ensure that $Ca_6[Al(OH)_6]_2(CrO_4)_3 \cdot 26H_2O$ was still present. Peaks corresponding to 10.10 and 5.15 Å are so dominant in the resulting XRD pattern that many chromate-ettringite peaks may be obscured (Table 5-1). However, a prominent peak at 9.87 Å matches the {100} peak determined for the. initial synthesized solid, again indicating both phases were present. An increase in the relative mass of monochromate with increasing temperature is to be expected. Indeed, one method described for synthesis of monosulfate is to heat a suspension of ettringite to 100ºC (Ghorab and Kishar, 1985).

5.4.2. Dissolution and Precipitation Experiments

As noted, the observed molar ratios of ions in solution do not agree with the ideal or measured solid stoichiometry of $Ca_6[Al(OH)_6]_3(CrO_4)_3 \cdot 26H_2O$. The excess CrO_4^{2-} in solution is consistent with the precipitation of the monochromate phase indicated by the XRD results, which would preferentially remove a greater fraction of Ca and Al from solution. The diminished Al concentrations observed in the higher pH samples may be the result of precipitation of aluminum hydroxides or oxyhydroxides. Solutions with pH >11.35 are near saturation with respect to boehmite, diaspore, and gibbsite.

Table 5-1. Comparison of powder X-ray diffraction peaks from synthetic $Ca_6[Al(OH)_6]_2(CrO_4)_3 \cdot 26H_2O$ with peaks from ettringite JCPDS Card 9-414 and experimental residual filtrates.

	Ettringite JCPDS 9-414		Initial Synthesized Cr(VI)-Ettringite		Solid Filtrate 25ºC, pH 10.5 Precipitation Experiment		Solid Filtrate 25ºC, pH 12.0 Dissolution Experiment		Solid Filtrate 25ºC, pH 12.5 Dissolution Experiment		Solid Filtrate 75ºC, pH 10.5 Dissolution Experiment	
h,k,l[a]	d(Å)	I/I_{max}	d(Å)	I/I_{max}	d(Å)	I/I_{max}	d(Å)	I/I_{max}	d(Å)	I/Imax	d(Å)	I/I_{max}
MC	--	--	--	--	10.21	83	10.21	68	10.27	53	10.10	97
100	9.73	100	9.87	74	9.87	27	--	--	--	--	9.87	32
101	8.86	14	8.93	10	--	--	--	--	--	--	--	--
110	5.61	80	5.73	100	5.69	20	5.71	1	--	--	--	--
MC	--	--	--	--	5.18	100	--	--	--	--	5.15	100
112	4.98	25	5.06	55	5.05	11	5.08	100	--	--	--	--
MC	--	--	--	--	--	--	--	--	4.83	100	--	--
200	4.86	8	--	--	--	--	--	--	--	--	--	--
104	4.69	35	4.73	45	4.72	2	--	--	--	--	--	--
314	4.41	4	--	--	--	--	--	--	--	--	--	--
113	--	--	4.46	10	--	--	4.48	5	4.49	1	--	--
203	4.02	2	4.08	12	--	--	--	--	--	--	--	--
114	3.88	50	3.92	81	3.91	8	--	--	--	--	--	--
Cal	--	--	--	--	3.86	5	3.87	2	3.88	2	3.87	8
210	3.67	8	3.74	7	3.72	2	--	--	--	--	--	--
204	3.60	16	3.64	10	--	--	--	--	--	--	--	--
212	3.48	30	3.53	45	3.50	7	3.55	11	3.56	3	--	--
MC	--	--	--	--	3.44	27	3.37	11	3.38	5	3.44	28
213	3.27	6	--	--	--	--	--	--	--	--	--	--
300	3.240	20	3.29	43	3.28	6	--	--	--	--	--	--
Cal	--	--	3.04	10	3.04	46	3.04	12	3.05	7	3.04	62
116	3.016	8	--	--	--	--	--	--	--	--	--	--
220	2.806	8	2.87	7	2.87	5	2.88	7	2.87	2	2.88	18
304	2.773	40	2.80	34	2.80	8	2.79	6	2.79	4	--	--
222	2.714	8	--	--	--	--	--	--	--	--	--	--
310	2.697	14	2.74	10	2.74	5	--	--	--	--	--	--
008	2.68	8	2.68	9	--	--	--	--	--	--	--	--
312	2.616	20	2.65	26	2.65	10	--	--	--	--	--	--
216	2.564	45	2.58	64	2.59	3	--	--	--	--	2.59	13
MC?	2.524	6	--	--	--	--	2.53	6	2.53	6	--	--
400	2.434	4	2.50	17	2.49	10	2.50	11	2.51	4	2.50	20
118	2.422	4	2.43	10	--	--	2.42	6	2.42	2	--	--
306	2.401	12	--	--	--	--	--	--	--	--	--	--
208	2.347	6	2.36	5	--	--	--	--	--	--	--	--
Cal	--	--	--	--	2.29	12	2.29	2	--	--	2.29	17
320	2.23	20	2.26	17	2.26	5	2.25	21	--	--	--	--
226	2.209	45	2.23	79	2.23	8	--	--	--	--	--	--
322	2.185	10	--	--	--	--	--	--	--	--	--	--
316	2.154	25	2.17	41	2.17	4	--	--	--	--	--	--
323	2.13	4	2.15	17	2.15	3	--	--	--	--	--	--
410	2.124	6	2.11	7	--	--	--	--	--	--	--	--
412	2.081	6	2.09	2	2.09	9	--	--	--	--	2.10	13
325			--	--	--	--	--	--	--	--	--	--
414	--	--	2.00	7	--	--	--	--	--	--	--	--

[a]"MC" denotes monochromate ($3CaO \cdot Al_2O_3 \cdot CaCrO_4 \cdot nH_2O$); "Cal"denotes calcite ($CaCO_3$)

Aqueous activities for Ca^{2+}, $Al(OH)_4^-$, and CrO_4^{2-} as well as Na^+ and NO_3^- were calculated with the geochemical speciation model MINTEQA2 (Allison et al., 1990) using the Davies Equation:

(3)

$$\log \gamma_i = -AZ_i^2\left(\frac{\sqrt{I}}{1+\sqrt{I}} - 0.24I\right)$$

The databases used by MINTEQA2 were first modified to include pertinent, updated thermodynamic data from available literature (Table 5-2). Ion activity products (IAPs) for the dissolution reaction

(4)

$$3CaO{\cdot}Al_2O_3{\cdot}CaCrO_4{\cdot}15H_2O = 4Ca^{2+} + 2Al(OH)^-_4 + CrO_4^{2-} + 4OH^- + 9H_2O$$

were calculated from the activities using

$$IAP = \{Ca^{+2}\}^4\{Al(OH)_4^-\}^2\{CrO_4^{-2}\}\{OH^-\}^4\{H_2O\}^9 \qquad \textbf{(5)}$$

At equilibrium, the IAP equals the solubility product, K_{SP}. The log IAPs calculated for all 25ºC samples (Table 5-3) vary by less than one log unit from –30.83 to –29.89 (Figure 5-2). The maximum value is associated with a sample with pH near the mid-range of values. Although the lowest value is associated with the

highest pH (12.15), the sample with the next highest pH (12.13) has a corresponding log IAP (-30.39) very near the average value of –30.38. Student t-tests indicate that the slope of the IAPs versus pH for all 25ºC samples is not significantly different from zero at the 95% confidence level (t = -0.74, df = 11 for all samples). An F-test indicates that the variance in log IAP values between samples is significantly different from the variance in the replicate values at the 95% confidence level (F = 23.9; df_1 = 12; df_2 = 21). Thus, the factors influencing such variability were more closely controlled within a given set of sample replicates than between samples. The charge balance errors for the dissolution samples, range from <1 to 9% (Table 5-3). Activities for two of the seven dissolution samples (post-precipitation samples) were calculated by estimating [NO_3^-] based on minimizing the charge balance errors. The average value of charge balance errors, excluding these samples, is 3.4%. The charge balance errors for precipitation samples ranged from < 1 to 7.5%, with an average value of 2.3%.

The mean log IAP value for the 25ºC dissolution and precipitation samples is –30.48 ±0.14 and –30.26 ±0.36, respectively. The reported errors are total standard deviations (t.s.d.), representing the error in both samples and replicates. A Student's t-test for samples with unequal variances shows that the difference between the means of the IAPs of the dissolution and precipitation samples are not significantly different than zero at the 95% confidence level (t = 1.45; df = 6). The average log IAP obtained from the means of both dissolution and precipitation experiments is –30.38 ±0.28 (t.s.d.).

5.4.3. Temperature-Dependent Experiment

The calculated log IAPs increase with increasing temperature, ranging from –30.83 ±0.01 at 5°C to –29.65 ±0.04 at 75°C (Table 5-4). Thus, a positive enthalpy of reaction, $\Delta H°_r$, for the dissolution of monochromate is indicated. The dependence of log IAP on the inverse of the temperature (Figure 5-3) appears to be linear (r^2 = 0.967), suggesting that the enthalpy of reaction, $\Delta H°_r$, is constant over the temperature range 5 – 75°C. Using the constant enthalpy model, the K_{SP} (T) can be written as

(6)

$$\log K_{SP} = \left(\frac{A}{T}\right) + B$$

where $A = -\Delta H_r° / (\ln(10)R)$ and $B = \Delta S°_r / (\ln(10)R$. The regression coefficients obtained from fitting our data to Equation (5) are A = -2042.07 ± 167.75 and B = -23.48 ± 0.55. The log K_{SP} values calculated using these linear regression coefficients were within one standard error of the measured K_{SP} values, with the largest residual value being 0.19 for the 45°C samples.

The temperature-dependent data were also fitted to a constant heat capacity model (Nordstrom and Munoz, 1994). The resulting coefficients were not significant (i.e. t-values < 1), implying that this model, or more complicated models such as the variable heat capacity model, are overparameterized and inappropriate for our solubility data. Therefore, the constant enthalpy model best represents the

temperature dependence of the log K_{SP} over the temperature range of 5 to 75ºC.

Table 5-2. Thermodynamic data used to update MINTEQA2 databases.

Reactions	kJ mol^{-1} $\Delta G°_r$	$\Delta H°_r$	J mol^{-1} K^{-1} $\Delta S°_r$	ΔC_P	log K_{SP}	Source*
$H_2O - H^+ = OH^-$	79.85	55.81	-80.66	-212.5	-13.99	1, 2
Aqueous Species						
$CrO_4^{2-} + 2H^+ = H_2CrO_4^o$	-39.8	-26.0	85	--	6.97	3
$CrO_4^{2-} + H^+ = HCrO_4^-$	-37.2	6.0	185	--	6.52	3
$2CrO_4^{2-} + 2H^+ - H_2O = Cr_2O_7^{2-}$	-97.2	-25.54	145	--	17.01	1, 3
$Ca^{2+} + CrO_4^{2-} = CaCrO_4^0$	-15.81	--	--	--	2.77	4
$Ca^{2+} + H_2O - H^+ = CaOH^+$	73.22	77.47	14.6	-38.0	-12.83	1, 2
$Al^{3+} + H_2O = AlOH^{2+} + H^+$	28.35	55.73	91.0	0.65	-4.97	1, 6
$Al^{3+} + 2H_2O = Al(OH)^{2+} + 2H^+$	57.70	122.6	218	-225	-10.11	1, 6
$Al^{3+} + 3H_2O = Al(OH)_3^0 + 3H^+$	95.15	176.4	--	--	-16.67	1, 6
$Al^{3+} + 4H_2O = Al(OH)_4^- + 4H^+$	131.3	181.4	167.7	-91.8	-23.00	1, 6
Solid Phases						
$Ca(OH)_2 = Ca^{2+} + 2H_2O - 2H^+$	-129.6	-129.6	0.02	31.71	22.70	1, 2, 7
$Al_2O_{3,\ corundum} = 2Al^{3+} + 3H_2O - 6H^+$	-96.63	-243.6	-491	-125	16.93	1, 5
$Al_2O_{3,\ \gamma\text{-Alumina}} = 2Al^{3+} + 3H_2O - 6H^+$	-104.6	-265.9	-533	-93.0	18.33	1, 5
$Al(OH)_{3,\ amph} = Al^{3+} + 3H_2O - 3H^+$	-61.65	-110.8	--	--	10.8	[
$AlOOH,\ _{boehemite} = Al^{3+} + 2H_2O - 3H^+$	-43.60	-116.2	-243	-23.5	7.64	1, 2, 6
$AlOOH,\ _{diaspore} = Al^{3+} + 2H_2O - 3H^+$	-40.00	-112.0	-241	-22.4	7.01	1, 2, 6
$Al(OH)_3,\ _{gibbsite} = Al^{3+} + 3H_2O - 3H^+$	-44.26	-105.3	-205	14.3	7.75	1, 2, 6
$Ca_6[Al(OH)_6]_2(CrO_4)_3 \cdot 26H_2O =$ $6Ca^{2+} + 2Al(OH)^{4-} + CrO_4^{2-} + 4OH^- + 26H_2O$	236.6 ± 3.9	77.5 ± 2.4	-534 ± 83	-1510 ± 140	-41.5 ± 0.30	4
$3CaO \cdot Al_2O_3 \cdot CaCrO_4 \cdot 15H_2O =$ $4Ca^{2+} + 2Al(OH)_4^- + CrO_4^{2-} + 4OH^- + 15H_2O$	173.1 ± 3.7	39.1 ± 3.2	-450 ± 10		-30.33 ± 0.28	8

*.Multiple numbers indicate sources for individual ion or solid phase data that were used in calculating data presented.

Sources: 1.) Cox, 1989; 2.) Shock, 1997, 3.) Ball and Nordstrom, 1998, 4.) Perkins and Palmer, 1999; 5.) Nordstrom, 1996; 6.) Hemingway, 1996; 7.) Garvin, 1987; 8.) This study

5.4.4. Thermodynamic Properties of $3CaO \cdot Al_2O_3 \cdot CaCrO_4 \cdot 15H_2O$

The free energy of reaction is related to the K_{SP} by

(7)

$$\Delta G°_r = -RT \ln K_{SP}$$

where R is the gas constant (8.31441 J mol^{-1} K^{-1}) and T is the temperature (K). Using Equation (7) and the log K_{SP} value of –30.33 obtained from the linear regression coefficients for Equation (6), we calculate $\Delta G°_{r,298} = 173.1 \pm 3.7$ kJ mol^{-1}. Using this value, the free energies of formation of the individual ions presented in Table 5-5 and

(8)

$$\Delta G°_{f,298,monochromate} = 4\Delta G°_{f,298}(Ca^{+2}) + 2\Delta G°_{f,298}(Al(OH)_4^-) + \Delta G°_{f,298}(CrO_4^{-2}) + 4\Delta G°_{f,298}(OH^-) + 15\Delta G°_{f,298}(H_2O) + \Delta G°_{r,298,monochromate}$$

we calculate $\Delta G°_{f,298,monochromate} = -9905 \pm 16$ kJ mol^{-1}. The uncertainty is based on the error associated with the K_{SP} value and the maximum possible errors associated with the free energies of the individual ions.

The enthalpy of reaction, $\Delta H_r°$, calculated from the slope of the regression curve (A = -2042.07 ±167.75 K) using $\Delta H_r° = -A \ln(10)R$ is 39.1 ±3.2 kJ mol^{-1}. The entropy of reaction, $\Delta S°_r$, calculated from the intercept of the regression curve (B = -

23.48 ±0.55) using $\Delta S°_r$ = B ln(10)R is –450 ±10 J mol^{-1} K^{-1}. The errors are based on the standard errors of the regressed slope and intercept.

Using the data in Table 5-5 and equations for $\Delta H°_{f,monochromate}$ and $\Delta S°_{,298,monochromate}$ analogous to Equation (8), we calculated the enthalpy and entropy of formation of monochromate to be $\Delta H°_{f,monochromate}$ = -11303 ±8.3 kJ $mol^{-1}$and $\Delta S°_{monochromate}$ = 1439 ±89 J mol^{-1} K^{-1}. The errors are based on the errors calculated for the dissolution reaction parameters and the maximum calculated errors associated with individual ions. A similar calculation of heat capacity resulted in $\Delta C_P°_{f,298,monochromate}$ = 373 ± 485 J mol^{-1} K^{-1}. This value is not significantly different than zero, given that the error exceeds the calculated value.

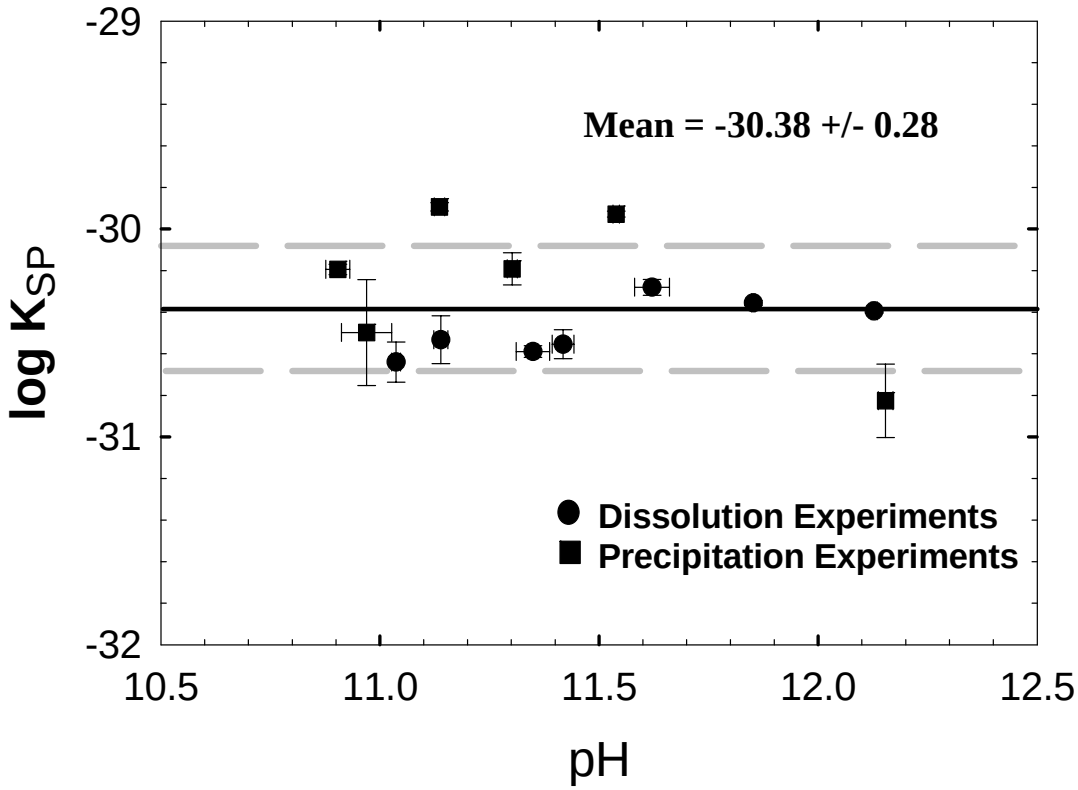

Figure 5-2. Calculated ion activity products versus pH for the monochromate phase from 25ºC dissolution and precipitation experiments. Dashed lines represent one standard deviation from the overall mean log K_{SP}.

Table 5-3. Calculated equilibrium activities and ion activity products for the monochromate phase in dissolution and precipitation experiments at 25ºC.

Sample Batch	Meas. pH	log $\{Ca^{+2}\}$	log $\{Al(OH)_4^-\}$	log $\{CrO_4^{-2}\}$	log $\{OH^-\}$	log $\{Na^+\}$	Ionic Strength (m)	C.B.[a] Error (%)	Log (IAP)
25ºC Dissolution Samples									
25-10.5	11.04 ±0.04	-2.63	-2.72	-2.83	-2.96	-3.07	0.0147	3.12	-30.63 ±0.10
25-11.0	11.14 ±0.02	-2.68	-2.80	-2.80	-2.86	-2.85	0.0145	1.03	-30.53 ±0.12
25-11.5	11.35 ±0.04	-2.80	-3.01	-2.78	-2.65	-2.47	0.0144	±1.53	-30.59 ±0.03
25-11.5r	11.42 ±0.02	-2.74	-3.23	-2.79	-2.58	-2.48	0.0150	4.54	-30.55 ±0.07
25-12.0	11.85 ±0.03	-2.85	-3.74	-2.91	-2.15	-2.05	0.0186	8.99	-30.36 ±0.01
25-12.0r	11.62 ±0.04	-2.39	-4.01	-3.20	-2.38	-1.82	0.0352	< 1%	-30.28 ±0.04
25-12.5	12.13 ±0.01	-2.46	-4.88	-3.30	-1.87	-1.67	0.0539	< 1%	-30.39 ±0.01
25ºC Precipitation Samples									
P25-10.5	10.90 ±0.03	-2.12	-2.98	-3.37	-3.09	-3.26	0.0558	-4.98	-30.19 ±0.02
P25-10.5r	10.97 ±0.06	-2.18	-3.12	-3.40	-3.03	-3.58	0.0480	-7.47	-30.49 ±0.25
P285-11.5	11.14 ±0.01	-2.11	-3.29	-3.40	-2.86	-2.61	0.0580	±1.86	-29.89 ±0.02
P25-11.5r	11.30 ±0.01	-2.19	-3.61	-3.41	-2.70	-2.55	0.0484	-3.53	-30.19 ±0.08
P25-12.0	11.54 ±0.06	-2.17	-3.98	-3.44	-2.46	-2.19	0.0568	-1.98	-29.92 ±0.01
P25-12.5	12.15 ±0.01	-2.22	-5.52	-3.50	-1.84	-1.71	0.0707	0.94	-30.82 ±0.18

[a] Charge balance error $= \frac{\sum_{cations} z_i c_i - \sum_{anions} z_j c_j}{\sum_{cations} z_i c_i + \sum_{anions} z_j c_j} \times 100$

Positive values indicate excess cations, negative values indicate excess anions; ± indicates both excess cations and anions within sample replicates.

Table 5-4. Calculated equilibrium activities and ion activity products for the monochromate phase in the temperature-dependent experiments.

Sample Batch	Meas. pH	log $\{Ca^{+2}\}$	log $\{Al(OH)_4^-\}$	Log $\{CrO_4^{-2}\}$	log $\{OH^-\}$	log $\{Na^+\}$	Ionic Strength (m)	C.B. Error (%)	log (IAP)
5º-10.5	11.79 ±0.04	-2.68	-2.79	-2.97	-2.89	-3.34	0.0117	3.71	-30.83 ±0.01
5º-10.5r	11.98 ±0.03	-2.75	-3.00	-3.07	-2.73	-3.17	0.0098	2.98	-30.77 ±0.22
5º-11.5	12.29 ±0.06	-2.88	-3.33	-2.98	-2.39	-2.49	0.0117	±4.07	-30.95 ±0.18
15º-10.5	11.64 ±0.02	-2.71	-2.97	-2.96	-2.70	-3.10	0.0116	±0.82	-30.58 ±0.12
15º-11.5	11.89 ±0.03	-2.79	-3.31	-2.88	-2.44	-2.49	0.0138	±0.93	-30.53 ±0.17
35º-10.5	10.95 ±0.02	-2.61	-2.88	-2.85	-2.73	-3.36	0.0148	2.14	-29.98 ±0.48
35º-11.5	11.11 ±0.05	-2.76	-3.16	-2.71	-2.57	-2.40	0.0169	1.38	-30.34 ±0.13
45º-10.5	10.57 ±0.04	-2.54	-2.71	-2.76	-2.93	-3.32	0.0184	5.03	-30.06 ±0.27
45º-11.5	11.30 ±0.06	-2.90	-3.29	-2.79	-2.10	-2.00	0.0216	±2.52	-29.36 ±0.13
60º-10.5	10.15 ±0.01	-2.55	-2.74	-2.85	-2.82	-3.16	0.0172	10.03	-29.84 ±0.03
60º-11.5	10.53 ±0.10	-2.70	-2.94	-2.84	-2.44	-2.37	0.0175	6.98	-29.30 ±0.40
75º-10.5	9.90 ±0.03	-2.61	-2.64	-2.80	-2.69	-3.14	0.0178	±2.97	-29.27 ±0.08
75º-11.5	10.03 ±0.02	-2.75	-2.80	-2.76	-2.56	-2.37	0.0175	2.19	-29.65 ±0.04

[a] Charge balance error

$$= \frac{\sum_{cations} z_i c_i - \sum_{anions} z_j c_j}{\sum_{cations} z_i c_i + \sum_{anions} z_j c_j} \times 100$$

Positive values indicate excess cations, negative values indicate excess anions; ± indicates both excess cations and anions within sample replicates.

Table 5-5. Thermodynamic data used in the calculation of formation parameters.

Species	kJ mol^{-1}		J mol^{-1} K^{-1}		References
	ΔG^o_f	ΔH^o_f	ΔS^o_f	$\Delta C^o_{p,f}$	
H_2O_{liquid}	-237.14	-285.83	69.95	75.351	1
	±0.04	±0.4	±0.03	±0.08	
OH^-	-157.3	-230.02	-10.7	-137.2	2
	±2.0	±0.6	±1.9	±16.7	
Ca^{2+}	-552.79	-543	-56.48	-31.5	3
	±2.0	±0.6	±1.9	±16.7	
CrO_4^{2-}	-724.2	-879	5.4	-261.9	3
	±1.0	±1.0	±0.5	±16.7	
$Al(OH)_4^-$	-1305	-1502.8	101.5	89.6	4
	±2.0	±1.6	±10	±12	
$Ca_6[Al(OH)_6]_2(CrO_4)_3 \cdot 26H_2O$	-15131	-17330	2190	2120	5
	±19	±15	±110	±530	
$3CaO \cdot Al_2O_3 \cdot CaCrO_4 \cdot 15H_2O$	-9905	-11303	1439	---	6
	±15.7	±8.3	±89		

*: Uncertainties are based on maximum values reported by Shock et al. (1997) over the temperature range of 0 to 100ºC.

**: $\Delta C^o_{P,f}$ from Shock et al., 1997

Sources: 1.) Cox et al., 1989; 2.) Shock et al., 1997: 3.) Ball and Nordstrom, 1998; 4.) Nordstrom and May, 1996; 5.) Perkins and Palmer, 2000; 6.) This study.

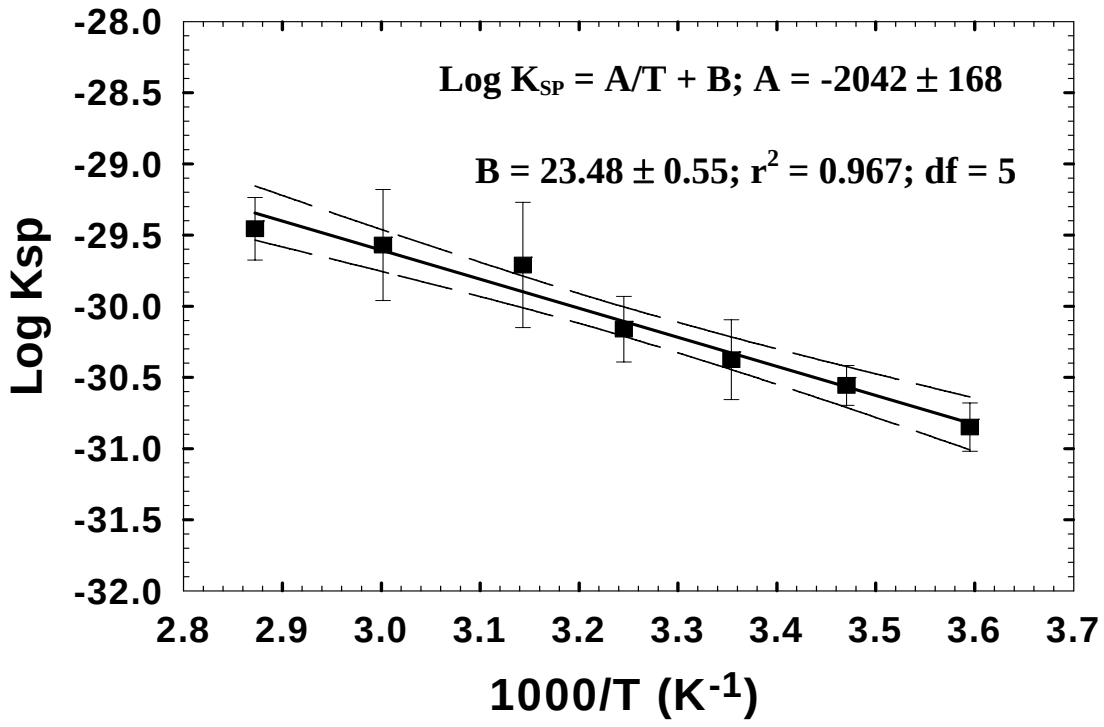

Figure 5-3. Log K_{SP} versus inverse temperature. The dashed lines are the 95% confidence intervals and the vertical bars are the standard deviations in the log K_{SP} for each temperature.

5.4.5. Stability Range for Monochromate

Based on the log K_{SP} values calculated for monochromate and the chromate analog of ettringite we can determine conditions under which these phases are stable. Based on analogy with the sulfate system, it is likely that monchromate will control the solubility of Cr(VI) in mature cements. The transition is given by

(9)

$$Ca_6[Al(OH)_6]_2(CrO_4)_3 \cdot 26H_2O \rightleftarrows 3CaO \cdot Al_2O_3 \cdot CaCrO_4 \cdot 15H_2O + 2Ca^{2+} + 2CrO_4^{2-} + 17H_2O$$

At equilibrium, this transformation can be expressed as

(10)

$$\log K_{Cr(VI)\text{-ettringite}} - \log K_{monochromate} \rightleftarrows 2\log\{Ca^{2+}\} + 2\log\{CrO_4^{2-}\} + 17\log\{H_2O\}$$

where $K_{monochromate}$ and $K_{Cr(VI)\text{-ettringite}}$ are the solubility products for the reactions given by Equation (4) and by **(11)**

$$Ca_6[Al(OH)_6]_2(CrO_4)_3 \cdot 26H_2O \rightleftarrows \{Ca^{2+}\}^6\{Al(OH)_4^-\}^2\{CrO_4^{2-}\}^3\{OH^-\}^4\{H_2O\}^{26}$$

respectively. Using the values of the solubility products at 25ºC ($\log K_{SP,Cr(VI)\text{-ettringite}}$ = -41.4 ±0.3) and Equations (5), (10), and (11), we generated the stability diagram in Figure 5-4. The solid lines denote the stability regions when $\{Ca^{2+}\} = 10^{-2}$. When $\{Ca^{2+}\}$ increases to 10^{-1}, the stability region for monochromate increases in

size and the resulting Cr(VI) concentrations are much lower. When $\{Ca^{2+}\}$ decreases to 10^{-3}, the stability region for monochromate decreases in size and the resulting Cr(VI) concentrations are much higher.

The solubility products for both monochromate and the Cr(VI)-analog of ettringite are temperature dependent and the stability regions therefore shift with temperature (Figure 5-5). The stability region for monochromate is small at 5ºC and becomes relatively large at 75ºC. There is, however, very little shift in the boundary between $Ca_6[Al(OH)_6]_2(CrO_4)_3 \cdot 26H_2O$ and $3CaO \cdot Al_2O_3 \cdot CaCrO_4 \cdot 15H_2O$ with temperature. These results indicate that consideration of the temperature of the system is important in determining the stability of these phases in concrete.

5.5 SUMMARY

Powder X-ray diffraction of solids present in a reactor at the end of dissolution and precipitation experiments using a Cr(VI) analog of ettringite revealed the presence of a secondary phase. This precipitate was identified as the Cr(VI) analog of monosulfate. The solubilty product of $3CaO \cdot Al_2O_3 \cdot CaCrO_4 \cdot 15H_2O$ for Equation (4) at 25ºC was calculated to be –30.38 ±0.28. Experiments conducted over the temperature range of 5 to 75ºC indicate that the enthalpy and entropy of reaction are 39.1 ±3.2 kJ mol^{-1} and 450 ±10 J mol^{-1} K^{-1}, respectively. The free energy of formation and enthalpy of monochromate calculated from our results and published partial molal quantities for key ions are –9905 ±16 and –11303 ±8.3 kJ mol^{-1}. $\Delta S°_{monochromate}$ is calculated to be 1439 ±89 J mol^{-1} K^{-1}. The results will be useful to scientists and engineers who are interested in chromium-concrete interactions.

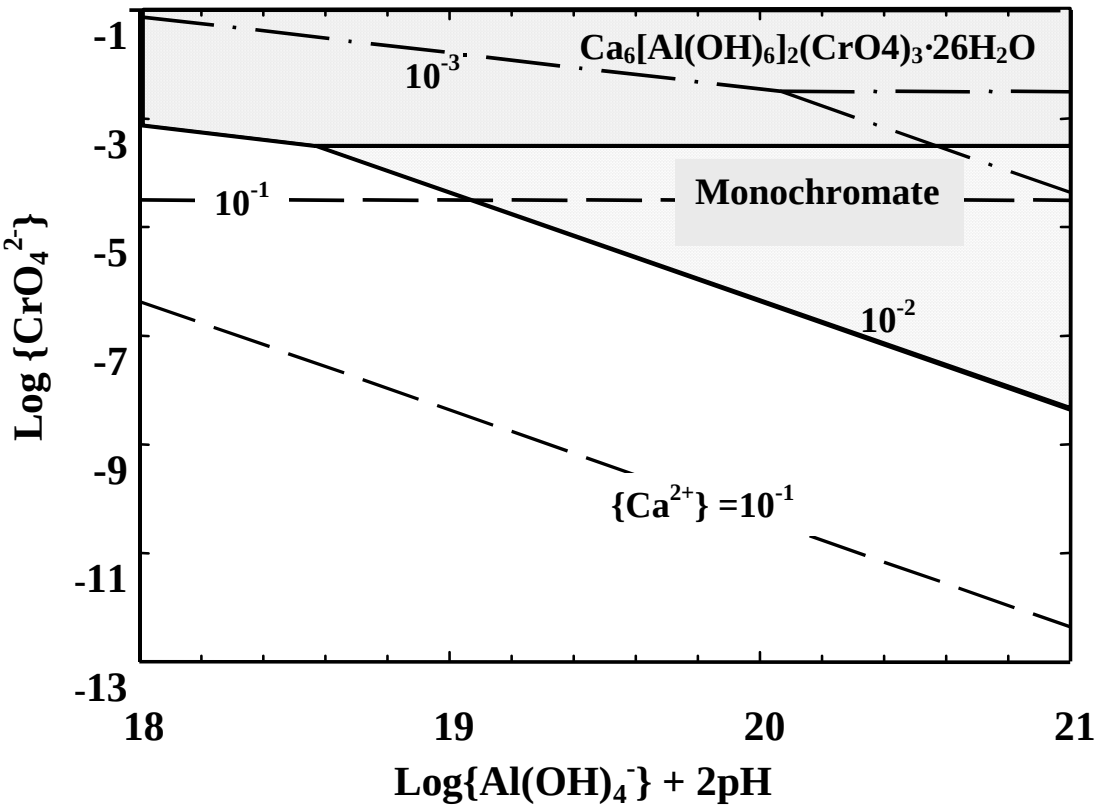

Figure 5-4. Stability diagram for Ca-Al-CrO_4^{2-}-H_2O system at 25ºC assuming unit activity of water. The numbers on the lines denote the activity of Ca^{2+} in solution: solid lines are for stability fields for $\{Ca^{2+}\} = 10^{-2}$; dashed lines for $\{Ca^{2+}\} = 10^{-1}$; dash-dot lines for $\{Ca^{2+}\} = 10^{-3}$.

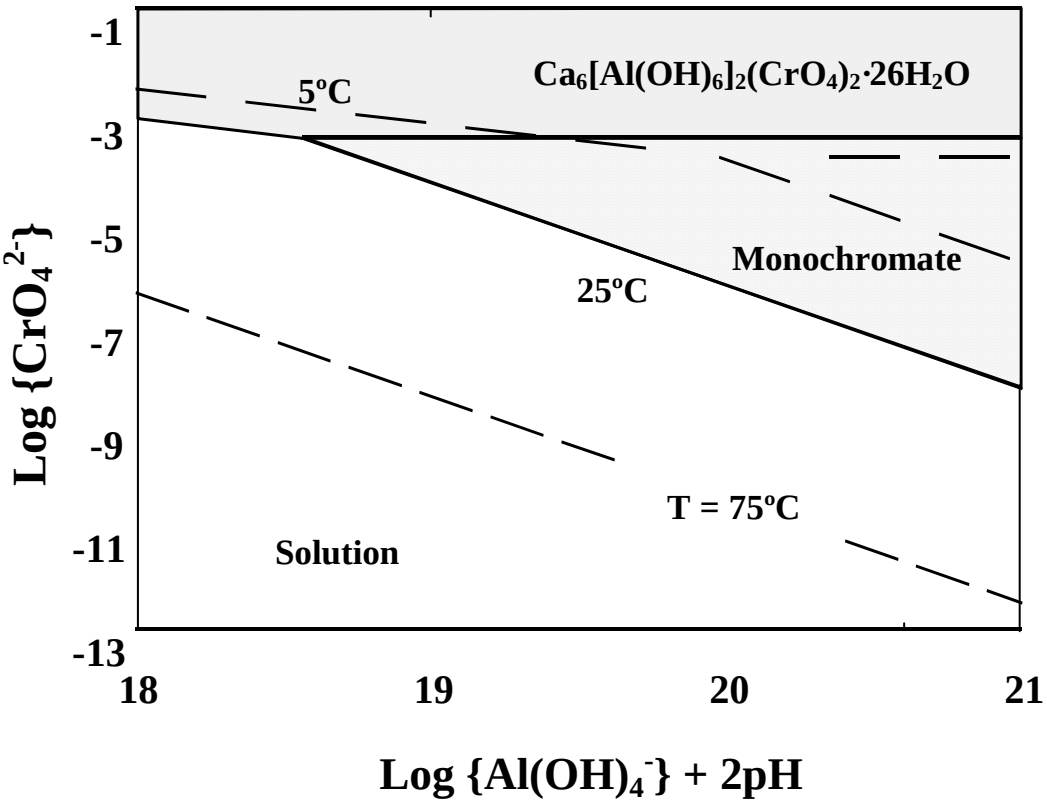

Figure 5-5. Stability diagram for Ca-Al-CrO_4^{2-}-H_2O system assuming unit activity of water and $\{Ca^{2+}\} = 10^{-3}$. The numbers on the line denote the temperature: solid lines denote 25ºC; dashed lines denotes 75ºC; dash-dot lines denote 5ºC.

Chapter 6. Solid-phase Characterization and Dissolution Reaction Pathway Studies of the $Ca_6[Al(OH)_6]_2(Cr_xS_{1-x}O_4)_3 \cdot 26H_2O$ Solid Solution Series

6.1 INTRODUCTION

Ettringite ($Ca_6[(Al(OH)_6)]_2(SO_4)_3\ 26H_2O$) is a naturally-occurring mineral as well as an important product of the hydration of portland-type cements and an important constituent in fly-ash. The identical charge, similar structure, and comparable thermochemical radii of CrO_4^{2-} and SO_4^{2-} (2.4 and 2.3 Å, Waddington, 1959) suggest that CrO_4^{2-} should readily substitute in the crystal structure of this commonly occurring phase and, indeed, several researchers have synthesized $Ca_6[Al(OH)_6)_2(CrO_4)_3 \cdot 26H_2O$ (Kumarathasan et al., 1990; Poellman et al., 1993). Palmer (2000) also observed Cr(VI)-rich ettringite-group crystals in samples of concrete which had been contaminated with chrome-plating solutions. Thus, substitution of CrO_4 for SO_4 in ettringites may provide an important solubility control on Cr(VI) concentrations in alkaline environments.

Previous studies have established the solubilities of ettringite and its pure chromate analog (Perkins and Palmer, 1999; 2000). Such data for the end member phases serves as a basis for modeling SO_4 - CrO_4 substitution in an ideal system. However, differences in bond strengths and interactions between SO_4 and CrO_4 within the ettringite structure may cause varying degrees of non-ideality. The ability to predict the distribution of CrO_4 in the SO_4-CrO_4-Ca-Al-H_2O system therefore requires that such interactions, if present, be taken into account. Although Poellman et al.

(1993) synthesized solid solutions between ettringite and its chromate analog, we are not aware of any solid-solution aqueous-solution (SSAS) system studies involving this system.

The purpose of this study is to investigate changes in solubilities and solid-phase characteristics resulting from partial SO_4 - CrO_4 substitutions in the ettringite structure. The results of this study will be useful in determining the potential for ettringite to control Cr(VI) concentrations and for utilizing sulfate solutions to promote the mobility of Cr(VI) incorporated in ettringite phases.

6.2 BACKGROUND

Ionic substitution in ettringite has been well established (Bensted and Varma, 1971; Dunn et al., 1983; Hassett et al., 1990; Hurlbut and Baum, 1960; 1993; Poellmann et al., 1990). However, there is relatively little available literature specifically addressing chromium substitution in ettringites. Previous studies of chromium-substituted ettringites dealt chiefly with X-ray and spectroscopic characterization of synthesized solids (Kumarathasan et al., 1990; Myneni, 1995; Poellman et al., 1993).

We previously measured the solubility of the $Ca_6[Al(OH)_6]_2(CrO_4)_3 \cdot 26H_2O$ (Perkins and Palmer, 2000), subsequently referred to as chromate ettringite or CrO_4-ettringite in this paper. The log solubility product (log $K_{SP,298}$) for the reaction

(1)

$$Ca_6[Al(OH)_6]_2(CrO_4)_3 \cdot 26H_2O = 6Ca^{+2} + 2Al(OH)^-_4 + 3CrO_4^{-2} + 4OH^- + 26H_2O$$

was determined to be –41.46 ±0.30. This value is significantly higher than the log K_{SP} of -44.90 ±0.32 previously determined for ettringite using an analogous reaction (Perkins and Palmer, 1999).

6.2.1. Solid Solution Theory

The concept of a solid solution refers to a homogeneous solid phase (as opposed to a mechanical mixture of solid phases) whose composition varies between pure end-members. This concept differs from that of gaseous or liquid solutions in that the constituents that make up the solid are confined to specific structural (exchange) sites within a rigid framework.

A solid solution is ideal if the substituting elements involved are completely indistinguishable. The closest approximation to such a theoretically ideal solid solution is the substitution of two isotopes of the same element on the same crystal site. In general, the more similar ions are with respect to size, electronegativity, and charge, the more readily they can substitute for one another.

Although a given crystallographic site may be occupied by several different ions, solid solutions are typically approached from the simplified standpoint of a binary system whose composition varies between two pure end-members. Such a system may be represented by the reaction:

$$BA + CA = (B_{1-X},C_X)A \qquad \textbf{(2)}$$

where B and C are the substituting ions and A represents the other components making up the solid. This reaction may be thought of as dissolution with the component with the higher concentration serving as the solvent.

The free energy resulting from such dissolution in an ideal system is, by definition, entirely attributed to the entropic contribution resulting from increased randomness:

(3)

$$\Delta G_{ideal} = -T\Delta S_{ideal} = nR(x \ln(x) + (1-x) \ln(1-x) = RT \Sigma (X_i \ln X_i)$$

where n is the number of mixing sites and R is the gas constant (8.31411 J mol^{-1}). Variations from ideality are expressed by excess functions. The change in free energy resulting from non-ideal dissolution may thus be defined by the excess free energy, G^E:

$$G_{non\text{-}ideal} = \Delta G_{ideal} + \Delta G^E \qquad \textbf{(4)}$$

If it can be assumed that the substituting ions are randomly distributed over all possible exchange sites, then variations from ideal dissolution will be due to different bonding energies (enthalpy changes).

$$\Delta G^E = \Delta G_{non\text{-}ideal} - \Delta G_{ideal} = \Delta H_{non\text{-}ideal} \qquad \textbf{(5)}$$

Increasing differences in bond energies or ion sizes may be expected to cause

non-uniform molecular interactions leading to preferred ion exchange sites and non-random distribution. The resulting deviation from ideality contributes to the excess free energy, which may then be expressed by:

(6)

$$\Delta G^{E} = \Delta H_{non\text{-}ideal} - T\Delta S_{non\text{-}ideal} = \Delta H_{non\text{-}ideal} - RT\left[\Sigma\left(X_i \ln X_i\right) - \Sigma\left(X_i \ln a_i\right)\right]$$

where a_i represents the activity of component "i" in the binary solution.

Excess parameters for a given solid solution may be expressed as a function of the component mole fractions, X_i. However, since component activities are themselves dependent on the relative component concentrations, excess functions are modeled with Margules equations, which allow the dependence on component concentrations to be expressed by the interaction parameter, W, itself independent of concentration. The interaction parameter may be thought of as the energy necessary to interchange one mole of ion A with one mole of B in a solid solution.

A binary solution in which the excess free energy, like that of the ideal free energy of dissolution, is symmetrical with a maximum value at $X_i = 0.5$, is referred to as a "regular solution." The excess free energy at any mole fraction within a given binary solid-solution series, $(B_{1-X},C_X)A$, may then be expressed through single-parameter Margules equation (e.g., Anderson and Crerar, 1993):

$$\Delta G^{E} = X_{BA} X_{CA} W_G \qquad \textbf{(7)}$$

Increasingly non-uniform ion interactions may result in excess functions which are not symmetric over the compositional field. The excess free energy for such a "sub-regular solution" may be expressed with a two-parameter Margules equation:

(8)

$$\Delta G^E = X_{BA}X_{CA}\,(X_{CA}W_{G1} + X_{BA}W_{G2})$$

Equation (8) is equivalent to mixing two symmetrical solutions having different interaction parameters. More typically, the excess free energy for a subregular solution is expressed through the Guggenheim expansion series:

(9)

$$G^E = X_{BA}\,X_{CA}\,[A_0 + A_1(X_{CA} - X_{BA}) + A_2\,(X_{CA} - X_{BA})^2 + \ldots]$$

An alternative form of the Guggenheim equation, utilizing dimensionless coefficients is also common:

(10)

$$G^E = RT\,X_{BA}\,X_{CA}\,[a_0 + a_1(X_{CA} - X_{BA}) + a_2\,(X_{CA} - X_{BA})^2\,]$$

6.2.2. Representation of Solid-Solution Aqueous Solution (SSAS) Systems

Two models based on mass-action equations have been popularized for assessing equilibrium conditions between solid solutions and aqueous solutions.

Letting

(11)

$$[A^{+6}] = [Ca^{+2}]^6 [Al(OH)_4^-]^2 [OH^-]^4 [H_2O]^{26}$$

the defining mass-action equations for the SO_4 and CrO_4 ettringites may be written

$$[SO_4^{-2}]^3[A^{+6}] = K_{SP,ettringite}\, a_{ettringite} \quad \textbf{(12)}$$

$$[CrO_4^{-2}]^3[A^{+6}] = K_{SP,CrO4\text{-}ettringite}\, a_{CrO4\text{-}ettringite} \quad \textbf{(13)}$$

where $K_{SP,CrO4\text{-}ettringite}$ and $K_{SP,\ ettringite}$ are the pure end-member solubility products and $a_{CrO4\text{-}ettringite}$ and $a_{ettringite}$ are the solid-phase activities. Thorstenson and Plummer (1977) combined the mass-action equations, using the solid-phase stoichiometry as coefficients, to give a stoichiometric saturation constant, $K_{SS,}$ for solid solutions whose composition remains invariant owing to kinetic restrictions. The stoichiometric saturation approach has been shown to be useful in modeling dissolution of many solid-solution systems under normal laboratory temperatures and timeframes (Glynn and Reardon, 1990). If dissolution occurs stoichiometrically,

(14)

$$Ca_6[Al(OH)_6]_2(Cr_xS_{1-x}O_4)_3 \cdot 26H_2O \rightleftharpoons$$

$$6Ca^{+2} + 2Al(OH)^-_4 + 3xCrO_4^{-2} + (3\text{-}3x)SO_4^{-2} + 4OH^- + 26H_2O$$

then, under steady-state conditions, a stoichiometric-saturation constant may be

obtained by multiplying Equations (12) and (13) raised to the 1-x and x powers respectively:

$$K_{SS} = [A^{+6}][CrO_4^{-2}]^{3x}[SO_4^{-2}]^{(3-3x)} \quad \textbf{(15)}$$

Equations (12) and (13) may also be added to derive a total solubility product, ΣΠ, to define thermodynamic equilibrium conditions (Glynn and Reardon, 1990). By adding the left-hand sides of Equations (12) and (13), the total solubility product may be calculated using aqueous activities. For the SO_4 – CrO_4 ettringite solid solution, the total solubility variable may thus be expressed by

(16)

$$\Sigma\Pi = [A^{+6}]\,[CrO_4^{-2}]^3 + [A^{+6}]\,[SO_4^{-2}]^3$$

where $[CrO_4^{-2}]$ and $[SO_4^{-2}]$ are activities of the ions in the aqueous solutions. At equilibrium the total solubility product may be equated to the solid-phase component activities and end member solubilities by:

(17)

$$\Sigma\Pi_{eq} = K_{SP,CrO4\text{-}ettringite}\, a_{CrO4\text{-}ettrringite} + K_{SP,\,ettringite}\, a_{ettringite}$$

$$= K_{SP,CrO4\text{-}ettringite}\, X_{CrO4\text{-}ettringite}\, \zeta_{CrO4\text{-}ettringite} + K_{CrO4\text{-}ettringite}\, X_{CrO4\text{-}ettringite}\, \zeta_{CrO4\text{-}ettringite}$$

where $X_{CrO4\text{-}ettringite}$ and $X_{ettringite}$ are the solid-phase mole fractions of CrO_4-ettringite and ettringite, respectively, $a_{CrO4\text{-}ttrringite}$ and $a_{ettringite}$ are the corresponding solid-phase

activities, and $\zeta_{CrO4\text{-}ettringite}$ and $\zeta_{ettringite}$ are the solid-phase activity coefficients. Equation (17) is typically referred to as the Lippman solidus equation as it relates the equilibrium total solubility product to the activity of the solid-phase components. In an ideal solid solution, the activity coefficients of the solid-phase components are equal to unity and the activities would then be equivalent to the corresponding mole fractions. The total solubility variable does not depend on the solid-phase composition and the aqueous activities can be equated to the end member solubilities. Therefore we can relate solid and aqueous phase compositions by assuming that solid-phase and aqueous-phase activities can be calculated. Thus, given that the solid-phase mole fractions of substituting ions in a binary system sum to unity, a "solutus" reaction expressing the equilibrium total solubility product as a function of the aqueous activity fractions, the end member solubility products, and the solid-phase activity coefficients may be represented by (Glynn and Reardon, 1990):

(18)

$$\Sigma\Pi_{eq} = \left(\frac{X_{CrO4,aq}}{K_{CrO4-ettringite}\,\zeta_{CrO4-ettringite}} + \frac{X_{SO4,aq}}{K_{ettringite}\,\zeta_{ettringite}} \right)^{-1}$$

Solidus and solutus curves may be plotted once the appropriate relationships have been determined. A plot displaying both curves and having two superimposed x-axis scales (one a solid mole-fraction, the other an aqueous activity fraction scale) is referred to as a "Lippman Diagram".

Glynn and Reardon (1990) provide a review of both the stoichiometric saturation and total solubility product models as well as examples of Lippman diagrams for several binary solid-solution systems. They show that the stoichiometric saturation ion activity product is related to the total solubility product variable by:

(19)

$$\Sigma\Pi_{SS} = \frac{IAP_{ss}}{X_{CrO4,aq}^{x} X_{SO4,aq}^{1-x}}$$

Because $\Sigma\Pi_{SS}$ values vary as a function of $X_{CrO4,aq}$ there is a continuum of possible ($X_{CrO4,aq}$, $\Sigma\Pi_{SS}$) values for an aqueous solution with respect to a given fixed-composition solid. Therefore, each solid-phase composition has a corresponding and different stoichiometric saturation curve, having a minimum at a value of $X_{CrO4,aq}$ numerically equal to that of $X_{CrO4\text{-ettringite}}$ and tending towards an infinite $\Sigma\Pi$ value as $X_{CrO4,aq}$ approaches 0 or 1. Glynn and Reardon (1990) also give equations expressing the total solubility products for pure end-members as a function of the end-member solubilities and aqueous activity fractions: **(20, 21)**

$$\Sigma\Pi_{CrO4-ettringite} = \frac{K_{CrO4-ettringite}}{X_{CrO4,aq}} \qquad \Sigma\Pi_{ettringite} = \frac{K_{ettringite}}{X_{SO4,aq}}$$

Thus, stoichiometric saturation and pure end-member curves may also be constructed on Lippman diagrams, providing a more complete graphical representation of binary SSAS systems.

In this paper we will discuss synthesis and solid-phase characterization of a series of CrO_4-SO_4 ettringite solid-solutions as well as dissolution reaction pathway experiments performed using this solid solution series. Data obtained from the dissolution experiments are then plotted on Lippman diagrams to aid in interpretation of the data with respect to the models summarized above.

6.3 EXPERIMENTAL METHODS

6.3.1. Synthesis of Synthetic $Ca_6[Al(OH)_6)_2(SO_4, CrO_4)_3 \cdot 26H_2O$ Solids

An initial series of solid ettringite phases with variable Cr(VI) contents was prepared by mixing 20.2 mmoles of tri-calcium aluminate ($Ca_3Al_2O_6$) previously synthesized by the modification of a method described by Odler and Abdul-Maula (1984) with 60.6 mmoles total of $CaSO_4 \cdot 2H_2O$ and $CaCrO_4$ in one liter of Nanopure water (> 18 MΩ). Four different solids were initially prepared from suspensions having total chromate mole fractions ($XCrO_4$) of 0.2, 0.4, 0.6, and 0.8. Two additional intermediate solid phases were later prepared by mixing 20.2 mmoles of commercially-prepared mono-calcium aluminate ($CaAl_2O_4$) with 40.5 mmoles of $Ca(OH)_2$, and 60.8 mmoles total of $CaSO_4 \cdot H_2O$ and $CaCrO_4$ in one liter of Nanopure water. The chromate mole fractions of the suspensions for these two solids were 0.7 and 0.9. All of the suspensions were mixed at 300 rpm using a magnetic stirrer at room temperature (~23ºC). To minimize CO_2 contamination, water used in the synthesis was purged with N_2 for at least 20 minutes and reactants were mixed in a N_2-filled glove box in which the atmosphere was continuously bubbled through 1 M

NaOH (e.g., Ewing and Shepard, 1994). After 72 hours, the contents were transferred, under N_2, to a ceramic filter funnel and rapidly vacuum-filtered through a 3.0-μm polysulfone filter to separate the solid precipitate. The precipitate was subsequently dried and stored in the glove box at a relative humidity of approximately 30%.

6.3.2. Characterization of Synthetic Solids

The synthesized solids were characterized by a number of methods. X-ray diffraction (XRD) analyses were performed on all synthesized solids. Fourier Transform Infrared Spectroscopy (FTIR) analyses were conducted on the four initial solids using a Perkin-Elmer 2000 unit and KBr pellets.

Replicate portions (5-7 mg) of each synthesized solid were digested in HNO_3 and analyzed to quantify the stoichiometry of the material. Total calcium and aluminum concentrations were determined by flame atomic absorption spectroscopy (AAS) using an air-acetylene flame for calcium and a nitrous oxide-acetylene flame for aluminum and a lanthanum matrix modifier for both sets of analyses. Hexavalent chromium concentrations were determined colorimetrically (3500-Cr D; APHA, 1995) by reacting samples with diphenylcarbazide and measuring the absorbance at 540 nm with a Beckman DU 640 spectrophotometer. Total sulfate concentrations were determined by high-performance liquid chromatography (HPLC). A Dionex 2010 HPLC unit, equipped with an Ionpac AS11 4 X 250-mm analytical column, a guard column, a Dionex anion self-regenerating suppressor, and conductivity detector was used for sulfate analyses. Typically, a 20 millimolar (mM) NaOH solution was used as the eluent.

The amount of water in each of the synthesized solids was determined by thermogravimetric analysis (TGA). TGA analyses were conducted with a Perkin-Elmer TGA7 thermogravimetric analyzer.

6.3.3. Initial Dissolution Reaction Pathway Experiments

A set of dissolution reaction pathway experiments was conducted at 25°C using the solids synthesized from 0.2, 0.4, 0.6, 0.7, and 0.8 $XCrO_4$ suspensions. The experiments were conducted in replicate by placing 0.80 g of synthesized solid in 250ml HDPE bottles along with a magnetic stir bar. The bottles were subsequently filled under N_2 with ultrapure water that had been purged with N_2, then adjusted to the desired pH with NaOH. As an additional precaution against CO_2 contamination, the capped HDPE bottles were sealed within N_2-filled glass mason jars. The jarred sample bottles were then placed in circulating water-baths to maintain the temperature within 0.5^oC of the desired value and mixed with magnetic stirrers.

Samples were collected at progressively longer intervals from 4 to >2600 hours after filling the bottles. An additional amount of the initial solid was added at that time (using ~2.5 g of solid / L of suspension) to see if significant changes would be induced in the concentrations, thus suggesting non-equilibrium conditions. All sampling was conducted in an N_2-filled glove box. After allowing the solids to settle out for several minutes, a 7-ml volume of suspension was withdrawn from near the top of each sample and filtered using a 0.45-μm polysulfone membrane filter. Separate cation and anion subsamples were prepared. A 5ml/liter solution of concentrated

HNO_3 was used to dilute and preserve the cation samples at pH < 2. Anion samples were diluted with ultrapure water and stored in HDPE vials.

An additional aliquot of 4 to 6 ml was removed for pH measurement. Measurements of pH were made at the time of sampling using an Orion Model 290A portable pH meter and Orion Model 9157BN-triode pH electrode. However, the earliest measured values were later determined to be suspect, likely due to contaminated buffers, and the pH values used in subsequent calculations were determined by minimizing charge balance errors. Total Ca, Al, SO_4, and hexavalent chromium concentrations were determined using the methods described for the solid digest. A representative portion of each of the solids remaining at the end of experiments were analyzed by XRD to determine whether the solid had experienced measurable re-crystallization or if additional phases could be identified.

The solid synthesized from the 0.6 $XCrO_4$ suspension was determined to be contaminated, as evidenced by a large, extraneous peak preceding those corresponding to SO_4 and CrO_4 in the HPLC chromatograms from the initial experiments. This peak was attributed to carbonate contamination, possibly resulting from synthesis of the tricalcium aluminate reagent. Similar contamination was noted in samples from the 0.7 $XCrO_4$ suspension after 960 hours, at which time that experiment was discontinued. This was also attributed to carbonate, most likely from atmospheric infiltration caused by failure of the mason jar seals.

6.3.4. Secondary (Spiked) Dissolution Reaction Pathway Experiments

A second set of dissolution reaction pathway experiments was conducted to circumvent potential effects resulting from possible coating of the initial solid by secondary solids. This round of experiments was conducted in an identical manner as the initial experiments except the initial solid was filtered out and analyzed by XRD after the third round of sampling at 385 hours (the approximate time in which total Ca and Al concentrations reached steady state conditions in the initial experiments). Additional fresh solid was then added to the solutions and again following subsequent sampling at one-, two-, and three-week intervals.

The design of the experiment was based on the idea that if steady-state conditions are the result of partial equilibrium with a secondary surface coating, the fresh solid should interact with this partially-equilibrated solution until saturation with another secondary solid, closer in composition to the original solid, is achieved. Repeating this procedure would then eventually bring the system into thermodynamic equilibrium with the solid of interest, bypassing the problems of diffuse ion exchange and recrystallization kinetic constraints created by any surface coatings.

The solids obtained from the 0.6 and 0.7 X_{CrO_4} suspensions were not used in these secondary experiments due to the apparent contamination described above. An additional solid was added so that these experiments used solids synthesized from 0.2, 0.4, 0.8, and 0.9 X_{CrO_4} suspensions.

Sample treatment and analysis were conducted as described for the initial reaction pathway experiment except that the pH probe and buffers were replaced. The

pH meter was calibrated using pHydrion® 7.00, 10.00, 11.00, and 12.00 pH buffers and checked against the pH 11.00 buffer to ensure the measured value was within 0.01 pH units. The 9157BN triode incorporates low Na-error glass, obviating the need for alkali interference corrections at the sodium concentrations / temperature combinations encountered (e.g., corrections < 0.01 pH units). Liquid-junction potential effects were minimized by appropriate conditioning and storage of the electrode and by allowing suspended sediment to settle prior to measurements.

6.4 EXPERIMENTAL RESULTS

6.4.1. Solid Characterization

XRD analyses of the synthesized solids resulted in diffraction patterns nearly identical to those of the endmembers, allowing for minor shifts in d-spacings and peak intensities (Table 6-1; Figure 6-1). The XRD peaks were assigned hkls based on the similarities of their d-spacings with endmember peaks for which hkls were previously established (Perkins and Palmer, 1999; 2000). Primitive unit cell dimensions were calculated by regression using the measured d-spacings, the assigned hkls, and the following equation for hexagonal minerals:

(22)

$$d = \frac{\sqrt{3}ac}{\sqrt{4c^2(h^2 + hk + k^2) + 3a^2l^2}}$$

Table 6-1. Comparison of X-ray diffraction peaks from synthetic $Ca_6(Al(OH)_6)_2(SO_4,CrO_4)_3 \cdot 26H_2O$ intermediates.

	0.10 X_{CrO4} Intermediate Solid Phase		**0.30XcrO4 Intermediate Solid Phase**		**0.57 XCrO4 Intermediate Solid Phase**		**0.73 X_{CrO4} Intermediate Solid Phase**		**0.79 X_{CrO4} Intermediate Solid Phase**	
h,k,l[a]	**d(Å)**	**I/I_{max}**	**d(Å)**	**I/I_{max}**	**d(Å)**	**I/I_{max}**	**d(Å)**	**I/I_{max}**	**d(Å)**	**I/I_{max}**
002	--	--	10.73	8	10.79	3	10.866	19	10.77	4
100	9.764	100	9.752	100	9.79	100	9.89	66	9.87	84
101	8.888	10	8.91	14	8.93	14	8.94	13	8.96	11
?	--	--	--	--	8.53	4	--	--	--	--
102	7.227	3	7.24	3	7.25	5	7.240	5	7.266	3
103	--	--	5.792	12	5.800	10	--	--	--	--
110	5.63	92	5.629	69	5.648	83	5.668	100	5.690	100
112	4.988	26	5.000	23	4.999	21	5.029	75	5.030	24
200	--	--	4.877	5	4.895	5	4.912	9	--	--
104	4.707	50	4.708	56	4.707	53	4.705	57	4.714	42
314	--	--	--	--	4.467	3	4.456	8	4.474	2
005	4.289	3	--	--	--	--	--	--	--	--
203	4.03	11	4.029	8	4.039	10	4.046	12	4.057	14
114	3.886	79	3.886	71	3.890	80	3.895	82	3.903	74
210	3.689	6	3.700	4	3.693	5	3.714	7	3.722	8
204	3.608	17	3.613	12	3.616	16	3.621	14	3.625	21
212	3.48	41	3.487	26	3.492	30	3.538	12	3.518	37
213	--	--	--	--	--	--	3.283	22	3.286	33
300	3.251	26	3.247	15	3.261	15	--	--	--	--
302	--	--	--	--	--	--	--	--	3.14	2
116	3.02	10	3.022	10	3.030	11	3.027	9	3.035	18
220	--	--	--	--	2.877	3	2.872	7	2.875	3
304	2.779	55	2.781	38	2.784	39	2.800	51	2.802	51
222	--	--	--	--	--	--	2.726	9	2.732	12
310	--	--	--	--	--	--	--	--	--	--
008	2.686	15	2.684	11	2.687	11	2.683	10	2.683	15
312	2.621	25	2.625	14	2.626	15	2.642	16	2.648	21
216	2.567	65	2.566	39	2.571	49	2.577	43	2.580	49
313	--	--	--	--	--	--	2.546	6	--	--
400	2.491	5	2.492	4	2.495	5	2.497	10	2.513	7
118	--	--	--	--	--	--	--	--	--	--
306	2.414	13	2.415	7	2.421	9	2.420	9	2.431	10
208	2.351	6	2.352	5	2.354	6	2.356	6	2.359	6
320	--	--	--	--	--	--	2.252	12	2.261	12
226	2.21	55	2.213	35	2.215	38	2.220	41	2.227	48
322	--	--	--	--	--	--	--	--	--	--
316	2.157	29	2.158	20	2.159	19	2.167	18	2.172	26
323	2.128	9	--	--	--	--	2.146	8	2.155	14
410	--	--	2.125	3	--	--	--	--	--	--
412	--	--	2.087	2	--	--	2.103	3	2.108	5
324	2.063	6	2.065	2	2.069	3	2.079	4	2.085	6
413	--	--	--	--	--	--	--	--	--	--
317	--	--	--	--	--	--	--	--	2.007	3
325	1.977	3	--	--	--	--	1.965-	5	1.971	7

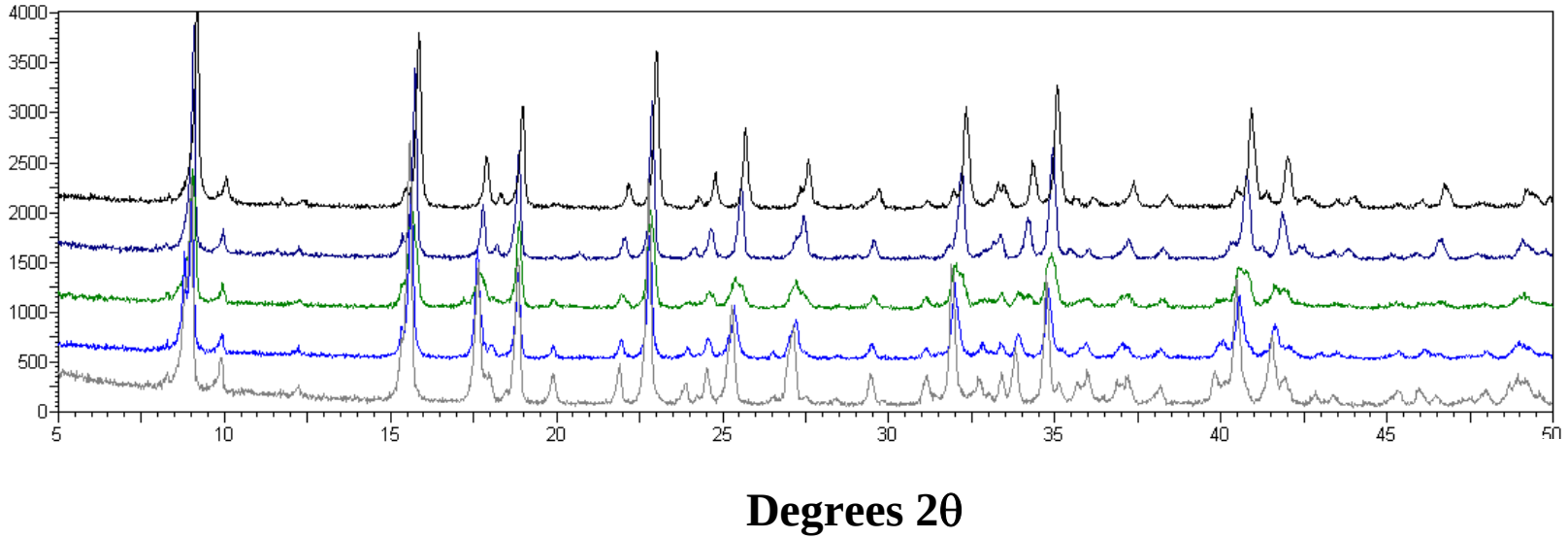

Figure 6-1. X-ray diffraction (raw data) patterns for synthesized 0.0$XCrO_4$ (top), 0.1 $XCrO_4$, 0.3 $XCrO_4$, 0.73 $XCrO_4$, and 1.00 $XCrO_4$ (bottom) ettringite solids showing shift to lower ^{o}2 theta with increasing $XCrO_4$.

A plot of the calculated unit cell dimensions versus the measured mole fraction of chromate (Figure 6-2) shows a nearly linear correlation. However, while a plot of the a_o dimensions versus composition shows a similar linear or broadly parabolic trend with composition, the calculated values for the c_o dimension appeared to vary randomly with composition. This may be attributed to the inter-column or channel positions of the SO_4 and CrO_4 ions within the ettringite structure, wherein they are not restricted with respect to space along the c-axis but are confined along the a-axes by the hydrated calcium-aluminum-hydroxide columns.

Chemical analyses of the solid digests revealed that each was more enriched in SO_4 than was the suspension from which it was synthesized (Table 6-2). This was expected given the lower solubility of the SO_4 ettringite end member. The sulfate enrichment is also a function of the higher concentrations of the $CaCrO_4$ ion pair relative to the $CaSO_4$ ion pair. The average Ca:Al:(SO_4+CrO_4) ratio from all of the synthesized solids, normalized to Ca was 6:2.22:2.96, which compares favorably with the expected ideal ratio of 6:2:3. The Ca to (SO_4 + CrO_4) ratio is nearly ideal. The excess of aluminum could be due to the presence of minor amounts (<1.5% by mass) of aluminum hydroxide.

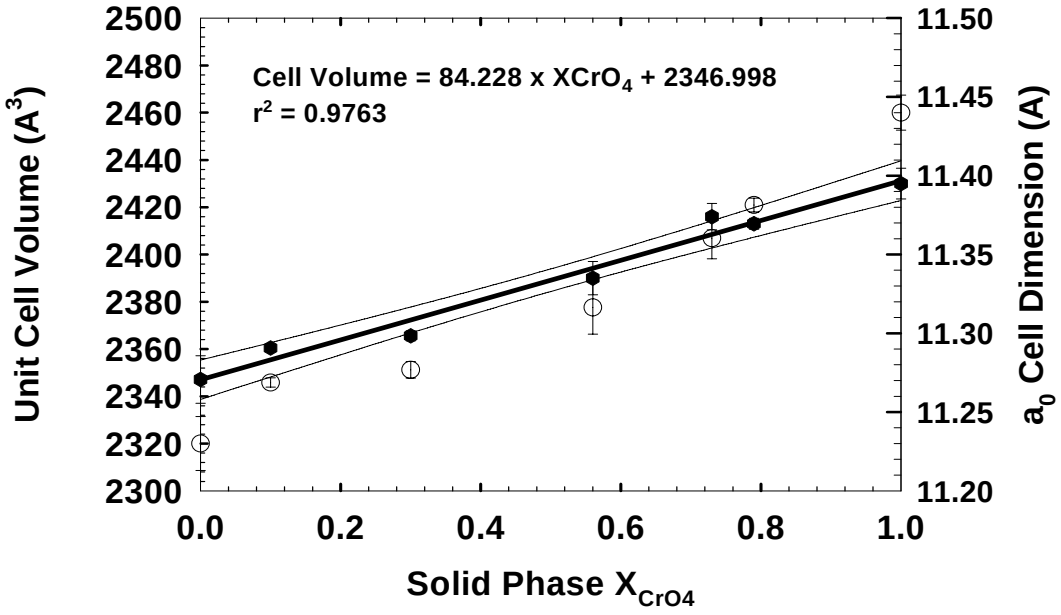

Figure 6-2. Calculated unit cell volumes (•) and a_0 cell dimensions (o) for synthesized SO_4 – CrO_4 ettringites as a function of the CrO_4 mole fraction.

Table 6-2. Results of solid digest analyses of synthesized $Ca_6(Al(OH)_6)_2(SO_4,CrO_4)_3 \cdot 26H_2O$ intermediates.

$XCrO_4$[a] in Reagents	Measured Solid Digest Concentrations (mM/L)				Molar Ratios Ca : Al : (SO_4+CrO_4) Normlzed to (Ca)			SolidCrO_4 Mole Fraction	Ratio of $XCrO_4$ in Reagents /Solid
	(Ca)	(Al)	(SO_4)	(CrO_4)					
0.20	0.96 ±0.037	0.333 ±0.006	0.46 ±0.015	0.051 ±0.002	6.00	2.06	3.19	0.10 ±0.001	2.00
0.40	1.21 ±0.12	0.41 ±0.061	0.39 ±0.026	0.17 ±0.017	6.00	2.03	2.77	0.30 ±0.008	1.33
0.50	0.95 ±0.030	0.36 ±0.013	0.316 ±0.007	0.157 ±0.008	6.00	2.25	2.99	0.33 ±0.006	1.51
0.60	0.91 ±0.100	0.34 ±0.029	0.247 ±0.028	0.208 <0.01	6.00	2.21	2.99	0.46 ±0.028	1.30
0.70[b]	0.137 ±0.007	0.049 ±0.028	0.029 ±0.002	0.039 ±0.002	6.00	2.13	2.94	0.57 ±0.006	1.22
0.80	0.99 ±0.075	0.40 ±0.021	0.131 ±0.009	0.039 ±0.002	6.00	2.42	2.92	0.73 ±0.023	1.10
0.90[b]	0.502 ±0.010	0.155 ±0.002	0.053 ±0.002	0.203 ±0.007	6.00	1.85	3.06	0.79 ±0.002	1.14

[a:] $XCrO_4$ = Mole Fraction of CrO_4 = $MCrO_4$ / ($MCrO_4$ + MSO_4)
[b:] Synthesized using monocalcium aluminate. Other solids synthesized using tricalcium aluminate

The FTIR spectrums from the initial synthesized solids (Figure 6-3) agree well with previous studies of ettringite and Cr(VI)-substituted ettringite (Bensted and Varma, 1971; Kumarathasan et al., 1990; Myneni, 1995). Peaks at ~1120 and ~883 cm^{-1} match peaks attributed to SO_4 and CrO_4. The relative variations in transmittance values for each of these peaks mimics the relative concentrations of the respective ions in the solids. The minor peaks at ~1390 cm^{-1} may be due to CO_3 contamination resulting from sample preparation or to OH-bending, as suggested by Kumarathason et al. (1990) for peaks at ~1427-1435 cm^{-1}.

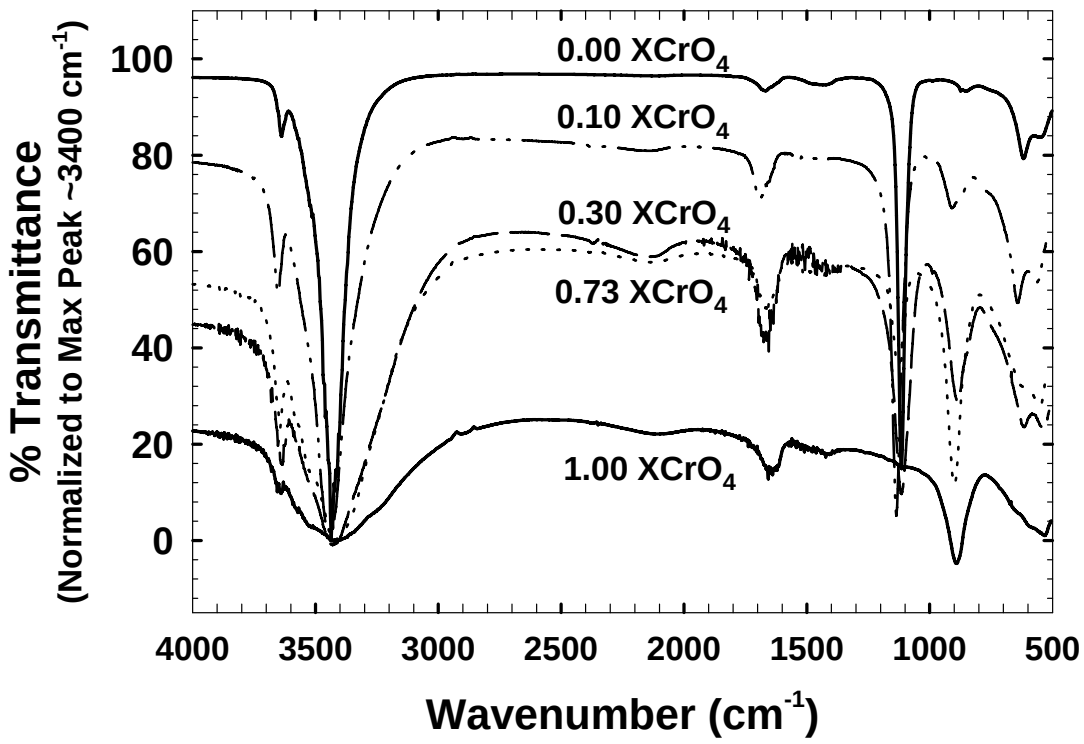

Figure 6-3. Fourier Transform infrared (FTIR) spectroscopy spectrum for a representative set of synthesized SO_4 – CrO_4 ettringites. Peaks at ~1140 and ~880 cm^{-1} match ν_3 peaks attributed to SO_4 and CrO_4, respectively while those at ~650 and 550 cm^{-1} are tentatively assigned to ν_3 vibrations for SO_4 and CrO_4 (Myneni,(1995). Peaks from 3700 to 1600 cm^{-1} are assigned to due to $\nu_2$and ν_3 vibrations in water or OH-stretching (Bensted and Varma, 1971).

Thermogravimetric analysis indicates that mass loss in each of the synthesized solids occurs over three distinct intervals as was previously noted in analyses of the end members (Figure 6-4). The greatest loss occurs between 40 - 180^o C, the range at which loosely bound water would be expected to be lost. The average mass loss of 32.7 ±2.2% over this interval corresponds to ~23 water molecules. An additional average mass loss of between 10 and 12% occurs between 180 and 540^{o}C

and corresponds to the loss of 7 to 8.5 additional water molecules. The last interval of mass loss (2.3 ±1.5%) from 540 to 900^{o}C corresponds to ~2 water molecules. The total measured mass loss for each solid is within 2.1% of the expected mass loss based on the ideal stoichiometry and molecular formula weight. The discrepancy is within the variance noted in replicate analyses of the same solid and is attributed to loss or gain of loosely bound water during sample handling and preparation. The sum of these analyses demonstrates that the synthesized solids are ettringite minerals having intermediate compositions ($Ca_6[Al(OH)_6]_2(SO4, CrO_4)_3 \cdot 26H_2O$) with between $0.10 \leq XCrO_4 \leq 0.79$. Unit cell dimensions vary linearly between pure end members. The slight variations from the expected stoichiometry (1.3 to 6.1%) are less than the corresponding analytical errors.

6.4.2. Initial Dissolution Reaction Pathway Experiments

Examination of the aqueous ion concentrations in the time-series samples (Table 6-3) indicates that the total concentration of Ca and Al increases with increasing $XCrO_4$. This is expected given the relatively higher solubility of the pure chromate ettringite phase as compared to that of the sulfate end member. Al concentrations achieved steady-state conditions in 200 to 400 hours. Ca concentrations appeared to reach near steady-state conditions within the same period but then show a slight decrease beyond 1000 hours. The decrease in Ca concentrations between 500 and 2000+ hours is only slightly larger than the maximum analytical error but appears to be consistent in all of the experiments.

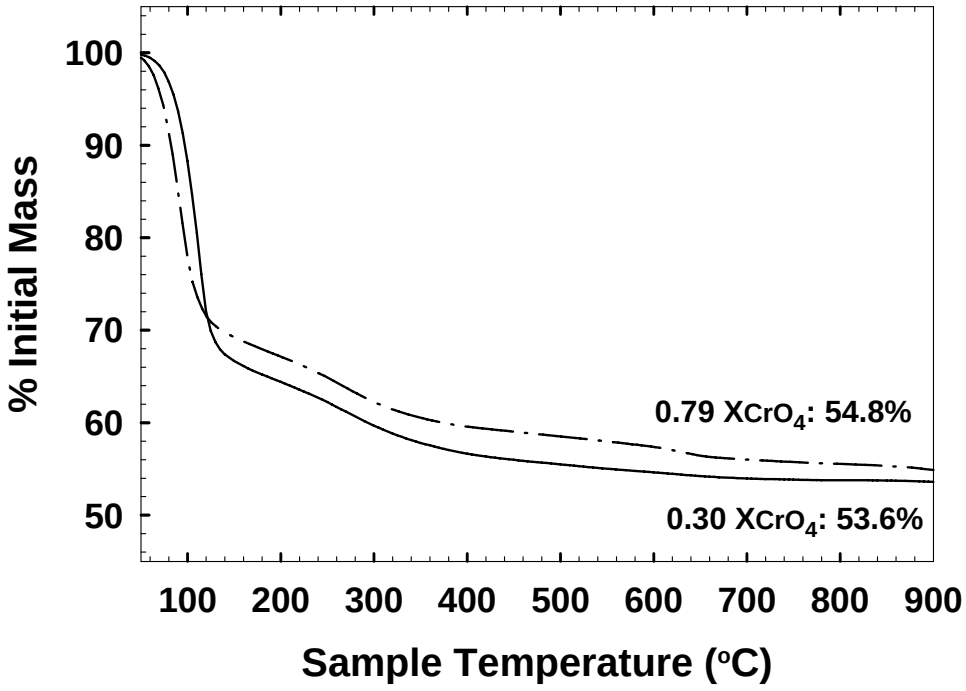

Figure 6-4. Thermogravimetric analyses of representative synthesized $SO_4 - CrO_4$ ettringites. Values listed are the percent of initial mass remaining at 900°C.

Table 6-3. Concentrations in initial dissolution reaction pathway experiments.

Solid $XCrO_4$	pH[a]	(Ca) mmol L^{-1}	(Al) mmol L^{-1}	(CrO_4) mmol L^{-1}	(SO_4) mmol L^{-1}	(Na) mmol L^{-1}	Duration (hrs)
0.10	11.15* ±0.035	2.222 ±0.035	1.049 ±0.001	0.262 <0.001	0.928 ±0.066	0.566 ±0.016	4
0.10	11.02* ±0.020	2.379 ±0.058	1.523 ±0.001	0.275 ±0.007	1.029 ±0.095	0.551 ±0.032	24
0.10	10.89*	2.278 ±0.016	1.52 --	0.318 <0.001	1.31 --	0.54 --	50
0.10	10.79* ±0.067	2.319 ±0.048	1.489 ±0.012	0.374 ±0.045	1.0384 ±0.080	0.54 --	120
0.10	11.07*	2.348 ±0.041	0.87 --	0.402 ± 0.008	1.111 ±0.057	0.54 --	220
0.10	11.13* ±0.070	2.436 ±0.064	0.807 ±0.572	0.419 ±0.030	1.024 ±0.023	0.504 ±0.013	1390
0.10	11.090 ±0.026	1.986 ±0.044	0.713 ±0.001	0.517 ±0.042	1.073 ±0.013	0.465 ±0.012	2640
0.10s[b]	10.923 ±0.059	2.473 ±0.026	0.697 ±0.006	0.787 ±0.005	1.259 ±0.001	0.514 ±0.004	2810
0.30	11.22* ±0.001	2.427 ±0.061	0.768 ±0.026	0.538 ±0.054	0.602 ±0.071	0.063 ±0.001	20
0.30	11.25* <0.001	2.564 ±0.027	0.849 ±0.008	0.595 ±0.004	0.605 ±0.002	0.065 ±0.003	50
0.30	11.18* ±0.034	2.516 ±0.028	0.868 ±0.074	0.296 ±0.006	0.640 ±0.062	0.060 ±0.003	265
0.30	11.26*	2.656 ±0.098	0.933 ±0.046	0.682 ±0.083	0.54 --	0.070 ±0.001	430
0.30	11.27* ±0.023	2.816 ±0.065	0.927 ±0.087	0.800 ±0.050	0.526 ±0.039	0.078 ±0.015	1080
0.30	11.123 ±0.012	2.308 ±0.082	1.024 ±0.020	1.501 ±0.097	0.558 ±0.002	0.131 ±0.005	2350
0.30[b]	11.271 ±0.001	3.02 ±0.17	1.074 ±0.031	1.318 ±0.009	0.364 ±0.006	0.101 ±0.007	2880
0.57	10.839 ±0.030	2.788 ±0.002	1.117 ±0.001	1.285 <0.019	0.558 ±0.006	0.184 <0.001	1
0.57	10.964 ±0.011	3.058 ±0.016	1.335 ±0.006	1.520 ±0.039	0.474 --	0.232 ±0.010	4
0.57	11.126 ±0.035	3.213 ±0.044	1.416 ±0.013	1.600 ±0.041	0.314 ±0.010	0.248 ±0.014	24
0.57	11.206 ±0.008	3.320 ±0.048	1.548 ±0.020	1.722 ±0.012	0.182 ±0.024	0.251 ±0.010	100
0.57	11.282 ±0.014	3.40 ±0.11	1.615 ±0.010	1.896 ±0.093	0.151 ±0.008	0.262 ±0.024	170
0.57	11.346 ±0.006	3.40 ±0.21	1.630 ±0.003	2.213 ±0.010	0.132 ±0.001	0.25 --	265

[a] pH values marked with "*" were calculated by minimizing speciated charge balance errors using MINTEQA2 software.

[b] indicates spiked samples, in which additional solid was added to the suspensions immediately following collection of the preceding sample.

Table 3(con't). Concentrations in initial dissolution reaction pathway experiments.

Solid $XCrO_4$	pH[a]	(Ca) mmol L^{-1}	(Al) mmol L^{-1}	(CrO_4) mmol L^{-1}	(SO_4) mmol L^{-1}	(Na) mmol L^{-1}	Duration (hrs)
0.57	11.435 ±0.007	3.739 ±0.037	1.655 ±0.025	2.280 ±0.004	0.123 <0.001	0.294 ±0.006	430
0.57	11.468 ±0.012	4.32 ±0.21	1.636 ±0.017	2.264 ±0.015	0.107 ±0.042	0.144 ±0.001	790
0.57	11.442 ±0.064	4.434 ±0.025	1.765 ±0.003	2.281 ±0.022	0.073 ±0.006	0.139 ±0.008	960
0.73	11.34* --	4.486 --	1.049 ±0.001	1.473 ±0.025	0.227 ±0.004	0.566 ±0.016	4
0.73	11.49* ±0.02	4.348 ±0.015	1.523 ±0.001	2.127 ±0.068	0.079 ±0.002	0.744 ±0.003	24
0.73	11.44* ±0.028	4.383 ±0.026	1.516 <0.001	2.271 ±0.088	0.074 ±0.001	0.76 ±0.009	50
0.73	11.48* ±0.028	4.615 ±0.001	1.567 ±0.097	2.40 ±0.13	0.070 ±0.002	0.755 ±0.002	120
0.73	11.31* ±0.15	4.425 ±0.010	1.478 ±0.019	2.39 ±0.11	0.0796 ±0.003	0.781 ±0.060	220
0.73	11.38* ±0.03	4.136 ±0.045	1.65 ±0.18	2.20 ±0.11	0.074 ±0.065	0.75 ±0.17	1390
0.73	11.484 ±0.010	3.616 ±0.035	1.547 ±0.071	2.30 ±0.11	0.071 ±0.009	1.00 ±0.21	2640
0.73[b]	10.739 ±0.004	4.53 ±0.53	1.426 ±0.081	3.42 ±0.37	0.065 ±0.008	1.37 ±0.24	2810

[a] pH values marked with "*" were calculated by minimizing speciated charge balance errors using MINTEQA2 software.
[b] indicates spiked samples, in which additional solid was added to the suspensions immediately following collection of the preceding sample.

SO_4 concentrations, like the Al concentrations, achieve steady-state conditions in under 400 hours. CrO_4 concentrations appear to increase slowly throughout the experiment. Excepting the 0.30 $XCrO_4$ experiment, the increases in CrO_4 are generally within the range of analytical error after 200 hours.

As previously mentioned, pH measurements taken during these experiments were suspect based on high charge balance errors (20 - 25%) and low readings in freshly-prepared pH 12 buffers. Therefore, pH values used in subsequent activity calculations were obtained by minimizing charge balance errors.

6.4.3. Secondary (Spiked) Dissolution Reaction Pathway Experiments

As expected, analyte concentrations, excepting SO_4, increased with increasing solid CrO_4 mole fraction (Table 6-4, Figures 6-4 and 6-5). The total concentrations of Ca and Al in all of the solutions varied only slightly prior to the introduction of fresh solid. Interestingly, Ca concentrations rose significantly after the first round of spiking with the solid while Al concentrations were largely invariant. However, Al concentrations rose after the second addition of fresh solid and then remained at steady-state conditions throughout the remainder of the experiment. A slight increase in Ca concentrations was noted in the solutions containing higher solid CrO_4 mole fractions.

CrO_4 and SO_4 concentrations were much more variable than was the case in the dissolution reaction pathway experiments. SO_4 concentrations rose after the first or second round of spiking with fresh solid, then decreased again. CrO_4 concentrations in the 0.10 XCrO_4 solution appear to have reached a steady-state condition after the second round of spiking. An increase in CrO_4 concentrations was observed in the other solutions throughout the duration of the experiment (Figure 6-5). The aqueous CrO_4 mole fractions increased with time for all experiments.

A maximum variation of 0.15 pH units was noted in all of the experiments throughout their duration (Table 6-4). However, an average decline of 0.1 (±0.04) pH units was observed in all of the solutions in the three weeks between the last addition of fresh solid and the final round of sampling. Speciated charge balance ranged between 0.5 and 11.3% with an average charge balance error of 4.6 ±2.9%.

Table 6-4. Concentrations in secondary dissolution reaction pathway experiments.

Solid $XCrO_4$	pH	(Ca) mmol L^{-1}	(Al) mmol L^{-1}	(CrO_4) mmol L^{-1}	(SO_4) mmol L^{-1}	(Na) mmol L^{-1}	Duration (hrs)
0.10	11.201	2.280	0.630	0.268	0.965	0.251	50
	--	±0.035	±0.007	<0.001	±0.053	±0.003	
0.10	11.191	2.285	0.650	0.284	0.901	0.246	215
	±0.006	±0.003	±0.008	±0.001	±0.003	±0.003	
0.10	11.205	2.226	0.625	0.240	0.858	0.260	385
	±0.035	±0.061	±0.005	<0.001	±0.001	<0.001	
0.10[a]	11.189	2.474	0.611	0.362	1.52	0.43	550
	±0.015	±0.014	±0.022	±0.043	±0.20	--	
0.10[a]	11.223	2.57	0.87	0.452	1.313	0.54	935
	--	±0.045	±0.009	±0.009	--	±0.001	
0.10[a]	11.072	2.536	0.654	0.516	1.240	0.230	1560
	±0.013	±0.049	±0.005	±0.012	±0.023	±0.004	
0.30	11.349	2.429	0.800	0.618	4.850	0.277	50
	±0.008	±0.014	±0.046	--	±0.010	±0.020	
0.30	11.354	2.451	0.830	0.671	0.462	0.262	215
	±0.013	±0.005	±0.003	±0.002	±0.012	<0.001	
0.30	11.328	2.522	0.822	0.738	0.465	0.272	385
	±0.034	±0.005	±0.001	±0.032	±0.012	±0.003	
0.30[a]	11.361	2.83	0.866	1.038	0.611	0.79	550
	±0.024	±0.16	±0.069	±0.046	±0.002	±0.15	
0.30[a]	11.32	3.036	1.06	1.16	0.32	0.304	935
	--	±0.040	±0.002	±0.021	--	±0.001	
0.30[a]	11.338	3.130	1.175	1.41	0.260	0.275	1560
	±0.038	±0.009	±0.022	±0.010	±0.010	±0.002	
0.73	11.566	4.237	1.530	2.092	1.364	.512	50
	±0.023	±0.028	±0.007	±0.009	±0.024	±0.001	
0.73	11.562	4.333	1.559	2.181	0.151	0.514	215
	±0.023	±0.053	±0.026	±0.083	±0.086	±0.004	
0.73	11.539	4.112	1.501	1.972	0.073	0.515	385
	±0.012	±0.070	±0.016	±0.080	±0.013	--	
0.73[a]	11.550	4.801	1.466	2.452	0.058	1.06	550
	±0.011	±0.003	±0.004	±0.016	±0.004	±0.36	
0.73[a]	11.521	4.76	1.587	3.174	0.075	0.907	935
	±0.004	±0.11	±0.034	±0.042	±0.001	±0.023	
0.73[a]	11.411	5.123	1.483	3.689	0.0573	1.066	1560
	±0.027	±0.041	±0.001	±0.073	±0.015	±0.018	
0.79	11.328	5.679	1.812	4.102	0.364	0.339	215
	±0.008	±0.081	±0.005	±0.003	±0.004	±0.004	
0.79	11.30	5.489	1.650	3.124	0.099	0.235	385
	--	±0.032	±0.014	±0.094	±0.008	±0.010	
0.79[a]	11.243	6.856	1.901	4.97	0.081	0.446	550
	±0.022	±0.015	±0.014	±0.12	±0.001	±0.002	
0.79[a]	11.277	7.708	1.694	6.671	0.084	0.465	935
	±0.003	±0.008	±0.001	<0.001	±0.001	±0.006	
0.79[a]	11.175	9.73	1.17	8.68	0.060	0.437	1560
	±0.019	±0.40	±0.13	±0.31	±0.004	±0.006	

[a] indicates spiked samples, in which additional solid was added to the suspensions immediately following collection of the preceding sample.

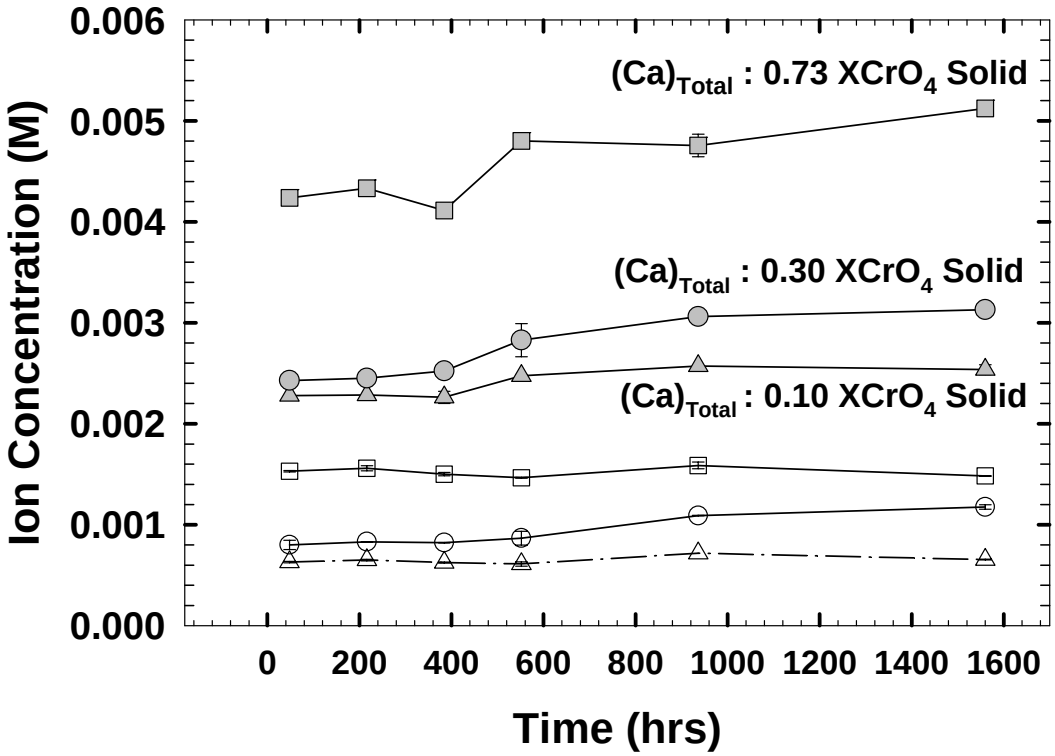

Figure 6-5. Total Ca and Al concentrations over time in selected secondary (spiked) dissolution reaction pathway experiments. Solid symbols represent Ca concentrations as noted; Al concentrations for same experiments are represented by identical but open symbols. Additional solid (~ 2.5 g/L) was added after the third, fourth, and fifth sampling rounds.

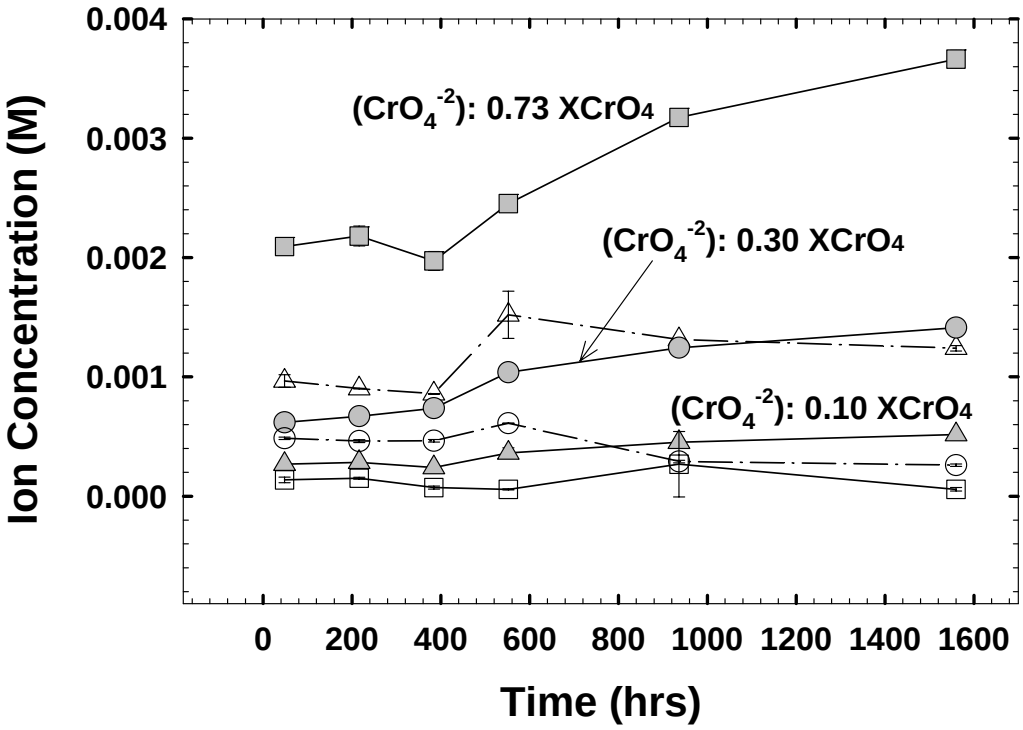

Figure 6-6. CrO_4 and SO_4 concentrations over time in selected secondary (spiked) dissolution reaction pathway experiments. Solid symbols represent CrO_4 concentrations as noted; SO_4 concentrations for same experiments are represented by identical but open symbols. Additional solid (~ 2.5 g/L) was added after the third, fourth, and fifth sampling rounds.

6.5 DISCUSSION

6.5.1. Solid Synthesis and Characterization Data

Changes in unit cell volumes with composition have been used to infer the nature of binary solid solution interactions based on empirical comparison of "volume mismatch terms" and excess free energies derived from calorimetry or solubility studies (Davies and Navrotsky, 1983; Navrotsky, 1987). The volume mismatch term for a regular binary solution is defined as:

$$\Delta V_{regular} = (V_C - V_B)/(0.5(V_C + V_B)) \quad \textbf{(23)}$$

where $V_C > V_B$. For subregular mixing models, the dual volume mismatch terms are

$$\Delta V_C = (V_B - V_C)/V_B \text{ and } \Delta V_B = (V_C - V_B)/V_C. \quad \textbf{(24)}$$

The mismatch term may be correlated with the previously defined interaction parameter, W_G. Dual interaction parameters, one for each component ($W_{G\text{-}B}$ $W_{G\text{-}C}$), may be correlated to the individual component mismatch terms (Equation 23) and used to calculate the excess free energy for sub-regular solutions.

The slopes and intercepts derived from correlation of experimentally-derived interaction parameters, W, with their corresponding mismatch terms, V, vary, not unexpectedly, with the different types of mineral groups involved. Navrotsky (1987)

provides a general correlation equation based on cation mixing for 4-, 6-, and 8-coordinated sites and a limited number of systems involving anion mixing:

$$W_{(G,G\text{-}A,\text{ or }G\text{-}B)} = 100.8\ \Delta V_G\ - 0.4\ \text{kJ mol}^{-1} \quad \textbf{(25)}$$

Assuming a regular solution and using Equations 23 and 25, we calculate the following parameters for $Ca_6[(Al(OH)_6)]_2(SO_4, CrO_4)_3\ 26H_2O$ solid solutions:

$$\Delta V_{G,regular} = (2430.0\text{-}2347.1\ \text{Å})/(0.5(2430.0+2347.0\ \text{Å}) = 0.0347 \quad \textbf{(26)}$$

$$W_{G,\ regular} = 100.8 \text{ x } 0.0347 - 0.4\ \text{kJ mol}^{-1} = 3.1\ \text{kJ mol}^{-1} \quad \textbf{(27)}$$

The maximum value of $\Delta G^E = 0.775\ \text{kJ mol}^{-1}$ obtained with Equation (7) and the value of $W_{G,regular}$ calculated in Equation (27) is relatively small in comparison with the maximum value of $\Delta G_{ideal} = 5.16\ \text{kJ mol}^{-1}$ calculated using Equation (3) at $X_i = 0.5$. Excess free energy values calculated using the dual mis-match terms and the sub-regular solution model (Equation 8) were identical to the values calculated for the regular solution model to two decimal places. The small differences in unit cell dimensions between end members as well as the linear relationship between unit cell volume and composition suggest a near-ideal solid solution.

All of the synthesized solids were enriched in SO_4 relative to the synthesis liquor. The degree of enrichment was greatest in the solids with compositions nearer the ettringite end member, as seen in the decreasing $XCrO_4$ ratios between the reagents

and the resulting solids (Table 6-2). If the assumption is made that all of the reagents were dissolved at the same rate and the synthesis solution composition with respect to the relative ratios of CrO_4 and SO_4 was the same as that of the reagents, this enrichment would suggest a lattice preference for the SO_4 ion. It is doubtful that such enrichment would be the result of aqueous speciation as SO_4^{2-} and CrO_4^{2-} should be the dominant S and Cr species under the experimental conditions (i.e., high pH, relatively low ionic strengths).

6.5.2. Dissolution Reaction Pathway Experimental Data

Aqueous activities for Ca^{2+}, $Al(OH)_4^-$, SO_4^{2-}, and CrO_4^{2-} as well as Na^+ were calculated with the geochemical speciation model MINTEQA2 (Allison et al., 1990) using the Davies Equation:

$$\log \gamma_i = -AZ_i^2 \left(\frac{\sqrt{I}}{1+\sqrt{I}} - 0.24I \right) \quad \textbf{(28)}$$

The databases used by MINTEQA2 were first modified to include pertinent, updated thermodynamic data from available literature (Table 6-6).

Table 6-5. Activities, IAPss, and ΣΠ values calculated for $Ca_6[Al(OH)_6]_2(SO_4,CrO_4)_3 \cdot 26H_2O$ dissolution reaction pathway experiments.

$XCrO_4$ (hrs)	Meas pH[a]	Log $\{Ca^{+2}\}$	Log $\{Al(OH)_4^-\}$	Log $\{CrO_4^{-2}\}$	Log $\{SO_4^{-2}\}$	Log $\{OH^-\}$	-Log IAP_{ss}[b]	-Log ΣΠ[b]
Initial (unspiked) dissolution reaction pathway samples								
0.10	11.14*	-2.854	-3.019	-3.936	-3.244	-2.853	44.55±	44.34
(4)							0.09	±0.09
0.10	11.02*	-2.835	-2.858	-3.927	-3.206	-2.978	44.48	44.26
(24)							±0.06	±0.07
0.10	10.88*	-2.854	-2.860	-3.855	-3.200	-3.110	45.08	44.88
(51)							±0.02	±0.02
0.10	11.19*	-2.851	-3.102	-3.756	-3.170	-2.926	44.70±	44.52
(221)							0.13	±0.14
0.10	11.23*	-2.846	-3.134	-3.740	-3.205	-2.864	44.58±	44.41
(1390)							0.35	±0.35
0.10	11.13*	-2.830	-3.226	-3.657	-3.126	-2.927	44.60	44.18
(1560)							±0.02	±0.02
0.10	11.09	-2.841	-3.155	-3.570	-3.533	-2.655	45.21	45.06
(2640)							±0.07	±0.07
0.10	10.92	-2.858	-3.200	-3464	-3.118	-3.075	45.31	45.16
(2810)[c]							±0.20	±0.20
0.30	11.22*	-2.833	-3.154	-3.632	-3.414	-2.779	44.86	44.58
(20)							±0.14	±0.15
0.30	11.25*	-2.814	-3.112	-3.603	-3.434	-2.752	44.57	44.30
(50)							±0.03	±0.03
0.30	11.18*	-2.824	-3.089	-3.561	-3.434	-2.822	44.83	44.56
(265)							±0.18	±0.18
0.30	11.26*	-2.799	-3.077	-3.561	-3.464	-2.738	44.38	44.11
(430)							±0.33	±0.32
0.30	11.27*	-2.789	-3.083	-3.481	-3.504	-2.725	44.29	43.97
(1080)							±0.23	±0.20
0. 30	11.12	-2.889	-3.032	-3.322	-3.460	-2.875	45.15	44.72
(2350)							±0.11	±0.15
0.30	11.27	-2.790	-3.012	-3.268	-3.669	-2.727	44.32	43.45
(2880)[c]							±0.07	±0.07
0.57	10.84	-2.818	-2.993	-3.263	-3.472	-3.159	45.59	45.23
(1)							±0.11	±0.11
0.57	10.96	-2.793	-2.917	-3.203	-3.552	-3.034	44.79	44.31
(4)							±0.03	±0.02
0.57	11.13	-2.775	-2.892	-3.190	-3.735	-2.872	44.20	43.49
(25)							±0.12	±0.14
0.57	11.21	-2.767	-2.854	-3.162	-3.977	-2.793	44.02	42.97
(100)							±0.14	±0.06

[a] pH values marked with "*" were calculated by minimizing charge balance errors.
[b:] Errors are standard deviations from replicates. IAPss values calculated assuming stoichiometry of initial solid.
[c:] Samples were spiked with fresh solid immediately after previous sampling round.

Table 6-5. (con't) Activities, IAPss, and ΣΠ values calculated for $Ca_6[Al(OH)_6]_2(SO_4,CrO_4)_3 \cdot 26H_2O$ dissolution reaction pathway experiments.

$XCrO_4$ / (hrs)	Meas pH[a]	Log $\{Ca^{+2}\}$	Log $\{Al(OH)_4^-\}$	Log $\{CrO_4^{-2}\}$	Log $\{SO_4^{-2}\}$	Log $\{OH^-\}$	-Log IAP_{ss}[b]	-Log ΣΠ[b]
Initial (unspiked) dissolution reaction pathway samples								
0.57	11.28	-2.769	-2.837	-3.122	-4.059	-2.716	43.52	42.52
(170)							±0.09	±0.15
0.57	11.36	-2.789	-2.833	-3.049	-4.118	-2.653	43.54	42.16
(265)							±0.17	±0.16
0.57	11.44	-2.752	-2.828	-3.054	-4.159	-2.563	43.01±	41.59
(430)							0.06	±0.06
0.57	11.47	-2.687	-2.835	-3.088	-4.249	-2.531	42.68±	41.18
(795)							0.06	±0.15
0.57	11.44*	-2.674	-2.802	-3.091	-4.402	-2.556	42.84±	41.15
(960)							0.27	±0.23
0.73	11.49*	-2.772	-3.023	-3.223	-3.873	-2.657	43.45	42.97
(4)							--	--
0.73	11.49*	-2.679	-2.866	-3.120	-4.370	-2.511	42.11±	41.21
(25)							0.06	±0.06
0.73	11.44*	-2.683	-2.867	-3.090	-4.392	-2.558	42.27±	41.34
(50)							0.10	±0.08
0.73	11.48*	-2.665	-2.877	-3.076	-4.424	-2.518	42.01±	41.04
(120)							0.07	±0.06
0.73	11.31*	-2.685	-2.879	-3.054	-4.364	-2.576	42.28±	41.34
(220)							0.05	±0.06
0.73	11.38*	-2.701	-2.831	-3.095	-4.224	-2.621	42.45	41.64
(1390)							±0.10	±0.10
0.73	11.48	-2.769	-2.858	-3.043	-4.398	-2.514	42.49	41.52
(2640)							±0.03	±0.06
0.73	11.35	-2.721	-2.897	-2.901	-4.456	-2.647	42.53	41.41
(2810)[c]							±0.30	±0.37
Secondary (spiked) dissolution reaction pathway samples								
0.10	11.20	-2.850	-3.240	-3.929	-2.797	-3.650	44.66±	44.21
(50)							0.06	±0.06
0.10	11.19	-2.848	-3.226	-3.904	-3.256	-2.808	44.73	44.78
(215)							±0.02	±0.02
0.10	11.18	-2.848	-3.243	-3.975	-3.276	-2.794	44.78	44.34
(385)							±0.20	±0.20
0.10	11.19	-2.841	-3.257	-3.810	-3.042	-2.810	44.16	43.72
(555)							±0.07	±0.07
0.10	11.23	-2.826	-3.187	-3.718	-3.106	-2.775	43.93	43.46
(935)								
0.10	11.08	-2.830	-3.226	-3.657	-3.126	-2.927	44.60	44.18
(1560)							±0.02	±0.02

[a] pH values marked with "*" were calculated by minimizing charge balance errors.
[b:] Errors are standard deviations from replicates. IAPss values calculated assuming stoichiometry of initial solid.
[c:] Samples were spiked with fresh solid immediately after previous sampling round.

Table 6-5. (con't) Activities, IAPss, and ΣΠ values calculated for $Ca_6[Al(OH)_6]_2(SO_4,CrO_4)_3 \cdot 26H_2O$ dissolution reaction pathway experiments.

$XCrO_4$ / (hrs)	Meas pH[a]	Log $\{Ca^{+2}\}$	Log $\{Al(OH)_4^-\}$	Log $\{CrO_4^{-2}\}$	Log $\{SO_4^{-2}\}$	Log $\{OH^-\}$	-Log IAP_{ss}[b]	-Log ΣΠ[b]
Secondary (spiked) dissolution reaction pathway samples								
0.30	11.34	-2.841	-3.155	-3.570	-3.533	-2.655	44.61	44.32
(50)							--	--
0.30	11.35	-2.839	-3.121	-3.535	-3.549	-2.645	44.44	44.18
(215)							±0.07	±0.06
0.30	11.33	-2.831	-3.125	-3.498	-3.548	-2.670	44.52	44.181±
(385)							±0.14	0.11
0.30	11.36	-2.812	-3.106	-3.364	-3.442	-2.637	43.89	43.53
(555)							±0.10	±0.12
0.30	11.32	-2.777	-3.017	-3.326	-3.725	-2.674	44.21	43.35
(935)							--	--
0.30	11.38	-2.782	-2.973	-3.228	-3.817	-2.660	44.20	42.96
(1560)							±0.15	±0.15
0.73	11.57	-2.693	-2.865	-3.122	-4.133	-2.432	41.80	40.98
(48)							±0.13	±0.07
0.73	11.56	-2.687	-2.857	-3.107	-4.088	-2.436	41.70	40.90
(215)							±0.13	±0.13
0.73	11.54	-2.697	-2.872	-3.144	-4.403	-2.460	42.22	41.20
(385)							±0.06	±0.01
0.73	11.45	-2.653	-2.885	-3.074	-4.517	-2.449	41.88	40.71
(555)							±0.02	±0.04
0.73	11.52	-2.694	-2.852	-2.947	-4.004	-2.478	41.48	40.62
(935)							±0.48	±0.03
0.73	11.41	-2.673	-2.881	-2.894	-4.526	-2.587	42.16	40.83
(1560)							±0.21	±0.13
0.79	11.33	-2.646	-2.796	-2.860	-3.725	-2.671	41.27±	40.73
(215)							0.01	±0.01
0.79	11.32	-2.613	-2.834	-2.988	-4.288	-2.701	41.93	41.11
(375)							±0.01	±0.02
0.79	11.24	-2.582	-2.777	-2.810	-4.394	-2.756	41.50	40.50
(555)							±0.07	±0.06
0.79	11.28	-2.582	-2.830	-2.688	-4.394	-2.721	41.18	40.11
(935)							±0.02	±0.02
0.79	11.18	-2524	-2.994	-2.610	-4.554	-2.825	41.18	40.11
(1560)							±0.02	±0.02

[a] pH values marked with "*" were calculated by minimizing charge balance errors.

[b:] Errors are standard deviations from replicates. IAPss values calculated assuming stoichiometry of initial solid.

[c:] Samples were spiked with fresh solid immediately after previous sampling round.

Table 6-6. Thermodynamic data used in modified MINTEQA2 database.

REACTIONS	kJ mol^{-1} $\Delta G°_r$	kJ mol^{-1} $\Delta H°_r$	J mol^{-1} K^{-1} $\Delta S°_r$	J mol^{-1} K^{-1} ΔC_P	log K_{SP}	Source[a]
$H_2O - H^+ = OH^-$	79.85	55.81	-80.66	-212.5	-13.99	1,2
Aqueous Species						
$Ca^{2+} + SO_4^{2-} = CaSO_4^0$	-12.05	5.44	58.6	196	2.11	2, 3
$CrO_4^{2-} + 2H^+ = H_2CrO_4^o$	-39.8	-26.0	85	--	6.97[b]	4
$CrO_4^{2-} + H^+ = HCrO_4^-$	-37.10	5.13	141.6	163.2	6.50	5
$2CrO_4^{2-} + 2H^+ - H_2O = Cr_2O_7^{2-}$	-83.45	20.7	210.3	661	14.62	5
$Ca^{2+} + CrO_4^{2-} = CaCrO_4^0$	-15.81	--	--	--	2.77	4
$Ca^{2+} + H_2O - H^+ = CaOH^+$	73.22	77.47	14.6	-38.0	-12.83	1,7
$Al^{2+} + H_2O = AlOH^{2+} + H^+$	28.35	55.73	91.0	0.65	-4.97	1,7
$Al^{3+} + 2H_2O = Al(OH)^{2+} + 2H^+$	57.70	122.6	218	-225	-10.11	1,7
$Al^{3+} + 3H_2O = Al(OH)_3^0 + 3H^+$	95.15	176.4	--	--	-16.67	1,7
$Al^{3+} + 4H_2O = Al(OH)_4^- + 4H^+$	131.3	181.4	167.7	-91.8	-23.00	1,7
Solid Phases						
$Ca(OH)_2 = Ca^{2+} + 2H_2O - 2H^+$	-129.6	-129.6	0.02	31.71	22.70	1,2,8
$CaSO_4 \cdot 2H_2O = Ca^{2+} + SO_4^{2-} + 2H_2O$	26.15	-0.46	-89.2	-333	-4.58	9
$Al_2O_{3,\ corundum} = 2Al^{3+} + 3H_2O - 6H^+$	-96.63	-243.6	-491	-125	16.93	1,7
$Al_2O_{3,\ \alpha\text{-Alumina}} = 2Al^{3+} + 3H_2O - 6H^+$	-104.6	-265.9	-533	-93.0	18.33	1,7
$Al(OH)_{3,\ amph} = Al^{3+} + 3H_2O - 3H^+$	-61.65	-110.8	--	--	10.8	7
$AlOOH,_{\ boehemite} = Al^{3+} + 2H_2O - 3H^+$	-43.60	-116.2	-243	-23.5	7.64	1,2,10
$AlOOH,_{\ diaspore} = Al^{3+} + 2H_2O - 3H^+$	-40.00	-112.0	-241	-22.4	7.01	1,2,10
$Al(OH)_3,_{\ gibbsite} = Al^{3+} + 3H_2O - 3H^+$	-44.26	-105.3	-205	14.3	7.75	1,2,10
$Ca_6[Al(OH)_6]_2(SO_4)_3 \cdot 26H_2O \rightleftharpoons 6Ca^{2+} + 2Al(OH)_4^- + SO_4^{2-} + 4OH^- + 26H_2O$	256 ± 1.8	204.6 ±0.62	-170 ±38	--	-44.90 ± 0.30	11
$Ca_6[Al(OH)_6]_2(CrO_4)_3 \cdot 26H_2O \rightleftharpoons 6Ca^{2+} + 2Al(OH)_4^- + CrO_4^{2-} + 4OH^- + 26H_2O$	236.6 ± 3.9	77.5 ± 2.4	-534 ± 83	-1510 ± 140	-41.46 ± 0.30	4

[a] Multiple sources indicate sources for individual ion or solid phase data that were used in calculating data presented. 1. Cox et al., 1989; 2. Shock et al., 1997; 3. Sverjensky et al., 1997; 4. Perkins and Palmer, 2000; 5: Baron and Palmer, 1998; 6. Ball and Nordstrom, 1998; 7. Nordstrom and May, 1996; 8. Garvin et al., 1987; 9. Nordstrom et al., 1990; 10: Hemingway and Sposito, 1996; 11. Perkins and Palmer, 1999.

[b] Calculated from ΔG°r from Ball and Nordstrom, 1998.

Equilibrium with pure phases was first assessed by calculating the saturation indices (SIs):

$$SI = \log (IAP / K_{SP}) \quad \textbf{(29)}$$

where the IAP is the ion activity product and K_{SP} is the solubility constant for the dissolution reaction as written in Equation (1). The calculated saturation indices (Figure 6-6) clearly indicate that all of the solutions were undersaturated with respect to CrO_4-ettringite, even in the higher $XCrO_4$ experiments. The solutions are all near saturation with respect to ettringite. This is expected given the much lower solubility of ettringite. However, there is a clear decline in SI values with increasing $XCrO_4$, with values dropping from the oversaturated to undersaturated conditions, implying that SO_4 concentrations were not controlled by equilibrium with pure ettringite.

Total solubility products were calculated using Equation (16) for all samples (Table 6-6) and are plotted on Lippman diagrams representing an ideal solid solution system in Figures 6-7 and 6-8. The calculated $\Sigma\Pi$ values for the experiments clearly plot above the ideal solutus curves (and, in fact, the values for the higher $XCrO_4$ solids plot above the solidus curves. This fact, together with the evolving CrO_4 and SO_4 concentrations, indicate that the solutions are not at thermodynamic equilibrium.

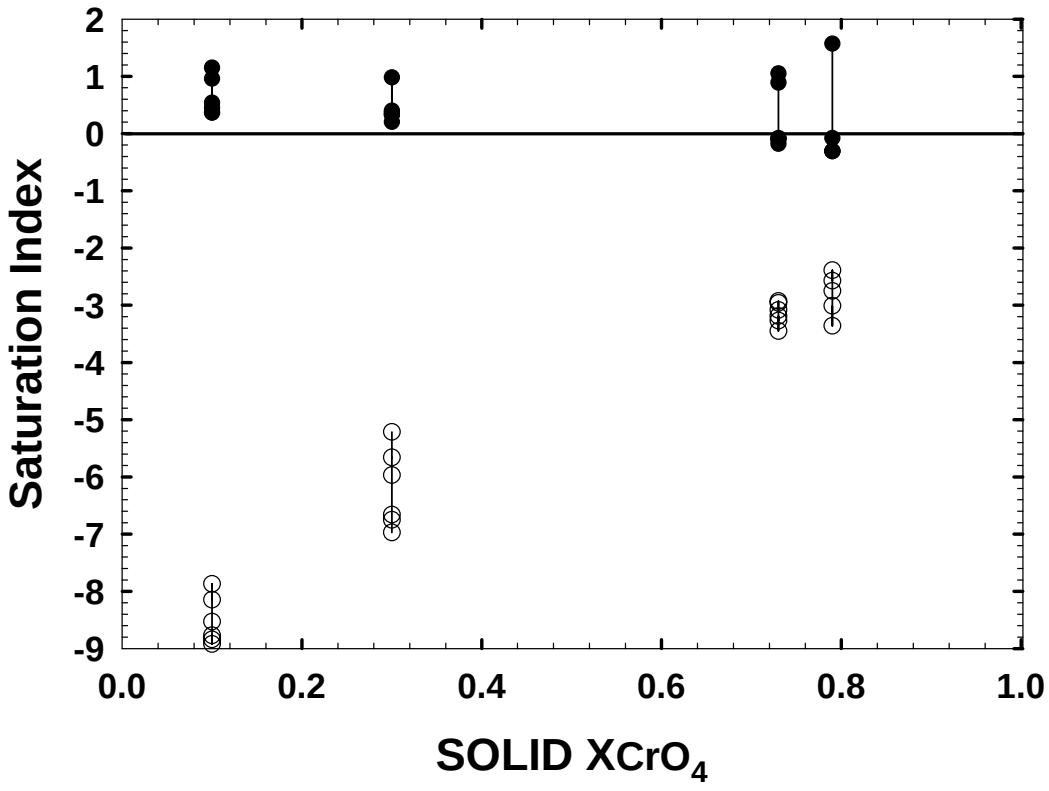

Figure 6-7. Plot of saturation indices for ettringite (•) and CrO_4-ettringite (o) as a function of solid phase $XCrO_4$ in second-phase (spiked) dissolution reaction pathway experiment samples.

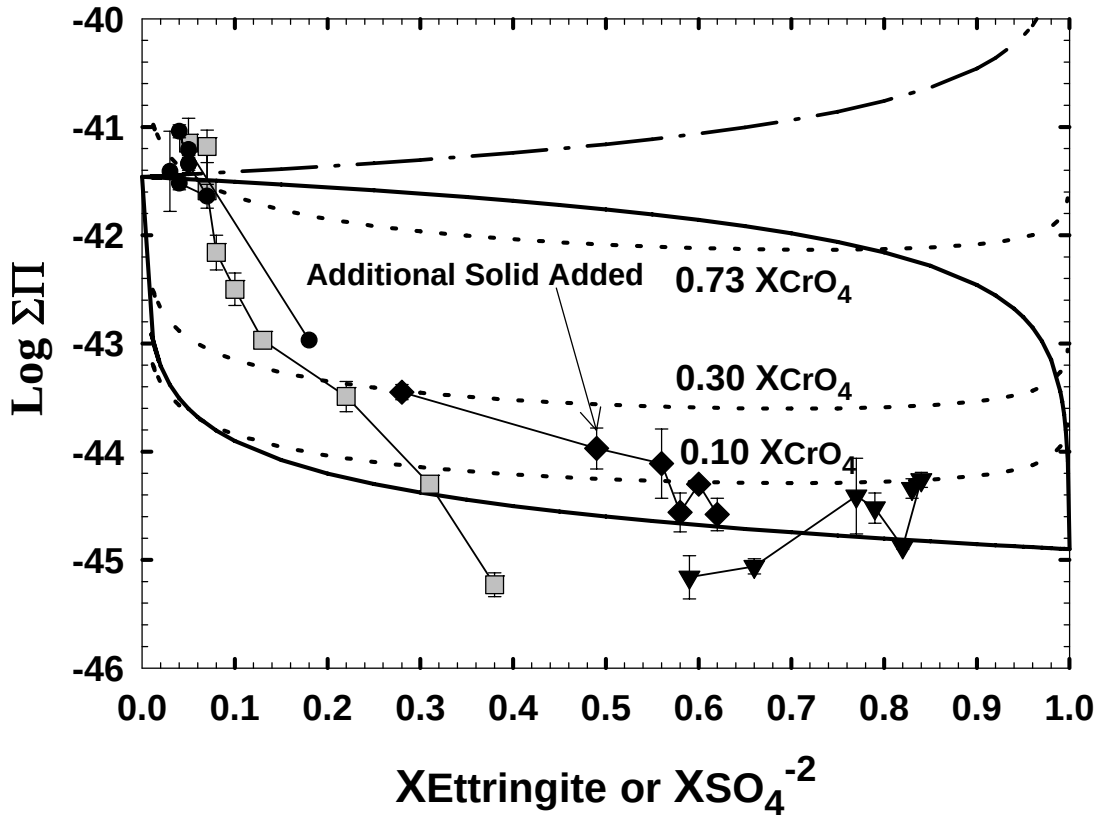

Figure 6-8. Lippman diagram showing total solubility products (ΣΠ) versus solid or aqueous $XCrO_4$ for initial dissolution reaction pathway experiments. ↔=0.10 $XCrO_4$ solid; _ = 0.30 XCrO4 solid; ◆ = 0.57 $XCrO_4$ solid; ℓ= 0.73 $XCrO_4$ solid. Dotted curves represent ideal stoichiometric saturation curves corresponding to a solid with the labeled CrO_4 mole fraction. The heavy dash-dot line at the top represents the saturation curve for the pure CrO_4-ettringite endmember.

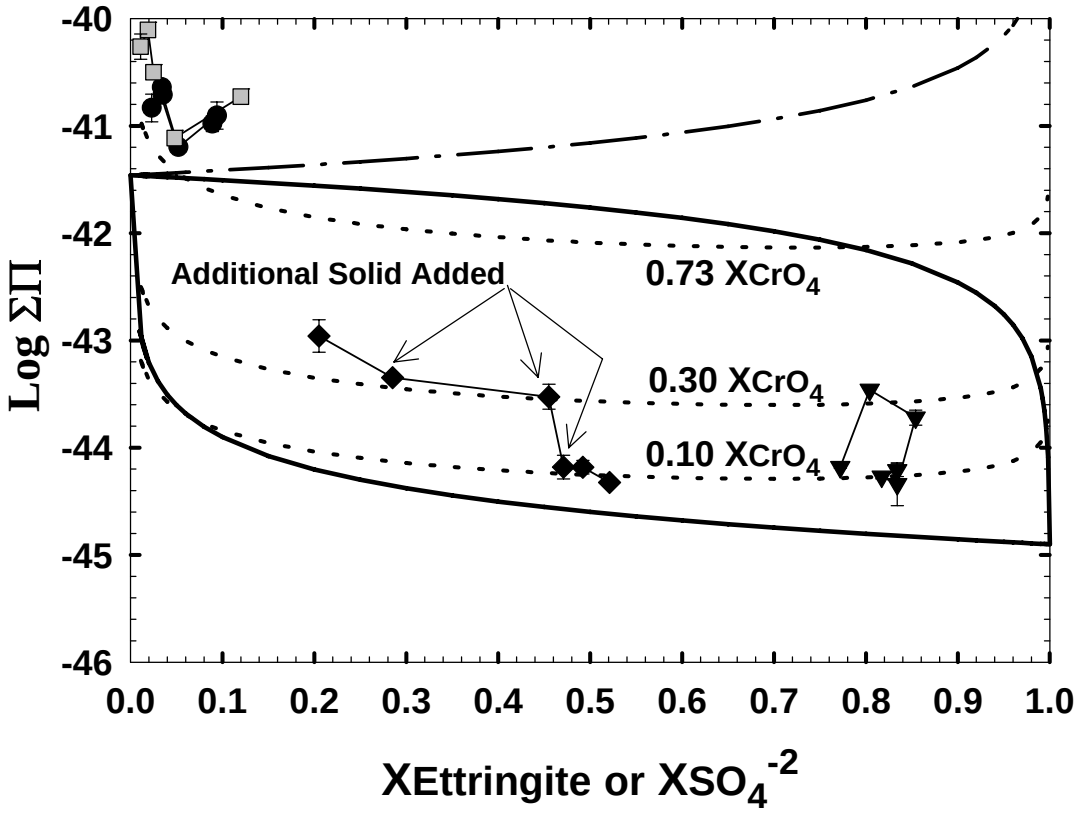

Figure 6-9. Lippman diagram showing total solubility products (ΣΠ) versus solid or aqueous $XCrO_4$ for secondary (spiked) dissolution reaction pathway experiments. ↔=0.10 $XCrO_4$ solid; _ = 0.30 XCrO4 solid; ℓ = 0.73 $XCrO_4$ solid; ◆ = 0.79 $XCrO_4$ solid. Dotted curves represent ideal stoichiometric saturation curves corresponding to a solid with the labeled CrO_4 mole fraction. The heavy dash-dot line at the top represents the saturation curve for the pure CrO_4-ettringite endmember.

However, the dissolution pathways represented by the calculated ΣΠ values track closely along the ideal stoichiometric saturation curves (as obtained from Equation (10)), particularly for the spiked samples (Figure 6-8). Such behavior has been noted in previous investigations of systems involving relatively low solubility solids and high solid to solution ratios (Plummer and Busenberg, 1987) and suggests stoichiometric saturation. Stoichiometric saturation is valid for systems, regardless of whether the phases involved are stable or metastable, as long as the composition of the solid remains fixed (Thorstenson and Plummer, 1977). Thus, for stoichiometric saturation to apply to the CrO_4 - SO_4 ettringite SSAS system, the shifts noted in the aqueous activity fractions would have to occur by precipitation of a secondary solid phase rather than by solid-state diffusion or recrystallization of the initial solid (Glynn et al., 1990).

Figure 6-9 presents a plot of log IAPss values, calculated using Equation (17) and assuming the stoichiometry of the initial solid, versus the compositions of those initial solids. The resulting IAP_{SS} values calculated for the secondary (spiked) dissolution experiment samples collected at 384 hours, prior to the addition of any additional solid, are nearly identical to those calculated for the samples collected at 1560 hours, after several rounds of spiking with additional solid. Variations in IAP_{SS} values calculated for the intervening samples may be assumed to be due to perturbations caused by introduction of new solids and the short period of time between samplings.

The aqueous concentrations at 384 hours are nearly stoichiometric with respect to ettringite-phases if SO_4 and CrO_4 concentrations are combined (i.e., Ca : Al : (SO_4 + CrO_4) ratios, normalized to Ca, are 6.0 : 1.7 : 2.9, 6.0 : 2.0 : 2.9, and 6.0 : 2.2 : 3.2 for the 0.10, 0.30, and 0.73 $XCrO_4$ solids, respectively). Given that the aqueous mole (and activity) fractions in the earliest samples are enriched with CrO_4 relative to the initial solid, the overall aqueous composition suggests that the secondary phase being precipitated is an ettringite phase or simply that the amount of secondary phase precipitated, while enough to significantly perturb the SO_4 : CrO_4 ratio, is not enough to significantly alter the overall aqueous stoichiometry within the precision range of the analytical techniques used. The latter scenario, which does not negate the former, is consistent with the observed changes in analyte concentrations from one sampling round to the next which were equivalent to or only slightly larger than typical analytical errors (~10^{-5} moles). The bulk composition of the initial solid can be assumed to have remained unchanged throughout the experiments because the high solid to solution ratios ensure that the reservoir of initial solid was far in excess of any secondary solid.

Stoichiometric saturation is appropriate in cases of very large solid / solution ratios when 1.) the initial solid, being the most soluble solid present, controls the extent of dissolution, and 2.) the change in the aqueous ratios is controlled by the precipitation of one or more secondary solid phases, which though present in small amounts relative to the initial solid, have significant mass relative to the aqueous rservoir of ions (Glynn et al., 1990). If stoichiometric saturation was achieved, the

persistent IAP_{SS} values may be assumed to be equivalent to the stoichiometric saturation constants (K_{SS}). K_{SS} values allow calculation of excess free energies, G^E, using (Plummer and Busenberg, 1987):

(30)

$$G^E = RT\,[\ln K_{SS} - X \ln(K_{SP,\,CrO4\text{-}ettringite}\,X) - (1\text{-}X)\ln(K_{SP,\,ettringite}\,(1\text{-}x))]$$

Combining Equations (30) and (10), results in an expression for ln Kss as a function of composition (Figure 6-9):

(31)

$$\ln K_{SS} = X_{ettringite}\,X_{CrO4\text{-}ettringite}\,[a_0 + a_1(X_{ettringite}\text{-}X_{CrO4\text{-}ettringite})]$$
$$+ X_{ettringite}\ln(K_{SP,ettringite}\,X_{ettringite}) + X_{CrO4\text{-}ettringite}\ln(K_{SP,\,CrO4\text{-}ettringite}\,X_{CrO4\text{-}ettringite})$$

K_{SS} values obtained by averaging those calculated from the 385 and 1560 hour data for 0.10, 0.30, 0.73, and 0.79 $XCrO_4$ samples and the 430 and 960 hour data for the 0.57 $XCrO_4$ sample were fit to Equation (31). It is not possible to fit these values to a single-parameter ("regular") form of this equation. The coefficients resulting from fitting G^E values to the two-parameter ("sub-regular") form of Equation (9) are a_0 = 2.03 ±0.76 and a_1 = 9.27 ±1.82 (n = 5, df = 3, r^2 = 0.987). The a_0 coefficient was marginally significant (t-value = 2.53) in this fitting; however, a_0 coefficients obtained by fitting either 385 or 1560 hour data alone were insignificant (t-values ≤1.3).

The calculated sub-regular coefficients indicate positive excess free energies over much of the range in which CrO_4-ettringite is the dominant component. The

resulting plot of free energies as a function of composition (Figure 6-10) implies a miscibility gap over the approximate range of $0.05 \leq X_{ettringite} \leq 0.65$ (binodal or double tangent points). Such a miscibility gap is inconsistent with the solid characterization of the synthesized intermediate phases which indicate miscibility throughout much of this range.

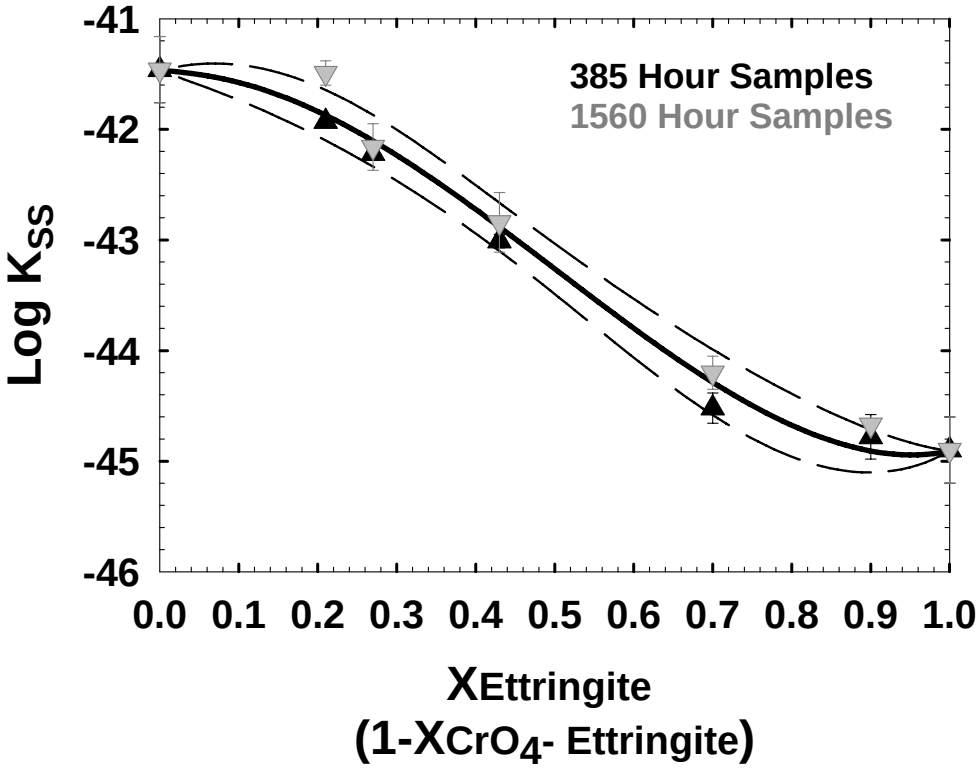

Figure 6-10. Plot of "Log Kss" values versus initial solid mole fraction. "Kss" values calculated for 385 (←) and 1560 hour (↔) data based on stoichiometry of initial solid . The heavy solid line represents best fit to Equation (31); short dashed lines represent 95% confidence intervals.

The calculated Guggenheim coefficients from which the free energies of mixing were derived are based on the assumptions that the reservoir of initial solid was far in excess of any secondary precipitates and, therefore, that the initial solid controlled dissolution. While the first of these assumptions is true with respect to the bulk solid, significant shifts in aqueous CrO4 / SO4 ratios brought about by precipitation of secondary phases could significantly alter the calculated IAPss values.

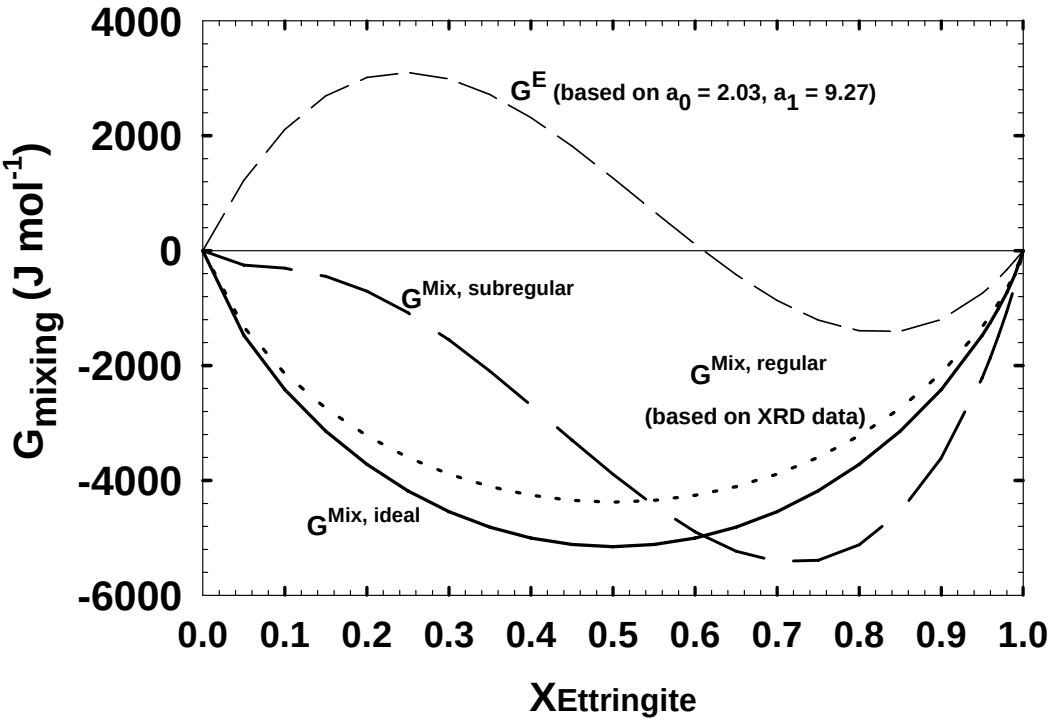

Figure 6-11. Plot of Gibbs free energies of mixing for SO_4 – CrO_4 ettringite solid solution system as a function of the solid-phase mole fraction. Solid line represents an ideal system. Dotted line represents "regular" system with excess free energies modeled using cell volume mismatch terms. Dashed lines represents a "subregular" system, with excess free energy, G^E, based on fitting of measured IAP_{SS} values.

If the extent of dissolution is controlled by these phases, which would be enriched with respect to SO_4, then the IAP_{SS} values, calculated assuming the stoichiometry of the initial solid, would be too high, with a larger degree of resulting error for the more CrO_4-enriched phases. IAPss (and hence, Kss) values calculated using larger XSO_4 values (corresponding to compositions of secondary SO_4-rich ettringite overgrowths) could more easily be fit either to a regular (one-parameter) solid solution model or a subregular solid solution model having a smaller a_1 coefficient which would be more consistent with the solid phase characterizations. However, without knowledge of the actual composition of secondary solids, accurate K_{SS} values cannot be calculated and a specific excess energy model (including fitting parameters) cannot be constructed

6.6 SUMMARY

A number of $Ca_6[Al(OH)_6]_2(Cr_xS_{1-x}O_4)_3 \cdot 26H_2O$ solid solutions over the range of $0.79 \geq XCrO_4 \geq 0.10$ were synthesized. Chemical analyses of the synthesized solids showed that each was more enriched in SO_4 than was the suspension from which it was synthesized. This enrichment is a function of the lower solubility of the SO_4 ettringite endmember and the higher percentage of total CrO_4 involved in ion pairing with Ca relative to total SO_4. The results from chemical analyses of solid digests, FTIR, and XRD analyses indicate a continuous solid solution series. Unit cell volumes calculated from XRD data appear to vary linearly over the compositional field, suggesting the solid solution series behaves as a regular (symmetric) system. An ion interaction parameter, $W_{G,}$ was calculated based on Navrotsky's (1987)

correlation of experimentally-derived interaction parameters with cell volume mismatch terms, V. The resulting W_G value of 3.1 kJ mol-1 is equivalent to a dimensionless Guggenheim coefficient, a_0, of +1.3.

Two sets of dissolution reaction pathway experiments were conducted by placing synthesized solids into NaOH solutions (pH ≈11.0) and tracking changes in aqueous solution compositions over time. The experimental suspensions were.spiked with fresh solid in the second set of experiments. Total solubility products, ΣΠs, were calculated from the analytical data and plotted on Lippman diagrams. The resulting plots indicate that the solutions dissolved incongruently. The dissolution reaction pathways plot well above the ideal solutus which, together with the continued evolution in solution compositions, indicates that thermodynamic equilibrium was not achieved over the duration of the experiments (> 2600 hours in some cases). The dissolution pathways do, however, plot close to the stoichiometric saturation curves in many cases. IAPss values calculated for samples collected at ~400 were nearly identical to those calculated for spiked samples collected at ~1600 hours while the ΣΠ values were more variable. These observations suggest stoichiometric saturation control beyond congruent dissolution. However, attempts to fit the IAP values calculated using the initial solid stoichiometries to an excess free energy model that was consistent with the solid-phase characterization data were not successful. We believe this is because the partial equilibrium conditions are controlled by SO_4-enriched secondary precipitates.

The experimental results indicate that $Ca_6[Al(OH)_6]_2(Cr_xS_{1x}O_4)_3 \cdot 26H_2O$ solid solutions can maintain significantly lower aqueous Cr(VI) concentrations than pure $Ca_6[Al(OH)_6]_2(CrO_4)_3 \cdot 26H_2O$, although this may not be the case for the higher $XCrO_4$ solids. Although thermodynamic equilibrium may not be achieved on time scales of interest, the experimental data suggests that the total solubility products can be expected to closely follow stoichiometric saturation curves while approaching equilbrium. Additional work is clearly required in order to develop more stringent mathematical models of this system, to determine distribution coefficients for precipitation of solid solutions, and to determine the times required for solid and aqueous solutions to arrive at thermodynamic equilbrium.

Chapter 7. Summary and Conclusions

7.1 SUMMARY OF RESULTS

The mobility of chromium, a prevalent and potentially harmful environmental contaminant, is likely to be controlled by precipitation and dissolution of solid phases under alkaline conditions. This dissertation adds greatly to our knowledge regarding the ability of one of the most common alkaline solids phases, ettringite ($Ca_6[Al(OH)_6]_2(SO_4)_3 \cdot 26H_2O$), to exert such control and clearly establishes fundamental parameters for this phase which were either previously unavailable or disputed. The salient points presented in the individual experimental chapters of this dissertation are presented here.

Chapter 2 presents the a study of the solubility of ettringite over a wide range of environmentally-relevant temperatures. Previously reported solubility values, written for the same reaction at 25ºC, varied by approximately 10 orders of magnitude and no previous studies regarding the temperature-dependence of the solubility could be located. The study presented is the first to establish enthalpy and entropy values based on solubility. The fundamental parameters established for ettringite should be of interest both to environmental workers and material scientists given the importance of this phase in common cementitious and refractory materials.

Chapter 3 presents the first solubility study of bentorite, the Cr(III)-analog of ettringite and a naturally-occurring mineral. This study also provides initial estimates of enthalpy for bentorite based on a limited number of temperature-dependent experiments. The results of the investigation indicate that a related

secondary phase(s), tentatively identified as $Ca_2Cr_2O_5 \cdot 8H_2O$, controls the concentration of Cr(III). This study should be of particular interest to workers designing cement-based waste stabilization.

The solubility study of $Ca_6[Al(OH)_6]_2(CrO_4)_3 \cdot 26H_2O$, the Cr(VI)-analog of ettringite, is the subject of Chapter 4. This study presents a set of fundamental thermodynamic properties for this phase. Although this is not known to be a naturally-occurring mineral, Cr(VI)-containing ettringite phases have been identified in chromium-contaminated concrete which indicates the potential importance of these phases in attenuation of chromium released in the environment. The solubility of this phase and that of ettringite provide solubility limits for ettringite solids in which substitution of CrO_4 for SO_4 is only partial. The study is the first to postulate the existence of a $CaCrO_4$ ion pair and provides an initial estimate for the ion pair formation constant derived by minimizing variations in IAPs with pH. Knowledge of such an aqueous complex may be critical to accurate modeling of the fate and transport of Cr(VI) in the environment.

Chapter 5 presents the first solubility values for $3CaO \cdot Al_2O_3 \cdot CaSO_4 \cdot nH_2O$, the Cr(VI)-analog of monosulfate, another important solid phase in cement systems. The thermodynamic parameters obtained from the solubility data allow construction of phase diagrams defining the stability boundary between $3CaO \cdot Al_2O_3 \cdot CaSO_4 \cdot nH_2O$ and the $Ca_6[Al(OH)_6]_2(CrO_4)_3 \cdot 26H_2O$.

A study of the $Ca_6[Al(OH)_6]_2(SO_4, CrO_4)_3 \cdot 26H_2O$ solid solution and solid solution / aqueous solution interactions is presented in Chapter 6. The experimental

results verify previous studies that indicated this solid solution series is continuous. It also provides the first estimate of the free energy interaction parameter, W, based on interpretation of variations in unit cell volumes obtained through XRD analyses of the synthesized solids. Incongruent dissolution of the solid solutions was noted and the solid solution / aqueous solution systems did not reach thermodynamic equilibrium over periods exceeding 2600 hours. Constant stoichiometric saturation values over time and reaction pathways plotted on Lippman diagrams suggested the extent of dissolution is at least initially controlled by stoichiometric saturation. However, the solutions may be at saturation with respect to SO_4-enriched secondary overgrowths. While a valid model for quantification of solid solution / aqueous solution interactions could not be developed from the available solubility data, this conceptual model provides a basis for further study of this complicated system.

7.2 OVERALL CONCLUSIONS

Little is known about potential controls on aqueous chromium concentrations in alkaline environments. This is particularly true in the case of Cr(VI), which generally occurs as an oxyanion which has low sorption tendencies under alkaline conditions. Ettringite, through its common occurrence in cements, fly-ash, and FGD wastes and its proven ability to substitute oxyanions, is potentially one of the most important solid phase controls on Cr(VI) in alkaline environments. However, no solubility data was previously available for Cr-substituted ettringites and the solubility of ettringite itself was the subject of considerable dispute. This dissertation presents for the first time fundamental solubility and thermodynamic parameters for

ettringite and its Cr(III) and Cr(VI) analogs as well as a conceptual model regarding the dissolution of ettringites which have undergone partial Cr(VI) substitution.

The resulting data shows that ettringite can limit the aqueous concentrations of Cr(VI) in alkaline conditions and, in conjunction with related calcium aluminum hydroxides, Cr(III) concentrations as well. The degree to which ettringite may limit chromium concentrations is, of course, dependent on the system in question, and in particular, the concentrations of other ettringite components (e.g., Ca^{+2} and OH^{-}) in the system under consideration. Conversely, the study also confirms that the concentrations of Cr(VI) in equilibrium with chromium-substituted ettringites may still be well above regulatory standards. Cr(VI)-substituted ettringites may therefore present secondary sources of chromium which could continue to maintain harmful levels of chromium in the environment after the initial contaminant source has been removed.

The $CaCrO_4$ complex, whose existence was inferred based on interpretation of the $Ca_6[Al(OH)_6]_2(CrO_4)_3 \cdot 26H_2O$ solubility data, is an aqueous species which may be important in modeling the fate and transport of Cr(VI) in most natural environments. Overall, this study represents a significant advance in our understanding of both chromium geochemistry and Ca-Al-SO_4-H_2O systems.

7.3 RECOMMENDATIONS FOR FUTURE WORK

Although this investigation has provided a thorough set of thermodynamic parameters for ettringite and its Cr(VI) analog, some issues remain unresolved or in need of additional refinement. Therefore, the following research is

recommended to improve our understanding of the interactions between chromium and the Al-SO_4-H_2O system.

1.) Significant changes in IAP values were noted in all of the experiments at pH approaching 13 and above. Similar results were noted by Warren and Reardon (1994) in their ettringite solubility study. Additional studies, including repeat solubility studies with more carefully controlled pH measurements and SEM observations of experimental residues may be warranted to determine the reason for these discrepancies. The upper and lower stability range of all the ettringite-type phases with respect to pH should be determined.

2.) There is considerable evidence from the bentorite solubility study as well as an earlier investigation of ettringite and chromium interactions by Kindness et al. (1994) that Cr(III) concentrations in the Ca-Al-Cr-SO_4 H_2O system are primarily controlled by Ca-Al hydroxides, possibly hydrogarnet. Given the prevalence of chromium contamination and proposals to isolate chromium wastes in cementitious materials, it is important that the controlling phase(s) be accurately identified and that solubilities and thermodynamic parameters for the phase(s) and their chromium analogs be determined.

3.) The bentorite solubility studies indicate a reversal in the trend of calculated IAPs with temperature between 35 and 60ºC. Such a reversal most likely represents a phase

change. The other phase(s) involved and the temperature-dependent stability boundary between this phase(s) and bentorite should be determined.

4.) The $CaCrO_4^0$ complex appears to account for a significant percentage (5-40%) of the total chromium present in the experimental solutions, particularly in the case of the $Ca_6[Al(OH)_6]_2(SO_4, CrO_4)_3 \cdot 26H_2O$ solid solutions. As Ca^{+2} is a major ion in most surface waters, this complex could be extremely important in understanding the geochemistry of chromium above pH 6.5 where CrO_4^{-2} is the dominant Cr(VI) ion. While this study presents an estimate of the $CaCrO_4^0$ formation constant, a more thorough investigation of this and other potential CrO_4 complexes, including determination of the temperature-dependence of their formation constants is warranted. The ion activities and solubility products obtained from the Cr(VI) analog and solid solution experiments should be recalculated if a significantly different $CaCrO_4^0$ formation constant is obtained through such studies.

5.) A great deal of work remains in order to develop a quantified model for $Ca_6[Al(OH)_6]_2(SO_4, CrO_4)_3 \cdot 26H_2O$ solid solution / aqueous solution reactions. In particular, short-term dissolution experiments could be performed in hopes of obtaining IAPss values corresponding to congruent dissolution. However, it this may not be possible if the rate of back-precipitation process is rapid.

The composition of secondary precipitates forming during dissolution should be determined. The stoichiometries of these overgrowths could then be used to calculate

IAPss values which should enable more accurate excess free energy models to be developed.

Precipitation experiments from supersaturated solutions with variable CrO_4 / SO_4 ratios should be conducted. The resulting solids should be carefully examined to determine whether heterogeneous layering is present. Long-term dissolution and precipitation experiments could also be conducted to verify thermodynamic equilibrium conditions which may be estimated via short-term experiments if the composition of the controlling reactive solid as well as the aqueous solution can be determined.

References

Allison J. D., Brown D. S., and Novo-Gradac K. J. (1990) MINTEQA2/PRODEFA2, A Geochemical Model for Environmental Systems: Version 3.0. U.S. Environmental Protection Agency.

Anderson, G.M. and Crerar, D.A. (1993*) Thermodynamics in Geochemistry: The Equilibrium Model*, Oxford University Press, 588 p.

APHA (1995) *Standard Methods for the Examination of Water and Wastewater*, 19th Ed., American Public Health Association, 1100 p.

Atkins M., Glasser F. P., and Kindness A. (1992) Cement hydrate phases: solubility at 25°C. *Cement and Concrete Research* **22**, 241-246.

Atkins M., Macphee D., Kindness A., and Glasser F. P. (1991) Solubility properties of ternary and quaternary compounds in the CaO-Al_2O_3-SO_3-H_2O System *Cement and Concrete Research* **21**, 991-998.

Ball J. W. and Nordstrom D. K. (1998) Critical evaluation and selection of standard state thermodynamic properties for chromium metal and its aqueous ions, hydrolysis species, oxides, and hydroxides. *Journal of Chemical Engineering Data* **43**(6), 895-918.

Baron D. and Palmer C. D. (1998) Solubility of $KFe(CrO_4)_2 \cdot 2H_2O$ at 4-75^{o}C. *Applied Geochemistry* **13**(8), 961-973.

Bensted J. and Varma S. P. (1971) Studies of ettringite and its derivatives. *Cement Technology* **2**(May/June), 73-76.

Bentor Y. K. (1963) High-temperature minerals in non-metamorphosed sediments in Israel. *Nature* **199**, 478-479.

Carlson E. T. and Berman H. A. (1960) Some observations on the calcium aluminate carbonate hydrates. *Journal of Research of the National Bureau of Standards: A. Physics and Chemistry* **64**(4), 333-341.

Cox J. D., Wagman D. D., and Mededev V. A. (1989) *CODATA Key Values for Thermodynamics*. Hemisphere Publishing Corporation, 271 p.

Damidot D., Atkins M., Kindness A., and Glasser F. P. (1992) Sulphate attack on concrete: limits of the AFt stability domain. *Cement and Concrete Research* **22**, 229-234.

Davies P. K. and Navrotsky A. (1983) Quantitative correlations of deviations from ideality in binary and pseudo-binary solid solutions. *Journal of Solid State Chemistry* **46**, 1-22.

Dunn P. J., Peacor D. R., Leavens P. B., and Baum J. L. (1983) Charlesite, a new mineral of the ettringite group, from Franklin, New Jersey. *American Mineralogist* **68**, 1033-1037.

Dzombak D. A. and Morel F. M. M. (1990) *Surface Complexation Modelling: Hydrous Ferric Oxide*. John Wiley and Sons, Inc, 393 p.

Ewing L. L. and Shepard M. I. (1994) A microcosm for soil-atmosphere gas transfer investigations. *Journal of Environmental Quality* **23**, 469-476.

Garvin D. P., Parker V. B., and White H. J. (1987) *CODATA thermodynamic tables - selections for some compounds of calcium and related mixtures: a prototype set of tables.* Hemisphere Publishing Corporation, 365 p.

Ghorab H. Y. and Kishar E. A. (1985) Studies of the stability of the calcium sulfoaluminate hydrates. Part I: Effect of temperature on the stability of ettringite in pure water. *Cement and Concrete Research* **15**, 93-99.

Ghorab H. Y., Kishar E. A., and Elfetouh S. H. A. (1998) Studies on the stability of the calcium sulfoaluminate hydrates. Part II: Effect of alite, lime, and monocarbonaluminate hydrate. *Cement and Concrete Research* **28**(1), 53-61.

Glynn P. D. and Reardon E. J. (1990) Solid-solution aqueous solution equilbria: thermodynamic theory and representation. *American Journal of Science* **290**, 164-201.

Glynn P. D., Reardon E. J., Plummer L. N., and Busenberg E. (1990) Reaction paths and equilibrium end-points in solid-solution aqueous-solution systems. *Geochimica et Cosmochimica Acta* **54**, 267-282.

Gougar M. L. D., Scheetz B. E., and Roy D. M. (1996) Ettringite and C-S-H portland cement phases for waste immobilization: a review. *Waste Management* **16**(4), 295-303.

Gross S. (1980) Bentorite, a new mineral from the Hatrurim Area, west of the Dead Sea, Israel. *Israel Journal of Earth-Sciences* **29**, 81-84.

Hampson C. J. and Bailey J. E. (1982) On the structure of some precipitated calcium alumino-sulphate hydrates. *Journal of Materials Science* **17**, 3341-3346.

Hassett D. J., McCarthy G. J., Kumarathasan P., and Pflughoeft-Hassett D. (1990) Synthesis and characterization of selenate and sulfate-selenate ettringite structure phases. *Materials Research Bulletin* **25**, 1347-1354.

Hemingway B. S. and Sposito G. (1996) Inorganic aluminum-bearing solid phases. In *The Environmental Chemistry of Aluminum* (ed. G. Sposito), CRC Press, 81-116.

Höglund L. O. (1992) Some notes on ettringite formation in cementitious materials; influence of hydration and thermodynamic constraints for durability. *Cement and Concrete Research* **22**, 217-228.

Hurlbut C. S. and Baum J. L. (1960) Ettringite from Franklin, New Jersey. *The American Mineralogist* **45**, 1137-1143.

JCPDS (Joint Committee on Powder Diffraction Standards) (1991) Powder Diffraction File, Swathmore, PA, International Centre for Diffraction Data.

Jones F. E. (1939) The quaternary system CaO-Al_2O_3-$CaSO_4$-H_2O at 25°C. *Transactions of the Faraday Society* **35**, 1484-1510.

Jones F. E. (1944a) The quaternary system CaO-Al_2O_3-$CaSO_4$-H_2O at 25° C. *Journal of Physical Chemistry* **48**(6), 311-355.

Jones F. E. (1944b) The quinary system CaO-Al_2O_3-$CaSO_4$-K_2O-H_2O at 25° C. *Journal of Physical Chemistry* **48**(6), 356-378.

Jones F. E. (1944c) The quinary system CaO-Al_2O_3-$CaSO_4$-Na_2O-H_2O (1 percent NaOH) at 25° C. *Journal of Physical Chemistry* **48**(6), 379-394.

Kindness A., Macias A., and Glasser F. P. (1994) Immobilization of chromium in cement matrices. *Waste Management* **14**(1), 3-11.

Kumarathasan P., McCarthy G. J., Hassett D. J., and Pflughoeft-Hassett D. F. (1990) Oxyanion substituted ettringites: synthesis and characterization; and their potential role in immobilization of As, B, Cr, Se and V. In *Materials Research Society Symposium*, 83-104.

Kuzel H. J. (1996) Initial hydration reactions and mechanisms of delayed ettringite formation in Portland cements. *Cement Technology*, 195-203.

Langmuir D. (1979) Techniques of estimating thermodynmic properties for some aqueous complexes of geochemical interest. *In Chemical Modeling in Aqueous Systems* (ed. E.A. Jenne) American Chemical Society, 353-387.

Lea F. M. (1970) *The Chemistry of Cement and Concrete*. Edward Arnold Ltd, 727 p.

McMurdie H. F., Morris M. C., Evans E. H., Paretzkin B., Wong-ng W., Zhang Y., and Hubbard C. R. (1986) Calcium Aluminum Sulfate Hydroxide Hydrate, $Ca_6Al_2(SO_4)_3(OH)_{12}\cdot 26H_2O$. *Powder Diffraction* **4**, 337.

Moore A. E. and Taylor H. F. W. (1970) Crystal structure of ettringite. *Acta Crystal* **B26**, 386-393.

Murdoch J. and Chalmers R. A. (1960) Ettringite ("Woodfordite") from Crestmore, California. *The American Mineralogist* **45** (November-December), 1275-1278.

Myneni S., Traina S. J., and Logan T. J. (1994) Retention of arsenate and chromate by ettringite in alkaline waste environments. *American Chemical Society, Division of Environmental Chemistry*, 525-527.

Myneni S. C. B. (1995) Oxyanion-Mineral Surface Interactions in Alkaline Environments: AsO_4 and CrO_4 Sorption and Desorption in Ettringite. Dissertation, The Ohio State University, 250 p.

Myneni S. C. B., Traina S. J., and Logan T. L. (1998) Ettringite solubility and geochemistry of the $Ca(OH)_2$ - $Al_2(SO_4)_3$ - H_2O system at 1 atm pressure and 298 K. *Chemical Geology* **148**(1), 1-19.

Navrotsky A. (1987) Models of Crystalline Solutions. In *Thermodynamic Modeling of Geologic Materials: Minerals, Fluids and Melts*, Mineralogical Society of America **17**, 35-77.

Nieboer E. and Shaw S. L. (1988) Mutagenic and other genotoxic effects of chromium compounds. In *Chromium in the Natural and Human Environments* (ed. J. O. Nriagu and E. Nieboer), John Wiley and Sons, Inc, 399-437.

Nordberg G. F. (1988) Current concedpts in the assessment of effects of metals in chronic low-level exposures; considerations of experimental and epidemiological evidence. *The Science of the Total Environment* **71**, 243-252.

Nordstrom D. K. and May H. M. (1996) Aqueous equilibrium data for mononuclear aluminum species. In *The Environmental Chemistry of Aluminum* (ed. G. Sposito), Lewis Publishers, 39-80.

Nordstrom D. K. and Munoz J. L. (1994) *Geochemical Thermodynamics*. Blackwell Scientific Publications, 493 p.

Nordstrom D. K., Plummer L. N., Langmuir D., Busenberg E., May H. M., Jones B. F., and Parkhurst D. L. (1990) Revised chemical equilibrium data for major water-mineral reactions and their limitations. In *Chemical Modeling of Aqueous*

Systems II (ed. D. C. Melchior and R. L. Bassett), American Chemical Society, 398-413.

Nriagu J. O. (1988) Production and Uses of Chromium. In *Chromium in the Natural and Human Environments* (ed. J. O. Nriagu and E. Nieboer), John Wiley and Sons, Inc. 81-103.

O'Brien P. and Kortenkamp A. (1994) Chemical models important in understanding the ways in which chromate can damage DNA. *Environmental Health Perspectives* **102**(Supplement 3), 3-10.

Odler I. and Abdul-Maula S. (1984) Possibilities of quantitative determination of the AFt-(ettringite) and AFm-(monosulphate) phases in hydrated cement pastes. *Cement and Concrete Research* **14**, 133-141.

Palmer C. D. (2000) Precipitates in a Cr(VI)-contaminated concrete. *Environmental Science and Technology*, **in review**

Perkins R. B. and Palmer C. D. (1999) Solubility of Ettringite ($Ca_6[Al(OH)_6]_2(SO4)_3 \cdot 26H_2O$) at 5-75ºC. *Geochimica et Cosmochimica Acta* **63**(12/14), 1969-1980.

Perkins R. B. and Palmer C. D. (2000) Solubility of $Ca_6[Al(OH)_6]_2(CrO_4)_3$-$26H_2O$, the chromate analog of ettringite; 5- 75ºC. *Applied Geochemistry* **in press**.

Plummer L. N. and Busenberg E. (1987) Thermodynamics of aragonite-strontianite solid solutions: results from stoichiometric dissolution at 25 and 76 C. *Geochimica Cosmochimica Acta* **51**, 1393-1411.

Poellman H., Auer S., Kuzel H. J., and Wenda R. (1993) Solid solution of ettringites, Part II: incorporation of $B(OH)_4^-$ and CrO_4^{2-} in $Ca_6Al_2O_6(SO_4)_3 \cdot 32H_2O$. *Cement and Concrete Research* **23**, 422-430.

Poellmann H., Kuzel H. J., and Wena R. (1990) Solid solution of ettringites, Part I: incorporation of OH^- and CO_3^{2-} in $3CaO \cdot Al_2O_3 \cdot 3CaSO_4 \cdot 32H_2O$. *Cement and Concrete Research* **20**, 941-947.

Reardon E. J. (1990) An ion interaction model for the determination of chemical equilibria in cement/water systems. *Cement and Conrete Research* **20**, 175-192.

Richard F. C. and Bourg A. C. M. (1991) Aqueous Geochemistry of Chromium: A Review. *Water Research* **25**(7), 807-816.

Shock E. L. and Helgeson H. C. (1988) Calculation of the thermodynamic and transport properties of aqueous species at high pressures and temperatures: Correlation algorithms for ionic species and equations of state prediction to 5kb and 1000°C. *Geochimica et Cosmochimica Acta* **52**, 2009-2036.

Shock E. L., Sassani D. C., Willis M., and Sverjensky D. A. (1997) Inorganic species in geologic fluids: Correlations among standard molal thermodynamic properties of aqueous ions and hydroxide complexes. *Geochimica et Cosmochimica Acta* **61**(5), 907-950.

Sugiyama M. (1994) Role of paramagnetic chromium in chromium (VI)-induced damage in cultured mammalian cells. *Environmental Health Perspectives* **102**(Supplement 3), 31-33.

Sverjensky D. A., Shock E. L., and Helgeson H. C. (1997) Prediction of the thermodynamic properties of aqueous metal complexes to 1000°C and 5 kb. *Geochimica et Cosmochimica Acta* **61**(7), 1359-1412.

Teramato H. and Koie S. (1976) Early hydration of a superhigh-early-strength Portland cement containing chromium. *Journal of the American Ceramic Society* **59**, 522-525.

Thorstenson D. C. and Plummer L. N. (1977) Equilbrium criteria for two-component solids reacting with fixed composition in an aqueous-phase; example: the magnesian calcites. *American Journal of Science* **277**, 1203-1223.

Viellard P. and Rassineux F. (1992) Thermodynamic and geochemical modelling of the alteration of two cement matrices. *Applied Geochemistry* (Supplementary Issue No. 1), 125-136.

Waddington T. C. (1959) Lattice energies. In *Avances in Inorganic Chemistry and Radiochemistry*, Vol. Vol. 1 (ed. H. J. Emeléus and A. G. Sharpe), Academic Press, 157-221.

Wagman D. D., Evans W. H., Parker V. B., Schumm R. H., Halow I., Bailey S. M., Churney K. L., and Nuttall R. L. (1982) The NBS table of chemical thermodynamic properties; Selected values for inorganic and C_1 and C_2 organic substances in SI units. *Journal of Physical and Chemical Reference Data* **11**(Supplement No. 2), 394 p.

Warren C. J. and Reardon E. J. (1994) The solubility of ettringite at 25ºC. *Cement and Concrete Research* **24**(8), 1515-1524.

Zamorani E., Sheikh A. A., and Serrini G. (1988) Physical properties measurements and leaching behaviour of chromium compounds solidified in a cement matrix. *Nuclear and Chemical Waste Management* **8**, 239-245.